Ana Virgínia Ferreira Azevedo

Modelação numérica da resposta dinâmica de proteções multi-material sujeitas a impactos balísticos

Ana Virgínia Ferreira Azevedo

Numerical modelling of the dynamic behaviour of stiff composite armour subject to ballistic impact

Tese apresentada à Universidade de Aveiro para cumprimento dos requisitos necessários à obtenção do grau de Doutor em Engenharia Mecânica, realizada sob orientação científica do Filipe Miguel Horta e Vale Teixeira-Dias, Professor Auxiliar com Agregação do Departamento de Engenharia Mecânica da Universidade de Aveiro e do Frederik Coghe, Major IMM do Departamento de Sistemas de Armas e Balística da Academia Militar da Bélgica.

O juri / The jury

Presidente / President

Professor Doutor José Fernando Ferreira Mendes
Professor Catedrático da Universidade de Aveiro

Vogais / Committee

Professor Doutor Marc Pirlot
Professor Ordinário da Royal Military Academy

Professor Doutor Jorge Manuel Costa da Fonseca Justo
Professor Adjunto do Instituto Superior de Engenharia do Porto

Professor Doutor Johan Gallant
Professor Militar da Royal Military Academy

Professor Doutor João Alexandre Dias de Oliveira
Professor Auxiliar da Universidade de Aveiro

Professor Doutor Frederik Coghe
Major IMM da Royal Military Academy

Agradecimentos / Acknowledgements

There are several people I would like to thank, for different reasons. First of all, I have no words to express how grateful I am to my two supervisors:
- Professor Filipe Teixeira-Dias, for his guidance, continuous advice, availability and above all for his friendship. Continues to be an example for me as a person and as a professional. Always present from a very early stage of my academic life, and one of the main responsible for me being here.
- Major IMM Frederik Coghe for all his daily support, patience, guidance and for his friendship. Thank you for proposing me this work and introducing me to the world of ballistics. It is a great honor to work with you.
I am also very thankful to my officemate Angel Miranda-Vicario for his help throughout my work and our project. My acknowledgements go also to Professor Marc Pirlot, the head of the Department of Weapon Systems and Ballistics of the Royal Military Academy of Belgium. Thank you Professor for having received me so well in your department.
To all my colleagues Colonel Johan Gallant, Major Alexandre Papy, Captain Véronique De Brie, Dr. Cyril Robbe, Dr. Nestor Nsiampa, Mr. André Chabotier, Dr. Bogdan Stribu, Ir. Iréne Ndindabahizi, Ir. George Kechagiadakis and to all my other colleagues at the Department of Weapon Systems and Ballistics of the Royal Military Academy of Belgium I would like to express my gratitude. Their presence and support was fundamental.
One special thanks goes to Bruno. Thank you for all your constant support, help and for being always with me.
Last, but not least, I thank my friends and family, particularly my mother, my father and my sister for their inconditional love.

Palavras-chave impacto balístico; projétil; simulação numérica; método dos elementos finitos; capacete balístico; material compósito

Resumo Face aos sucessivos eventos relativos a ataques terroristas, é imperativo realizar investigação cientifica e desenvolvimento em questões relacionadas com a proteção balística. O objetivo principal do trabalho que aqui se apresenta é desenvolver um novo capacete balístico capaz de parar projéteis de alta velocidade, usando modelos de elementos finitos, validados com base em resultados de testes experimentais. O modelo de capacete aqui apresentado é composto por quatro diferentes camadas, onde: (i) a primeira é capaz de deformar e fraturar o projétil, especialmente o núcleo de aço, ajudando a reduzir a sua velocidade; (ii) a segunda camada absorve energia cinética do projétil, (iii) a terceira limita a deflexão da face anterior e, finalmente, (iv) a quarta camada absorve a onda de choque do impacto inicial e garante a distância necessária para evitar o contato dessas camadas com a cabeça. Foi também realizado um estudo numérico detalhado das diferentes partes do projétil 7.62 $\times$ 39 M43. Obteve-se uma boa correlação entre os resultados numéricos (usando o software LS-Dyna^{TM}) e experimentais para os modelos do projétil quer do equipamento de proteção pessoal (capacete). Atingiu-se também uma boa correlação em termos de velocidade de impacto em função da profundidade de deformação do novo desenho de capacete balístico. Realizou-se uma análise numérica mais detalhada para a configuração do capacete relativa à camada de absorção da onda de choque. Um primeiro conjunto de simulações consistiu em introduzir limites rígidos nas extremidades das três primeiras camadas. Um segundo conjunto de simulações considerou as três primeiras camadas anexadas a uma estrutura rígida, fixa no capacete. A partir dos resultados numéricos, conclui-se ser possível projetar uma camada de absorção da onda de choque de maneira a reduzir significativamente o risco de traumatismo craniano causado pelo impacto no capacete. Uma distância mínima entre a cabeça e o capacete pode, portanto, ser determinada para um novo modelo de capacete balístico capaz de parar o projétil M43 Kalashnikov.

Keywords ballistic impact; projectile; numerical simulation; finite element method; ballistic helmet; composite material

Abstract

With the current events concerning terrorist attacks, it is imperative to perform research and development on issues related to ballistic protection. The need to protect soldiers from high impact velocity threats has become increasingly important and challenging. Within the scope of this work the aim is to develop an optimised armour configuration for an advanced ballistic helmet design, which is able to defeat impacts from high velocity rifle bullets. This is done using finite element modelling supported by results from experimental tests. The design presented here is based on four different layers, where: (i) the first layer is designed to break and erode the projectile, (ii) the second layer absorbs the kinetic energy of the projectile, (iii) the third layer minimises the back face deflection and, finally, (iv) a fourth layer absorbs the shock wave of the initial impact and provides the necessary standoff (required by the back face deflection) for the first three layers, so that direct contact between these layers and the head does not occur. The results obtained by simulation with the finite element method (using LS-Dyna^{TM}) demonstrate that the models agree with the experimental results. A detailed numerical study of the different layers as well as the 7.62$\times$39 M43 projectile was made. A good correlation between numerical and experimental results of the ammunition and armour materials was achieved, as well as between numerical and experimental results in terms of the depth of indentation as a function of impact velocity of the new ballistic helmet design. The last two sets of numerical analysis made for the helmet shell configuration was relative to the shock absorbing layer. The first set of simulations consisted of introducing rigid boundaries to the composite layer of the flat panel. A second set of simulations considered the composite layer of the flat panel to be attached to a rigid frame, without fixing this frame. From the simulation results, a shock-absorbing layer can be designed in such a way as to significantly reduce the risk on behind-helmet blunt trauma, and with acceptable force transfer to the head. An optimum standoff distance was determined for a ballistic helmet concept able to stop the M43 Kalashnikov projectile.

Contents

Part I

Introduction and state-of-the-art

Chapter 1

Goal and thesis outline

1.1 Goal

This thesis aims at developing an extensive knowledge base on the dynamic behaviour of different composite armour configurations. The characterization of the dynamic behaviour of different composite armour configurations involves both the assessment of the ballistic resistance and the dynamic deflection during impact. The aforementioned knowledge base is applied to determine an optimised armour configuration for an advanced ballistic helmet design using finite element modelling for both ballistic and material tests based on results from experimental tests. This not only involves the classical ballistic problem of stopping the bullet, but also determining the risk of head and brain injury for non-penetrating impacts. The main idea behind the research here presented is to create a new concept of helmet able to defeat high velocity rifle bullets using available ballistic materials.

This work is aimed at evaluating if protection against these kinds of high-velocity rifle threats can be obtained by using a composite, four-layer armour concept within the current weight and biomedical accepted constraints for military (and/or police) helmets [Crowley et al., 1992]. The new helmet design is composed of a first layer made of a hard, ceramic outer shell. This first layer is backed by an energy absorbing layer, composed of fibre-based composite material responsible for stopping the incoming projectile. Envisioned levels of protection concern typical semi-armour piercing military ammunition equipped with soft- or hard-cored penetrators (respectively the 7.62 $\times$ 39 M1943 Kalashnikov and the 5.56 $\times$ 45 NATO Ball round), the ceramic outer shell is necessary to break (fragment) these cores before effectively absorbing their kinetic energy with the fibre-composite material.

The risks on skull fracture and traumatic brain injury are (mainly for the former) largely influenced by the dynamic back face deflection of the helmet shell. Although the back face deflection will in part also be determined by the characteristics of the two first layers, research has shown that a tailored sandwich concept of a third and fourth layer can largely decrease the total required thickness of the helmet to avoid direct loading of the head from the impact zone [Coghe et al., 2010]. It has also been shown that an optimised design of these last two layers would not only lead to a reduced back face signature, but also to an increase in ballistic resistance, leading to a win-win situation [Coghe et al., 2010]. The fourth shock-absorbing layer (in combination with the system to ergonomically fit the helmet to the head) will also reduce the risk on traumatic brain

injury due to the altered impulsive loading of the head through the helmet shell. In order to have a set of minimum requirements based on acceptable loadings to the human head, this research project makes relative comparisons between existing helmet designs and the proposed design, and assesses the performance of the latter, applying relevant injury criteria.

The work is developed in a partnership between the Department of Mechanical Engineering of the University of Aveiro and the Department of Weapon Systems and Ballistics of the Royal Military Academy of Belgium.

1.2 Thesis outline

This thesis is divided in three parts, each subdivided in a total of nine chapters.

The first part of this thesis includes chapters 1 to 5. A brief presentation of the subject of investigation is made in Chapter 1, presenting the goal of this thesis and also a thesis outline, where a glimpse of the contents of each chapter is given to the reader. In Chapter 2 the history of ballistic helmets and the evolution of the helmet materials are presented. The general motivation of this work is also presented in Chapter 2. The non-penetrating injury resulting from the rapid deformation of the inside of the helmet shell, known as the Behind Helmet Blunt Trauma is presented in Chapter 3 as well as the associated types of head injuries such as skull fractures and traumatic brain injury. A number of head impact criteria that are available to estimate the injury levels and also the different helmet and body armour standards important for this research are presented. The main objectives of this research work are also presented in this chapter. Chapter 4 is dedicated to materials and geometry of all ammunition and armour used. Chapter 5 presents the finite element model in order to better understand the numerical material models that are needed in this work. Part II of this document, which includes Chapters 6 to 8, deals with the finite element analysis and numerical modelling of the new helmet design. Chapter 6 is an overview on finite element analysis and the use of this method to impact problems. The numerical validation using experimental data of the ammunition and armour materials presented in this thesis is covered in Chapter 7. The third chapter regarding numerical modelling is Chapter 8, where the numerical model of a new ballistic helmet design is presented. Also, in this chapter a finite element model approach used to see the influence of the shock-absorbing layer on the risk on behind-helmet blunt trauma and a suitable standoff based on a maximum force injury criterion are presented.

Part III (including chapter 9) ends this thesis. In this chapter the main conclusions are pointed out and possible future lines of research and work are suggested.

Chapter 2

Ballistic helmets

Combat helmets are amongst the oldest forms of personal protective equipment, and are known to have been first worn by the Akkadians/Sumerians in the 23rd century BC, and are used until now [Rank, 2019]. Today's militaries often use high-quality helmets made of ballistic materials such as aramid fibres, which offer improved protection. Such helmets typically offer protection for the head from shrapnel and fragments.

Aramid body armour and helmets are the most commonly used type of personal ballistic protection and they can play an important role in stopping a projectile.

By effectively shielding the wearer from bullets and fragments, protective gear has improved overall survival rates, and aramid helmets have reduced the frequency of penetrating head injuries [Sone et al., 2017]. Helmets, however, cannot completely protect the face, head, and neck, nor do they prevent closed brain injuries, often produced by blasts [Terrio et al., 2009].

Ballistic resistant garments, like vests, jackets and helmets were mainly designed for protection from shrapnel and bomb fragments. It is common practice nowadays for both military personnel and regular police to use aramid ballistic protection and ceramic plates to protect from fragments and small-arms threats [Brown, 2003]. The military standards [NATO Standardization Agency, 2016] that are used to rate the effectiveness of aramid and ceramic materials vary according to the end use and even to the military service branch testing them. In general, the effectiveness of a material is evaluated based on its ability to completely stop a penetrating projectile. Some military standards also evaluate the material deformation and target deformation after impact. Protection from small calibre arms is quite challenging because of the high velocities, low aspect ratios and hard surfaces of the projectiles [Bhatnagar, 2016]. Nevertheless, new armour design efforts continue to pursue the reduction of deformation of helmets and vests after an impact from a projectile. Explosive devices are far greater threats to soldiers in combat [Wade et al., 2007]. Although statistically less probable, protection from rifle, machine gun, and submachine gun projectiles remains critical in the development of military armour.

A typical military helmet consists of three basic components, namely the helmet shell, a comfort padding and a retention system [Ivins et al., 2007]. Optional accessories are often included in the system to fulfil other requirements. Additionally, modern helmets are often equipped with some accessories for specific functions. For example, helmets for paratroopers are enhanced by modified chin straps without interfering with their overall performance [Ivins et al., 2007]. Also, different colour toned camouflage

covers are used according to environmental characteristics, not to mention the advanced electronic devices including audio-visual head gear, hands-free communication sets as well as real-time physical monitors are often mounted on modern helmets.

This chapter describes the changes in helmet design and materials, since the times of the Napoleonic era to modern Advanced Combat Helmets (ACH). One of the key advances was the development of a composite material in the 1960s, which led to today's aramid-based helmets. A large group of nations are investing in research to improve armour protection systems (personal and vehicle) through better design and materials as well as better manufacturing processes. A brief introduction into the evolution of military helmets is presented and also a review of the different helmet materials. The last section of this chapter presents the actual threat of terrorism attacks.

2.1 History of the ballistic helmet and helmet materials

Ballistic protection equipment for the head is a very important research subject and in the previous decades the topic has received extensive attention in various areas. Within the range of helmets, there are various types, such as, for example, military helmets, police helmets, motorcycle helmets, sports helmets and helmets for emergency services. They all have in common the fact that they are in part designed and used to protect their users from possible brain damage in situations of impact. Specifically, this doctoral work focusses on ballistic helmets for military and police operators. This type of equipment is normally used for protection in case of threats that combine high speed and low mass. Materials and construction techniques became more advanced as weapons became more powerful with time. Initially manufactured from leather and brass, and then bronze and iron during the Bronze and Iron Ages, helmets soon came to be made entirely from forged iron in many societies after around 950 AD [Mdlinger et al., 2013].

The Napoleonic era saw the introduction of ornate helmets (see Figure 2.1a), which continued to be used by the French army and later on by the British until World War I. However, it was necessary to make these helmets safer, thus enabling protection against fragments, grenades and ricochetted projectiles. This led to the first modern helmet, the French Adrian helmet (see Figure 2.1b) built from hardened steel with an inner liner that is adjustable to accommodate different head sizes. This model was later adopted by the American army resulting in the Hadfield steel helmet (see Figure 2.1c)[Military Trader, 2009].

Steel helmets similar to the French Adrian helmet were soon adopted by other nations. The original World War I French and British helmet designs were adapted by the US Army to form the Hadfield steel helmet. The Hadfield helmet was eventually redesigned for lower weight, better comfort, and higher protection to produce the famous World War II M1 (see Figure 2.1d) steel helmet. A modernisation of this model was later made, resulting in lighter helmet, were more comfortable and with a higher level of protection. The military helmet M1 also know as "steel pot", was used by the United States military from World War II until 1985. The M1 helmet has become an icon of the American military and over 22 million were manufactured by the end of World War II [Stanton, 1994]. The M1 helmet model was produced in only one size, which was a great disadvantage [Gerald, 2008].

In the early 1960s, the US Army launched a study with the aim of replacing the

M1 helmet by a lighter helmet and whose configuration conferred more protection to the user. Around 1972, the Personnel Armour System for Ground Troops (PASGT) helmet, which was the first helmet to use aramid fibres was released to the market. In Figure 2.1e it is possible to see an example of this model, which presents a lower weight compared to the previous model and provides better protection with regards to brain damage caused by ballistic impacts. All previous military helmets were made from steel, but from the PASGT onwards, manufacturers began to use lighter metallic alloys and polymer matrix composites [Kulkarni et al., 2013, Gerald, 2008]. The PASGT helmet is a one-piece structure composed of multilayers of aramid ballistic fibres (Kelvar 29 Type II fabric) and phenol-formaldehyde (PF) and polyvinylbutyral (PVB) resin. The helmet is manufactured using a compression molding technique [Adanur, 1995]. After introducing the PASGT helmet the aramid fibres have become the standard raw (and most common) material for making ballistic helmets [Brown, 2003].

There have also been developments in helmet retention systems. The M1 "steel pot" used a nylon stripe suspension system, sweatband and chinstrap. The PASGT helmet and its variants also used similar retention systems. The Belgium Army still uses a variant of the PASGT military helmet: the Schuberth combat helmet. This military helmet is made out of aramid fibres and the suspension system of this helmet is shown in Figure 2.2.

The PASGT model covers a large part of the head, has better ventilation conditions and is designed in four different sizes (S, M, L and XL). However, the US Army continued to perform research for possible lighter models which led to the PASGT model being further developed in two improved helmets, the Advanced Combat Helmet (ACH) shown in Figure 2.1f and the Light Weight Helmet (LWH) of the Marine Corps shown in Figure 2.1g. The current generation of US military helmets, such as the Advanced Combat Helmet (ACH), is also constructed of a thermoset resin shell matrix with aramid fibre. The helmet shell provides ballistic protection from fragments and also can stop 9 mm projectiles. Compared to the PASGT helmet, the ACH helmet allow easier mounting of night-vision goggle brackets and the front brow is eliminated to improve upwards visibility, higher ballistic protection and is lighter. These helmets are, however, only designed to stop fragments and hence do not give sufficient protection against high velocity small calibre rifle bullets.

The ACH and LWH helmets switched to a multi-pad that had better impact protection while providing increased comfort. The combat helmet liner system shown in Figure 2.3 consists of a one-piece protective impact liner with variable thicknesses (back is thicker than front) and 22 adjustable comfort pads provided in four shapes (oblong, trapezoid, tapered trapezoid, and triangle) and two thicknesses. The comfort pad set also includes four pads for added stability and two sweat bands for moisture absorption [Wendy, 2019]. The inner part of modern helmets (ACH for example) is made from a combination of high quality materials such as leather, polyester fabric, nylon webbing, polypropylene webbing, nylon fittings, and brass press studs. The helmet shell is also fitted with deformable plastic foam liners to cope with blunt impacts. Each material is selected to provide maximum performance and comfort for each aspect of the harness design. The harness is mounted in the helmet using a stainless steel shell body with PVC edge trimming 5-point suspension system assembly, a head band with brow and back cushioning pads, a perforated crown, a chin strap fitted with quick release buckles, and a chin cup.

(a) Napoleonic era [IMA, 2019].

(b) Adrian style helmet [Military Trader, 2009].

(c) Hadfield helmet[IMA, 2019]

(d) M1 [Kulkarni et al., 2013].

(e) PASGT [MKU, 2018].

(f) ACH [Kulkarni et al., 2013].

(g) LWH [Corporation, 2017].

Figure 2.1: Evolution of helmet design.

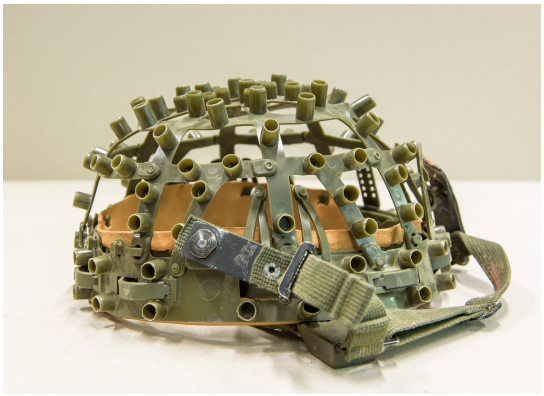

Figure 2.2: Schuberth helmet suspension system.

(a) Example of a helmet liner system [Wendy, 2019].

(b) Helmet liner system installed [Wendy, 2019].

Figure 2.3: Helmet inner padding systems.

Figure 2.3 shows the use of inner pads in a helmet as the helmet-to-person interface.

The next major advance in helmet technology resulted from a combination of advances in materials and manufacturing processes. Continued improvement in materials (like the ultra-high-molecular-weight polyethylene fibres (UHMWPE)) had also led to advances in helmet performance. New materials are also under evaluation for mitigating the effect of impacts on the head. Both recoverable and non-recoverable energy-absorbing materials are being considered for use as helmet pads. Another factor in helmet protection [Grand view research, 2016] is the way the constituent materials are assembled. For example, in unidirectional UHMWPE panels, varying fibre orientation and fibre architecture can provide better balance between resistance-to-penetration and deformation mitigation.

The main disadvantage of composite helmets is when energy absorption occurs after a ballistic impact and can destroy the compressed tissues and also in some cases, can cause delamination of fabric layers in the composite material [Kulkarni et al., 2013]. However, helmets made out of aramid fill all required standards and their cost is relatively low compared to other materials. The helmets made out of aramid are the most widely used military helmet in the armies of all countries.

Protective equipment must be robust, in order to protect more effectively the user,

and simultaneously be lightweight to be comfortable and easy to carry. With the continued investigation in this subject, researchers and companies came to the conclusion that one possible metallic material capable of providing significant improvements in ballistic protection is titanium [Seeber et al., 2018]. Kane and Smith [Kane and Smith, 1968] studied helmets made of pure titanium and with three different alloys to identify which led to the ballistic properties, formability in shaping the helmet and the commercial availability of the studied alloys. The three different types of alloys that were studied are: 6Al-4 V, 4Al-3 Mn and 5Al-2.5 Sn. Pure titanium demonstrated a lower ballistic performance compared with these alloys. The 5Al-2.5 Sn titanium alloy was the one that gave the best results for the helmet application. The main advantage of titanium alloys is their energy absorption. The main disadvantages of this material are however the high cost and the weight when compared to aramid materials.

New manufacturing technologies and techniques have enabled the production of ballistic helmets using thermoplastic ultra-high-molecular-weight polyethylene (UHWMPE) fibres, which exhibit the highest strength-to-weight ratio currently seen in any thermoplastic fibre material [Kulkarni et al., 2013]. The Enhanced Combat Helmet (ECH), which has been under development since 2007, is made of UHWMPE reinforced with carbon fibres [Kulkarni et al., 2013]. These new helmets are up to 15% lighter in weight than the previous generation and achieve equivalent ballistic protection as those heavier models [Freitas et al., 2014]. The use of UHMWPE in the construction of the helmet shell continues to be explored to increase the level of ballistic protection beyond that of the ECH, without an increase in weight [Kulkarni et al., 2013, Vargas-Gonzalez et al., 2011].

One of the issues currently being faced by private manufacturers is the high deformation response of the backface during ballistic impact. For that reason, significant research is being made to understand the behaviour of lightweight materials like aramid or polyethylene, in order to improve their ballistic performance regarding behind-helmet blunt trauma (BHBT).

Gerald [Gerald, 2008] compares and investigates two types of design for the interior padding system, and determine whether the difference in design and material properties affect the severity of the head injury suffered by the soldier. This author tested the use of polymeric foams such as polyurethane foam (PU), expanded polypropylene (EPP) and polystyrene (EPS) as energy absorbing materials and compared them with a regular suspension system composed by a strap, strip and back rest. As expected, results indicated that the difference in the density of the foam pads influences the level of stress and pressure on the head. Compared to the regular suspension system, where nylon and leather straps are of higher stiffness, and the standoff gap between the head and the helmet is larger, there is less room for deformation and hence most of the deformation energy will be imparted onto the head, causing skull fracture and serious head injuries, including life threatening. The ideal interior cushion pad would be one that is low in stiffness but with sufficient thickness to allow more space for deformation. Othman [Othman, 2009] studied the ballistic limit and the maximum deflection of the helmet made of four different types of composites namely carbon fibre-reinforced polyester, glass fibre-reinforced polyester, Kevlar fibre-reinforced polyester and Kevlar 29 fibre-reinforced phenolic, and found that the ballistic limit was highest for carbon reinforced polyester and lowest for Kevlar 29 reinforced phenolic.

In 2013, Kulkarni et al. [Kulkarni et al., 2013] provided a comparative study on the design, materials, and ballistic and blast performance of the combat helmets used by

the US Army, based on a comprehensive and critical review of existing studies. The authors established that the curvature given to a helmet during its manufacturing from flat laminates has a significant effect on the ballistic limit of a helmet. The authors also reinforce the idea that UHMWPE/carbon fibre composites can provide higher ballistic protection at a reduced weight than the composites used in current helmet designs.

Cordeau [Cordeau, 2016] conducted, at the DGA (Direction Générale de l'Armement of France) Land Systems laboratory, an interesting experimental test to better understand helmet capabilities against the non-penetrating impact of rifle projectiles and the rebound phenomena. The author studied the impact of 7.62×51 Ball and 7.62×51 AP projectiles against aramid-based helmets at nominal velocities and at different impact incidences. The tests presented in this paper illustrated the importance of correctly measuring the helmet impact angle.

In 2005, Walsh [Walsh et al., 2005] explored new ballistic material solutions for military helmets. The focus of this work was to identify materials and design opportunities that could be used to engineer a lighter helmet that met prescribed baseline performance specifications. The preliminary conclusions based on ballistic and mechanical data were that thermoplastic-based systems can yield a 10 to 25% weight reduction over conventional thermoset (PVB phenolic) helmet materials, while maintaining equivalent protection levels.

In general, increased helmet weight implies increased stiffness due to either more layers of composites or increased mass of the matrix. Helmets with higher structural stiffness tend to exhibit lower dynamic back face deflection during a ballistic impact. As the helmet weight is reduced, the current generation of combat helmets tends to exhibit greater back face deflection for the same ballistic impact conditions compared to the previous generation of helmets. Achieving equivalent ballistic protection (in terms of perforation or projectile defeat) at a lighter weight is a significant achievement. The tradeoff of greater dynamic back face deflection at reduced weight may, however, result in other damage or injury mechanisms coming to the forefront, such as blunt trauma injuries [Freitas et al., 2014].

The ultimate goal is for these new materials and hybrids (combination of different composite materials) to manifest themselves into new head protection systems that enable either the same level of protection at lower weight to result in helmets with significantly higher protection at similar weight. Thermoplastic matrices, together with both aramid and UHWMPE fibres, have tremendous potential, but they carry some complexities that must be addressed if these materials are to be used successfully in new helmet applications. The key complexities are the relative soft structural response of these materials, making both static and dynamic deformations a potentially limiting criterion in certain applications. The two leading providers of innovative ballistic helmets are Gentex Corporation and Revision Military, both located in the US [Corporation, 2017]. The core business of Gentex Corporation, is helmet system platforms and capability upgrades (respiratory and chemical, biological, radiological, and nuclear protection products, eye and face protection products, and hearing protection and communications products). Revision Military [Military, 2017a] was founded in 2001, and develops and delivers purpose-built protective soldier equipment for military use worldwide. The company, which began by developing eyewear, has expanded to face, head and torso protection and continues to develop innovative capabilities for integrated, performance-enhancing soldier systems.

To develop innovative helmets, and higher performance armour systems in general,

it is necessary to develop evaluation methods that can efficiently predict injuries and trauma, thus assuring that the soldier protection can resist specific threats. The risk of injury or trauma that can arise from head and neck movements (accelerations, rotations, displacements, etc.) are additional considerations.

2.2 Motivation - Actual threat

The work here presented explores in more detail the relationship between back face deformation and materials response (including monolithic, hybridized, and alternative fibre orientations), and correlates this with the influence on the ballistic response of the new helmet concept. The goal is to develop sufficient understanding to enable the most robust and optimal use of these materials.

Today, with the current events concerning terrorist attacks, it is imperative to perform research and development in issues related to ballistic protection. The need to protect soldiers from high impact velocities, such as, for example, small calibre impacts, has been stimulating and renewing the interest in new materials and structures. The development of protection systems against small calibre projectiles, originated by either terrorist attacks or war scenarios, plays an important role in the development of defence armour applications.

A ballistic impact is a high velocity impact often caused by a low mass object such as small fragments or small arms projectiles. Applications of research in this field include body armour and armoured vehicles. A typical military-style ballistic helmet only offers protection against high-velocity fragments (which until the conflicts in Iraq and Afghanistan was also the only required level of protection as in conventional warfare, the fragmentation threat from artillery and mortar fire, bombs, etc. is by far the most common threat).

In 2010, the International Committee of the Red Cross (ICRC) illustrated the importance of protecting the head from ballistic impacts as wounds to the head and torso are the most lethal [Giannou and Baldan, 2009]. The lethality of penetrating head wounds is approximately 75% and they account for slightly less than 50% of combat deaths, and only about 8% of survivors [Giannou and Baldan, 2009]. Head wounds kill either through devastating brain injury or through asphyxiation of the comatose patient who would otherwise survive the injury [Giannou and Baldan, 2009].

In 2008, a study was conducted at a zonal hospital of the Indian Army. This study reported and examined the case of soldiers killed in counter-terrorist operation in the Kashmir valley between January 1999 to December 2006. The highest percentage of all deaths were due to head injury (23.4%) [Arora et al., 2009].

Modern protective equipment has reduced fatalities, from primary injury mechanisms uncovering previously hidden secondary injuries. The traumatic brain injury (TBI) problem is acute for military personnel as exemplified even by the medical side alone: there have been approximately 1.4 million soldiers serving in Iraq and Afghanistan, 3.6% of which return with injuries, and approximately 60% of injured soldiers have some form of mild traumatic brain injury (MTBI) or TBI, and about 20% of these have serious TBI [Wallsten and Kosec, 2005, Bilmes and Stiglitz, 2008].

In 2011 DuBose et al.[DuBose et al., 2011] presented a study on severe TBI occurring in the context of modern military conflict from 2003 to 2007. Blast (61.9%) and gunshot

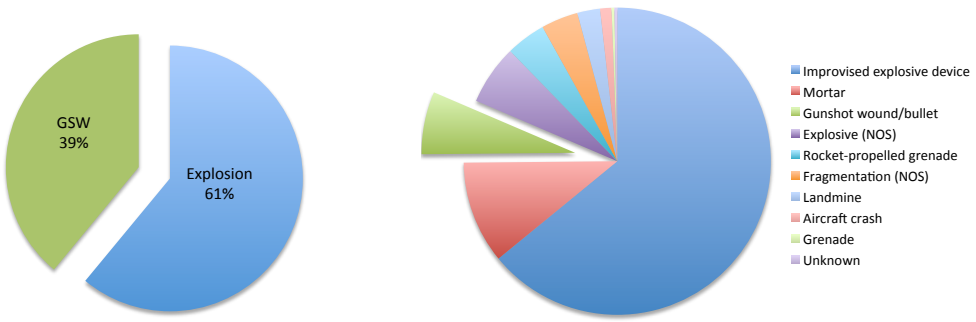

(a) Head injuries (from gun shot wounds (GSW) and explosion) of the British military in Iraq and Afghanistan between March 2003 and October 2014 [Keene et al., 2016].

(b) British military fatalities due to head, neck and face injuries in Iraq and Afghanistan, by cause, March 2003 through March 2007 [Wade et al., 2007].

Figure 2.4: Example of head injury data in war scenarios.

wounds (19.5%) accounted for the majority of combat injuries.

Between March 2003 and June 2005, 401 US marines died from combat injuries during Operation Iraqi Freedom. A report from the US Marine forces shows that 33.7% died from a primary head or neck lethal injury [Lidn et al., 1005].

Although blast and fragments continue to be the main cause of injuries, it is not possible to neglect the fatalities caused by projectiles, as can be seen in Figure 2.4. The presented data (71 combat-related fatalities) shows the number of lethal casualties deemed to have died from their injuries after arriving at a medical treatment facility during recent conflicts in Iraq and Afghanistan. Figure 2.4 (a) shows that of the 71 British military who died from wounds between March 2003 and October 2014, 44 (62%) had severe head injuries. The primary mechanism of head injury was due to explosions (61%) and the remaining 17 (39%) died due to gun shots to the head (GSW) [Keene et al., 2016], Figure 2.4 (b) shows that the most common causes of head, face, and neck injury among battle casualties were improvised explosive devices (64%), mortars (11%), GSW (7%) and other explosives (6%). According to this information, it is necessary to create/develop a helmet not only to stop fragments but also projectiles [Wade et al., 2007].

Although efforts have been made to increase the level of protection offered by helmets, the mass constraints (for continuous usage like in a military context the maximum allowable weight is 2 kg [Arbogast et al., 2003]) do not allow for any significant increase in protection by adding additional layers of protective materials. Several helmet manufacturers claim to have developed ballistic helmets offering protection against bullets, but these helmets generally have never been evaluated for the risk on behind-helmet blunt trauma (BHBT) caused by the dynamic deflection of the helmet shell upon impact. This is mainly due to the lack of an internationally accepted test method and associated pass/fail criterion. Nevertheless, specialised helmets (typically made of titanium to reduce the dynamic deflection) offering protection against handgun threats have been developed, which largely eliminate the risk on BHBT. Unfortunately, these helmets weigh approximately 2.5-3.0 kg, which excludes them from being worn over

extended periods, and they are hence typically only for special intervention forces.

Both in military and in law enforcement operations, the most commonly found small calibre threat is the ubiquitous Kalashnikov, also known as the AK-47 (or simply AK). Recent criminal investigations and the recent terrorist activities in Belgium and abroad have only confirmed the universal presence of the AK-47 weapon system. Some examples are:

- May 24, 2014: a gunman opens fire in the Jewish Museum of Belgium in Brussels, killing three people and critically wounding a fourth. An AK-47 Kalashnikov weapon is recovered after the arrest of the gunman [Wikipedia, 2016b];
- January 7, 2015: two gunmen open fire in the office of the Charlie Hebdo magazine (Paris, France), killing twelve people and wounding another eleven [Parisien, 2015, Wikipedia, 2016a]. The gunmen used Kalashnikov assault rifles. In the following days three other shootings with Kalashnikov rifles resulted in 17 more people killed;
- January 15, 2015: during anti-terrorist operations in Verviers (Belgium), three terrorists are killed during a heavy firefight with the police [Wikipedia, 2016a]. At the scene and during further searches, four AK-47 assault rifles were recovered [fivr/Belga, 2015];
- November 13, 2015: 130 people are killed by terrorists using gunfire and bombs in Paris (France) [Wikipedia, 2016c]. Another 368 are wounded. Most of the casualties are due to AK-47 gunfire [News, 2015];
- November 20, 2015: Terrorists take 170 hostages and kill 20 of these in a mass shooting at the Radisson Blu hotel in Bamako, the capital city of Mali. Two of the victims had Belgian nationality. The perpetrators were using AK-47 ammunition (weapons not confirmed) [Associated Press in Bamako, 2015];
- March 15-18, 2016: during anti-terrorist operations in Brussels (Belgium), four policemen (three Belgian and one French) were shot and one terrorist was killed. Several Kalashnikov rifles were recovered at the crime scenes [News, 2016];
- March 22, 2016: a bombing at the Brussels international airport in Zaventem (Belgium) kills fourteen people. One Kalashnikov rifle is retrieved at the crime scene [Brants, 2016].

According to this information the soldiers should be protected against this specific threat. Consequently, the research presented in this thesis intends to develop a new concept of helmet able to defeat high velocity rifle bullets, namely the 7.62×39 mm M43 projectile using regular ballistic materials.

Chapter 3

Introduction

This chapter begins by describing what is the consequence of a ballistic impact to the head through the explanation of the Behind Helmet Blunt Trauma (BHBT), which is the injury caused to the head by the Back Face Deformation (BFD). There are two different types of head injuries, skull fracture and brain injury. Due to the fact head injuries cover such a broad scope of injuries, there are many causes − including accidents, falls, physical assault, or traffic accidents − that can cause head injuries.

An injury criterion is defined as a "physical parameter (or a function of several physical parameters) that correlates well with the injury severity of the body region under consideration" [NATO, 2007]. In this work the injury criteria focuses on the head. The three main groups in which the head injury criterion levels can be separated are presented in this chapter. In the final section of this chapter the main existing armour standards concerning helmets are shown and explained.

3.1 Behind Helmet Blunt Trauma (BHBT)

Behind Helmet Blunt Trauma (BHBT) is the injury caused to the head by the BFD. BHBT has emerged as a collection of serious injury types with a common origin experienced by soldiers on the battlefield. Figure 3.1 shows examples of minor, moderate, and significant or critical classes of injuries caused to the head by the BFD [Freitas et al., 2014].

The effects of the impact of a non-perforating projectile to the back face of a helmet is the BFD. The Back Face Signature (BFS) of the BFD is the maximum depth of the indentation in a head dummy (or ballistic clay, for laboratory tests). This value is measured for each shot that does not penetrate the helmet. Being an important parameter, significant research is under way on how to measure the BFD and correlate it to injury criteria.

An interesting paper written by Sarron et al. [Sarron et al., 2004] describes the dynamic effects of the impact of a 9 mm calibre bullet on cadaveric skulls protected by aramid, polyethylene or aluminium plates. From this study, the authors concluded that ballistic helmets made of composite materials could be optimised to avoid extensive transient deformation and thus reduce the impact and blunt trauma to the head. The authors, however, also claim that deformation cannot be completely removed, which is why the gap between the helmet and the head must be maintained at more than 12 mm.

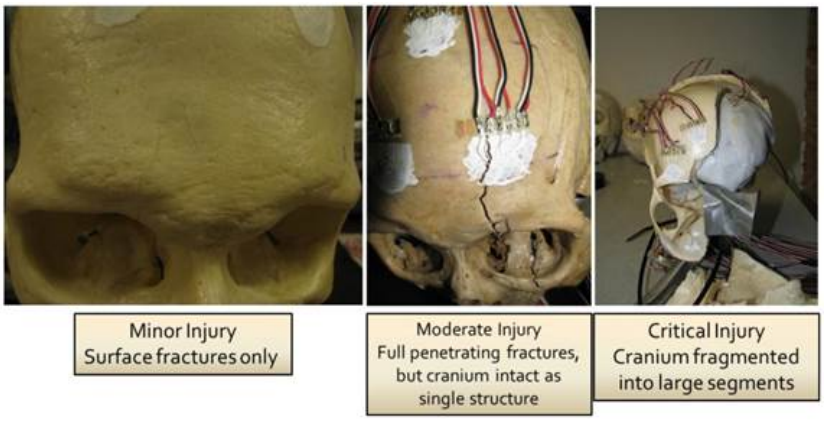

Figure 3.1: Illustration of different types of damage [Freitas et al., 2014].

This specific distance between the helmet and the head prevents skull fracture.

Recently, Grobert et al. [Grobert et al., 2016] proposed a new prototype of head-shaped measurement setup for ballistic impact tests on combat helmets. Experimental tests were conducted and force-time sequences caused by the helmet-head contacts during impact were obtained. The authors concluded that the actual movement of the head starts significantly (approximately 1.5 ms) later after the impact. Additional ballistic test series need to be performed with different helmet types to compare the outputs and the differences of the material behaviour.

Rafaels et al. [Rafaels et al., 2015] did experiments to study the injuries to the head from backface deformation of an ultra-high molecular weight polyethylene (UHMWPE) ballistic helmet due to the non-penetrating impact of 9 mm full metal jacket projectiles with impact velocities in the range of 400-460 m/s. The results of this study demonstrate a high risk of skull fracture due to BHBT and the necessity to prevent BHBT as a design constraint in future helmets and other protective gear.

Some studies have been conducted in order to understand and analyse the effect of the BFD of a helmet after an impact. Van Hoof et al. [van Hoof et al., 1999, van Hoof et al., 2001] studied the mechanical response of a composite helmet to a frontal ballistic impact. These authors developed a finite element numerical model, to predict the interactions between the helmet and the human head. They used a .22 FSP (Fragment Simulating Projectile) with a mass of 1.1 g and an impact velocity of 586 m/s. From this study, the authors concluded that the helmet back face deformations were significantly higher than expected and predicted by previous analyses from other authors [van Hoof et al., 1999]. Other relevant conclusions are that local effects are much more significant than any global (e.g. rigid body) movements of the helmet-head system, thus permitting to neglect the latter.

In 2011, Hisley et al. [Hisley et al., 2011], developed a way to experimentally replicate and measure the BFD on a helmet that can be correlated to injury criteria. In this study, a helmet performance test methodology was developed using digital image correlation (DIC). A new metric (available energy for potential impact to a soldier's head) has been developed utilising DIC data that allows the computation of a conservative estimate of the blunt criterion. The blunt criterion (BC) equation used in this article as a prospective measure to predict head injury from blunt, less-than-lethal projectiles.

The BC equation is of the form:

$$BC = \ln\left(\frac{E}{TD}\right) \tag{3.1}$$

where E [J] is the impact kinetic energy, T [mm] is the thickness of the skull, and D [cm] is the diameter of the projectile (if impact area is circular). The BC has been demonstrated to correlate very well with experimental data published from cadaver and animal studies [Dehmer and Yen, 2010]. This experimental methodology advances the state-of-the-art in helmet BFD evaluations from using only static, post impact metrics (deformation into clay) to dynamic, fully profiled (volume, velocity, etc.) helmet BFDs.

Li et al. [Li et al., 2016] recently evaluated head injury risks arising from the BFD of the ACH under ballistic impact. These authors concluded that a slightly larger standoff than the regular ballistic helmet of 2 mm distance leads to a significant reduction in head injury risk. Also, the authors observed that a 45° oblique impact at the front leads to a lower head injury risk than a 90° frontal impact. The simulation results show that a 2.5% increase in the thickness of the helmet leads to a 6.2% decrease in the maximum von Mises stress in the compact cranial bone. That is, a thicker helmet provides better protection of the head, as expected. Moreover, for a helmet protected head under ballistic impact, it is seen that a high risk of skull fracture does not necessarily mean an equally high risk of injury to the brain tissue.

3.2 Anatomy of the human head

In these two next sections the different parts of the head are presented in order to understand their functions and how a ballistic impact can lead to a head injury and consequently the different types of head injury. The human head can be considered to be a multilayered structure. There are many different layers of protecting the brain (Figure 3.2), with the first layer of protection being the skull which acts as armour, shielding the brain from blows. The next layer of protection of the meninges which has three membranes that surround the brain and spinal cord to keep it from being damaged by contact with the inside of the skull. The final layer of protection is the cerebrospinal fluid (CSF) that the brain and spinal cord float [Schmitt et al., 2014]. The mass of a human adult (50% percentile) head is about 4.5 kg [Claessens, 1994].

The skull consists of two parts: the cranial bones and the facial bones. The cranial bones are composed of eight bones and these are connected by sutures. The facial anatomy includes fourteen bones [Tse et al., 2014]. Figure 3.3 shows the cranial bones and facial subdivisions of human skull. The outermost layer os called dura mater and it is considered as the thickness layer [Claessens, 1994].

3.3 Type of head injuries

Head combat injury may be broadly defined as temporary or permanent damage to one or more of the head components from a blow or impact to the head such as might be encountered on a battlefield. In general terms, head injuries can be grouped into four categories as follows: scalp damage, skull fracture, traumatic brain injury, and neck injury, or a combination of above.

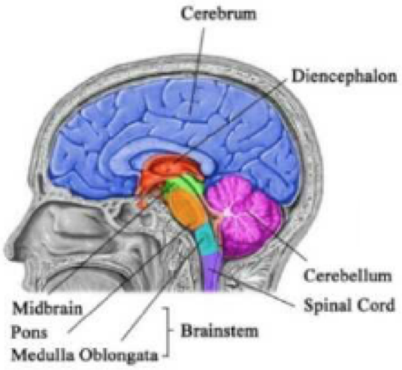

Figure 3.2: Internal structures of the human brain (adapted from [Tse et al., 2014]).

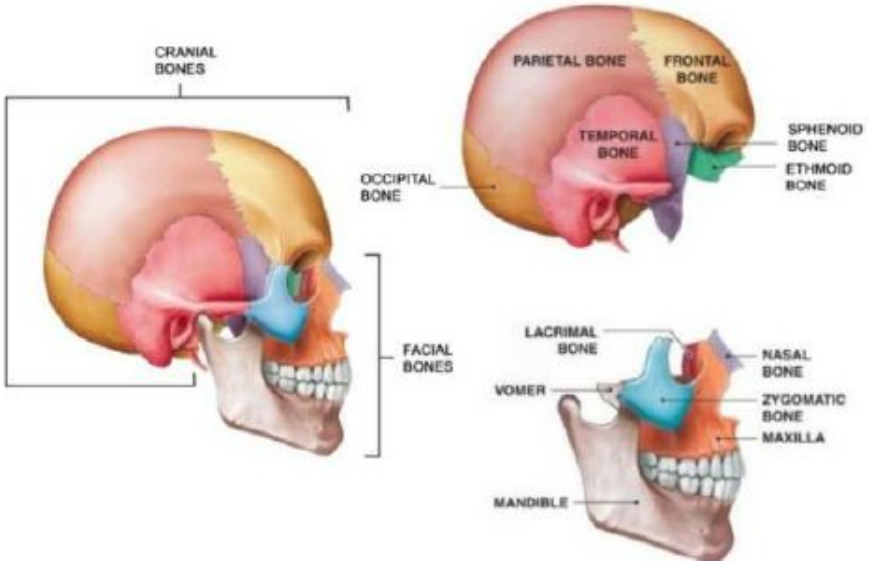

Figure 3.3: Cranial bones and facial subdivisions of human skull [Tse et al., 2014].

Scalp damage does not have the same importance as brain injury or skull fracture [Voo et al., 1994]. The seriousness of neck injury is also low compared with brain injury or skull fracture [Moss et al., 2009]. Compared with skull fracture, brain injury is far more serious, and needs to be given particular importance when considering the projective effect of the helmet under direct impacts [Moss et al., 2009]. In this section, only skull fracture and brain injuries are described.

3.3.1 Skull fractures

Skull fracture is not a major criterion for helmeted-head impact due to the fact that brain damage by acceleration will occur well before the impact load causes a depressed skull fracture [Sparks, 2012]. However, during a projectile impact a skull fracture may occur due to penetration of the skull. There is a need to investigate skull fracture in relation to helmet type and/or helmet standard testing boards [Sparks, 2012].

Pintar et al. [Pintar et al., 2013] studied two different types of helmet-to-head contact forces from experiments. They used a human head finite element model to determine localised responses, and compared outputs to skull fracture and brain injury thresholds. Based on results from a limited sample size, the authors concluded that skull fracture criteria may be better used to distinguish the two specific helmet types than the brain injury criteria, while the pressure criterion may be too sensitive.

In 2008, a PhD thesis by Raymond [Raymond, 2008] defined the behaviour of the fracture of the tempo-parietal region of the head under ballistic blunt impacts. In this study, 14 heads of fresh Post Mortem Human Subject (PMHS) with intact scalp were used. The results show that a risk of 50% of skull fracture corresponds to a maximum force of approximately 6 kN. Also, they show that the weight, age, gender and thickness of the skull are not significant factors in the prediction of fracture. The thickness of the soft tissue, however, is an important factor.

It is possible to find some data for low-rate skull fracture, concussion and diffuse axonal injury [Yoganandan et al., 1995, Bass and Yoganandan, 2015]. However, all these data have been derived from animal and human studies using observations from crash tests and laboratory experiments with lower stress and strain-rates than those from projectile and blast threats. Thus, a translation of these low stress-rate data from animals, physical models, and mathematical simulations to the ballistic trauma case is not expected to be reliable. As a consequence, the design of protection from typical military threats is compromised because the actual design thresholds are unknown.

In general, the impact responses are described in terms of head acceleration and impact force and therefore depend on the inertial properties of the head and the impacted surface. During direct head impacts, skull deformation can lead to a number of fracture patterns depending on the impact conditions. The three main types of fracture include penetrating fractures, depressed comminuted fractures and remote linear fractures [Raymond, 2008]. The risk on skull fracture from a ballistic impact is mainly due to a direct loading path from the projectile, and is determined by the BFS of the helmet shell during an impact event. Analysing the available literature for the maximum allowable dynamic loading of the head (generally based on experiments on cadavers) a threshold in the range of 4.0-6.2 kN seems to have been identified by several researchers for frontal head impact (see Table 3.1). In these studies, mainly drop tests against a rigid flat surface were performed. Table 3.1 summarises the peak force values reported for skull fracture for frontal impacts.

Table 3.1: Peak force for skull fracture for frontal impacts [Schmitt et al., 2014].

Force [kN]	Reference
4.2	Nahum et al. 1968 [Nahum et al., 1968]
5.5	Hodgson et al. 1971 [Hodgson et al., 1973]
4.0	Schneider and Nahum 1972 [Schneider and Nahum, 1972]
6.2	Advani et al. 1975 [Advani et al., 1975]
4.7	Allsop et al. 1988 [Allsop et al., 1988]

The reported fracture forces do, however, vary depending on the impactor surface area [Voigt and Thomas, 1973]. These force values can be related to the linear acceler-

ation of the head through Newton's second law.

3.3.2 Traumatic Brain Injury

Brain injuries are clinically classified into two broad categories: diffuse injuries and focal injuries. Diffuse brain injuries form a spectrum ranging from mild concussion to diffuse white matter injuries. Forces acting on the brain can produce complex movements and deformation. An acceleration injury occurs when a blunt object strikes the freely mobile head. Injuries to the brain have in recent times been referred to as Traumatic Brain Injury (TBI), thus distinguishing them from the more generic designation of Head Injury [Sparks, 2012]. TBI can be defined as any type of failure or damage affecting brain function and resulting from non-intrusive mechanical head loading of the contact or non-contact type.

The transmission of stresses to the brain from any substantial impact on the head can lead to TBI. The effects on brain function depend on the magnitude and direction of the force impacting the head. Therefore, it is important to understand the link between blunt trauma and how the helmet attenuates the effects of the impact. For lower severity ballistic or blunt impacts, the transfer of momentum and rate of change of momentum from an impact can be sufficiently attenuated by the helmet, preventing brain tissue injuries. Thus, an understanding of brain tissue and brain physiological tolerance must be linked to the magnitude of the transfer of force or other mechanical parameters from the impact on the helmet onto the head and into the brain. TBI can be caused by a number of events: falls, motor vehicle accidents, bicycle accidents, collisions, blast exposure, and blunt head trauma. More than 5 million US citizens alive today have had a TBI. A study, conducted in 2009 showed that of 3973 soldiers who served in Iraq, 23% had a clinically confirmed history of TBI [Terrio et al., 2009].

Over time, there has been considerable research and interest in studying TBI from both medical and biomechanical perspectives. Modelling brain injury through biomedical engineering, due to mechanical impact loads and blasts, has been the focus of significant research [Daniel and Remy, 2005, Aare and Kleiven, 2007]. In particular, helmet protection and its mechanical behaviour have been an area of research for the safety of the human head [van Hoof and Worswick, 2000].

Jazi et al. [Salimi Jazi et al., 2014] studied the effect of a military helmet with pads on the acceleration levels, inflicted pressure and shear stresses in a finite element model of a human brain subjected to a ballistic impact. Based on the results of the simulations in this work, those authors concluded that the stiffness of the foam has a prominent role in reducing the level of the load transferred to the brain. Also, they concluded that the frontal impact was the most severe due to the minimum contact area of the pad and the helmet.

Tan et al. [Tan et al., 2012] performed experimental tests and numerical simulations on helmeted Hybrid III headforms using spherical projectiles and found that foam cushioning systems help to reduce the head acceleration. In general, there is reasonable correlation between numerical and experimental observations and also on quantitative parameters, such as accelerations, helmet damage and deflections for frontal and lateral impacts and for the two different absorbing systems. In terms of energy absorbed by the helmet/ head, the maximum difference between the experimental tests and numerical simulations is approximately 13%. The energy absorbed is the energy difference between

the projectile impact and the projectile rebound.

The terms used in order to qualify head lesions are generally very technical. Consequently, they are codified following specific scales in order to simplify the interpretation of the lesional criteria. One of the most used, is the Abbreviated Injury Scale (AIS). *AIS is an anatomically based, consensus derived, global severity scoring system that classifies an individual injury by body region according to its relative importance on a 6 point ordinal scale (1= minor to 6 = maximal). AIS is the basis for the Injury Severity Score (ISS) calculation of the multiple injured patient* [AAAM, 2018]. The head injuries classified according to the Abbreviated Injury Scale (AIS) are presented in Table 3.2. The AIS is a standardised system for categorising the type and severity of injuries arising from vehicle crashes (but not limited to vehicle crashes) and each category represents a specific threat-to-life probability associated to an injury.

Table 3.2: The AIS classification and injury description [Raymond, 2008].

AIS score	Injury Description
1	Not classified
2	Close, simple/ undisplayed, diastatic, linear
3	Comminuted, compound but dura intact, depressed < 2 cm, displaced; superficial penetration injury < 2 cm beneath entrance
4	Complex; open with torn, exposed or loss of brain tissue; massive; large areas of skull depressed > 2 cm
5	Major penetrating injury > 2 cm penetration
6	Crush injury

The Head Injury Criterion (HIC), is a criterion based on acceleration response and is a measure of the average acceleration of the head in the case of an impact.

Table 3.3: The HIC, AIS codification by severity. [Raymond, 2008]

HIC (15 ms)	AIS code	Level of brain concussion and head injury
135-519	1	Headache or dizziness
520-899	2	Unconscious less than 1 hour - linear fracture
900-1254	3	Unconscious 1-6 hours - depressed fracture
1255-1574	4	Unconscious 6-24 hours - open fracture
1575-1859	5	Unconscious longer than 24 hours - large hematoma
> 1860	6	Non survivable

Risk on traumatic brain injury due to ballistic impacts is mainly due the rapid acceleration of the head, and differential movement of the head and the brain (due to inertia effects) can lead to brain tissue damage.

3.4 Injury criteria

A number of head impact criteria are available to estimate the injury levels, which can be separated in three main categories: (i) those based on linear accelerations measured at the centre of gravity of the head; (ii) those based on translational and angular (rotational) accelerations at the centre of gravity of the head, and (iii) those derived from measured or estimated brain stress and strain levels. All the injury criteria presented in this section take in account the global movement of the head.

3.4.1 Translational acceleration based injury criteria

Several head injury criteria have been proposed using translational acceleration.

- Wayne State Tolerance Curve (WSTC)

  The WSTC is considered to be the foundation of research on human head injury criteria. This curve evolved from the works of several authors [Lissner et al., 1960, Gurdjian et al., 1953, Gurdjian et al., 1961] and [Patrick et al., 1963], and gives tolerable average acceleration magnitude in the Anterior-Posterior (A-P) direction as a function of the duration of the acceleration. It is still the basis for most currently accepted injury criteria. The curve is shown in Figure 3.4. Slight cerebral concussion without any permanent effects was considered to be human acceptable. Only linear accelerations were used in the development of the curve, which was obtained from different experiments with post-mortem human subjects (area I in Figure 3.4); from experiments with animals (area II in Figure 3.4 [Gurdjian et al., 1961]); and from experiments with human volunteers (area III in Figure 3.4 [Patrick et al., 1963]). The WSTC is based only on direct frontal impacts, and cannot be applied to non-contact loading conditions nor to other impact directions.

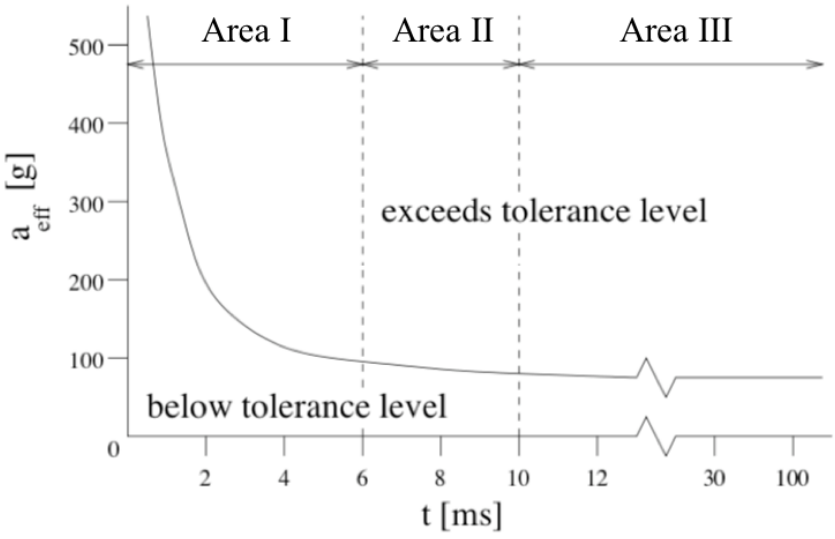

Figure 3.4: Wayne State Tolerance Curve (WSTC) [Patrick et al., 1963].

- Severity Index (SI)

  Gadd [Gadd, 1966] argued that neither the average acceleration nor the peak acceleration observed in an impact are sufficient to accurately determine the response of the head to an impact. According to Gadd, the resulting injury potential is highly dependent upon the acceleration pulse and therefore pulses with the same average acceleration but different shapes can have very different effects. To account for both the acceleration pulse shape and its duration, he suggested integrating the acceleration signal over its entire duration. Gadd further maintained that injury potential was a non-linear function of the acceleration magnitude. Therefore, he suggested that an exponential weighting factor (greater than 1) should be applied to the acceleration and that the result be integrated over the duration of the acceleration. This led to the following injury criterion, called the Severity Index:

$$\mathrm{SI} = \int_0^T a(t)^{2.5} \mathrm{d}t \tag{3.2}$$

  The exponent factor 2.5 only applies to the head and is primarily based on a straight-line approximation of the WSTC plotted on log-log scales between 2.5 and 50 ms. Gadd proposed a tolerance level for concussion for frontal impact of 1000, which agreed with the WSTC-curve. In 1971, Gadd [W. Gadd, 1971] suggested a threshold of 1500 for non-contact loads on the head. The SI has received significant scientific criticism, because it deviates considerably from the WSTC-curve [Stattenschek and Tauffkirchen, 1970].

- Head Injury Criterion (HIC)

  The most commonly acknowledged and widely applied head injury criterion is the Head Injury Criterion (HIC). This head criterion results from the evolution of the Wayne State Tolerance Curve (WSTC) developed by Gurdjian et al.[Gurdjian et al., 1953]. In 1972, the HIC was proposed as a new criterion (see equation 3.3) by the National Highway Traffic Safety Administration (NHTSA) to identify the most damaging part of the acceleration pulse by finding the maximum value of the function:

$$\mathrm{HIC} = \max \left\{ (t_2 - t_1) \left[\frac{1}{t_2 - t_1} \int_{t_1}^{t_2} a(t) \mathrm{d}t \right]^{\alpha} \right\} \tag{3.3}$$

  where $a(t)$ is the resultant linear acceleration time history, measured in multiples of g and t_1 and t_2 are the two time instants chosen in such a way as to maximise the HIC, subject to the constraint that they do not differ by more than a prescribed interval.

  In 1985 Prasad and Mertz [Prasad and Mertz, 1985] emphasized that acceleration of the head and the pulse duration are important parameters for assessing injury severity. Such criteria are in wide use in the automotive industry (FMVSS-208, EuroNCAP), but the injury risk functions using these parameters are not universally accepted.

Yang and Dai [Yang and Dai, 2010] studied the rear effect using the HIC when a helmeted head form is impacted by a bullet at different impact angles and various impact locations. The rear effect happens when the interior of the helmet is deformed and contacts with the human head and can provide crucial insights to injury. These authors concluded that at larger impact angles, the HIC score gets smaller and therefore there is less damage to the brain. Based on the HIC scores obtained from impact simulations at various impact locations, an impact at the back is the most dangerous. When the bullet hits the back of helmet, the largest HIC score has been observed, compared to the situations when the bullet hits other parts of the helmet. The work has, however, a number of assumptions and limitations. For example, the head model does not consider soft tissue over the skull, such as muscle and skin. Additionally, the 9 mm Parabellum projectile was modelled as one solid material instead of the real structure including a copper jacket and a lead core. In addition, the mechanical properties used in the helmet model do not seem to be correct since the authors use properties for aramid fibres and not aramid composites. Depending on the direction of impact the results will be different since firstly the fibres are oriented in only one direction and secondly they do not take into account the matrix to give ductility to the material. However, simulation studies have shown that both the impact angle and impact position have great effect on the HIC score. With a larger impact angle, the bullet will more likely skid over the surface of the helmet and have less kinetic energy transferred to the helmet. However, the HIC scores do not necessary have the same trend as the values for von Mises stress, maximum/minimum brain pressure or maximum principal strain in the brain because the HIC only depends on the resultant linear accelerations.

Although this criterion is widely used, it is recognised as inadequate to fully explain brain injury outcome. For military helmets, HIC and similar concepts incorporating global skull rotational parameters [Newman et al., 2000] assume rigid body motion of the head/brain system and do not consider local deformations that may be crucial for assessing the injury potential from ballistic impacts [Bass et al., 2003].

- Peak linear acceleration (PLA)

  The PLA is the maximum linear acceleration value. This method ignores impact duration. Nevertheless, some studies present time duration limits for some peak acceleration values [King et al., 2003].

3.4.2 Rotational linear acceleration-based injury criteria

The brain is composed of a natural viscoelastic material. Its mechanical response is dependent on the magnitude of the acceleration, and the rate and change of rotational velocity [King et al., 2003].

- Generalised Acceleration Model for Brain Injury Threshold (GAMBIT)

  Newman [Newman, 1986] attempted to present a generalised model for brain injury threshold, which takes into consideration the combined effects of both translational and rotational kinematics. The Generalised Acceleration Model for Brain Injury Threshold (GAMBIT) borrows from classical engineering treatment of the design

of systems in which combined axial and shear stresses are both simultaneously generated because of the particular location and direction of the applied load. The premise for such an approach is that whatever the combination of normal and shear stresses, the material failure can be forecast on the basis of an assumed "equivalent" maximum principal or shear stress or strain. The GAMBIT equation is of the form:

$$G(t) = \left[\left(\frac{a(t)}{a_c}\right)^n + \left(\frac{\alpha(t)^m}{\alpha_c}\right)\right]^{1/s} \tag{3.4}$$

where $a(t)$ and $\alpha(t)$ are the instantaneous values of linear and rotational acceleration, respectively, n, m and s are constants selected to fit the available data, and a_c and α_c represent critical tolerance levels for those accelerations. A GAMBIT value of 1 represents a probability of 50% for an irreversible head injury [Newman, 1986].

- Head Injury Power (HIP)

  Newman et al. [Newman et al., 2000] reasoned that the translational and rotational kinetic energy change rate could be a possible biomechanical function for head injury assessment. The authors proposed different coefficients for the different directions that be chosen to normalise HIP. It is computed using both linear and angular accelerations measured at the centre of gravity of a Hybrid III dummy head as shown in the following equations:

$$\begin{aligned} \text{HIP} = Aa_x \int a_x \mathrm{d}t + Aa_y \int a_y \mathrm{d}t + Aa_z \int a_z \mathrm{d}t \\ +B\alpha_x \int \alpha_x \mathrm{d}t + C\alpha_y \int \alpha_y \mathrm{d}t + D\alpha_z \int \alpha_z \mathrm{d}t \end{aligned} \tag{3.5}$$

  The HIP has units of power. Each term in this expression represents the change in kinetic energy for one degree of freedom, where the first there represents the linear contributions and the last there the angular contribution. The coefficient A represent the mass of the human head, 4.5 kg and B, C and D represent the appropriate moments of rotational inertia for the human head which denote the injury sensitivity for each one of the degrees of freedom. The appropriate moments of inertia for the human head are: C =0.016 Nms^2, D =0.024 Nms^2 and E =0.022 Nms^2. a_x, a_y and a_z [m/s^2] are the linear acceleration components along the three aces of the inertia reference space attached to the dummy head and the α_x, α_y and α_z [rad/^{2}] are the angular acceleration components around the three axes of the inertial reference space attached to the dummy head [Marjoux et al., 2008]. HIP can measure directional sensitivity, sensitivity for rotational accelerations, and sensitivity for angular and linear velocities. These are some of the advantages of this criterion compared to HIC.

- Rotational Injury Criterion (RIC)

  In 2012 Kimpara and Iwamoto [Kimpara and Iwamoto, 2012] proposed the Rotational Injury Criterion (RIC), which was derived by substituting the resultant

linear acceleration of the Head Injury Criterion equation for the resultant angular acceleration. The authors proposed in their studies that RIC of 1.03×10^7 would lead to a 50% mild traumatic brain injury (MTBI) probability.

- Power Rotational Head Injury Criterion (PRHIC)

  Kimpara and Iwamoto [Kimpara and Iwamoto, 2012] also proposed the Power Rotational Head Injury Criterion (PRHIC), which is calculated as the integrated power of the rotational head motion. The goal was to propose a new predictor for head injuries associated with angular head accelerations from data sets for six degrees of freedom at the head's centre of gravity. The equation for this criterion is the same as the Head Injury Criterion equation, where the resultant linear acceleration is substituted by the HIP (only the rotational components). The maximum time duration for PRHIC (and also the RIC) is 36 ms, which was the original time duration set for the HIC. The authors proposed that PRHIC 8.70×10^5 would lead to 50% MTBI probability.

3.4.3 Stress and strain-based injury criteria

Brain injury [Lee and Haut, 1989] is reported to correlate well with stress, strain and strain rate. However, strains and strain rates in the brain are difficult to measure [van den Bosch, 2006]. This can nevertheless be achieved using anatomically detailed and accurate finite element head models, from where stresses and strains are used to compute injury parameters in the skull and intracranial contents. These models bring a detailed injury assessment closer to reality, since they enable stresses and strains to be analised. Bandak [Bandak, 1995, Bandak, 1997] developed the following three measures representing the general types of brain injuries experienced in traffic accidents.

- Cumulative Strain Damage Measure (CSDM)

  This method was presented by Bandak and Eppinger [Bandak and Eppinger, 1994] to evaluate the strain related damage within the brain. The idea behind their hypothesis is the possibility to evaluate the relative effects of rotational and translational accelerations, in both the sagittal and coronal planes, on the development of strain damage in the brain. The CSDM is often considered the most promising stress- and strain-based injury criterion, since it is based on the brain's tissue strain. This is an important parameter, mainly when the brain is submitted to considerable rotational and translational impact [Aare et al., 2003].

- Dilatation Damage Measure (DDM)

  The DDM is a pressure-based injury criterion proposed by Bandak [Bandak, 1997], which evaluates brain injury caused by large dilatational stresses. The DMM estimates the instantaneous volume fraction of the brain matter that experiences negative dynamic pressures that can cause vaporization of the cerebral fluids, and contusion [Ciarlet et al., 2004].

- Relative Motion Damage Measure (RMDM)

  RMDM was also proposed by Bandak to evaluate injuries related to brain movements located at the inner surface of the cranium. The RMDM estimates the

percentage of the bridging veins that have stretched beyond a limit curve in a calibrated strain vs strain-rate diagram [Ciarlet et al., 2004]. Unfortunately, the majority of the finite element head models do not incorporate the bridging veins. Nevertheless, RMDM does not require the modelling of the bridging veins, but rather the monitoring of the relative displacement between node pairs. Each pair represents a bridging vein tethered between the skull and the brain.

3.5 Body armour standards

After the appearance of ballistic vests made with aramid fibres in 1970, standards started to appear for these items in order to assess and check their level of ballistic protection against projectile impacts.

The most common standards for civilian and police ballistic threats used by fabric and fibre suppliers are those developed in the United States and in the European Union. The main US ballistic standard is from the National Institute of Justice (NIJ) and identifies four levels of threat and two subcategories. In the European Union the main standards are the German VPAM (Vereinigung der Prüfstellen für Angriffshemmende Materialien und Konstruktionen), and the British Home Office Scientific Development Branch (HOSDB) standard for police forces. The main military standard focussed on personal protection and is provided by NATO. The NATO standard, namely STANAG, however, describes only levels of protection against fragment impacts. For this reason, when the military forces wanted to introduce ballistic protection against projectiles in their personal protection equipment they have been forced to be guided by the civilian standards available for this market until recently.

At the moment, there is only one standard specific for ballistic helmets from VPAM named "Durchschusshemmender Helm mit Visier und Nackenschut" (Bullet-resistant helmet with visor and neck protection), released in 2009. Also, the NIJ is working on a new helmet standard, a replacement for the retracted NIJ 0106.01 standard, which is still under revision.

Since there are not many specific standards for ballistic helmets, the standards for body armour are also referred in this work. It is also common for the ballistic helmet companies to refer to the body armour standards from NIJ, VPAM, HOSDB or STANAG in their catalogues.

3.5.1 Standardization Agreement (STANAG) 2920

The aim of this agreement is to standardise methods of classification (testing procedures, criteria and methods of designation) and to classify ballistic protection on the basis of standardised ballistic tests. The test results are intended to aid in comparison of the degree of ballistic protection provided by various body armours. The agreement is intended to cover testing with small arms bullets or fragment simulating projectiles.

The standard discussed here, is the 1^{st} edition of the AEP 2920, Ed. A, V2 entitled Procedures for the Evaluation and Classification of Personal Armour − Bullet and Fragmentation Threats [NATO Standardization Office, 2015], presented in Table 3.4. This procedure agrees within NATO's classification of personal armour for protection, includes standard techniques and reproducible test procedures for evaluating the level of protection of combinations of items, components or representative material samples used

in personal armour systems and the method to designate the performance by use of a set of identifiers.

Bullets and fragments are identified in classes to facilitate the designation following the ballistic tests. The standard applies to material samples, components such as flexible armour and helmet shells, personal armour items (helmet, face and eye protection, and plates), and combinations of flexible armour with hard armour.

Tests according to STANAG 2920 (Edition A Version 2) are conducted by firing the projectiles onto the test specimen at different velocities. By altering the velocities, in order to obtain perforating and non-perforating shots, an estimate of the V_{50} can be obtained, which is the velocity of the bullets where 50% of the bullets do not perforate, and 50% of the bullets do perforate.

3.5.2 Body Armour standard for NIJ - 0101.06

To ensure that body armour continues to be effective in protecting policemen and homeland security officers, the NIJ established a body armour standard and testing program in 1972, which has been updated several times to reflect the design and manufacturing developments of body armour and test methods. The latest version − NIJ 0101.06 for Ballistic Resistance of Body Armour − is one of the most comprehensive, stringent and rigorous body armour compliance standards available today. NIJ 0101.06 tested and certified body armour ultimately means increased protection for the user.

In the official NIJ 0101.06 Ballistic Resistance of Body Armour Standard, John Morgan, Deputy Director for Science and Technology, National Institute of Justice stated: *"The NIJ Standard - 0101.06, 'Ballistic Resistance of Body Armor' is . . . a technical document that specifies the minimum performance requirements that equipment must meet to satisfy the requirements of criminal justice agencies and the methods that shall be used to test this performance. This standard is used by the NIJ Voluntary Compliance Testing Program (CTP) to determine which body armor models meet the minimum performance requirements for inclusion on the NIJ Compliant Products List."* [Mukasey et al., 2008].

This ballistic resistance standard increases safety in three ways: by increasing performance against today's emerging threats; by improving reliability; and by increasing durability for body armour, ensuring it will cope with the stress it may endure by being worn 10 hours a day, five days a week, 52 weeks a year, over several years.

The NIJ 0101.06 standard lays out the minimum requirements for performance and testing methods for all personal protective vests and rates the various kinds of available body armour. When body armour is being tested, self-regulating NIJ-certified laboratories will put the body armour through various tests to ensure they are up to NIJ performance standards.

The NIJ has the authority to retest body armour already in use to ensure performance standards do not change over time. Their performance standards mean that commercially available body armour will meet the minimum performance requirements it sets forth. Table 3.5 is provided by the Office of Science and Technology of the National Institute of Justice. These levels range from low-velocity or low-mass projectiles at Level I, to very high-velocity, high-mass projectiles at Level IV. The NIJ standard used in this work is shown in Table 3.5. These standards only consider soft, lead-core bullets and armour-piercing projectiles with high-hardness rigid penetrators, such as typical rifle threats.

Table 3.4: Threat class and acceptable test projectiles for kinetic energy threats according to STANAG 2920 [NATO Standardization Agency, 2016].

Category	Calibre	Class	Projectile mass [g]	Minimum Core Hardness [HRC]	Core mass [g]	Acceptable projectile
A Lead core projectiles	9x19	A1	8.0 ± 0.1			According to STANAG 4090
	4.6x30	A2	2.6 ± 0.1			RUAG FMJ SX
	5.56x45	A3	3.6 ± 0.1			FN SS 92/M 193
	7.62x51	A5	9.3 ± 0.1			According to STANAG 2310
	Emerging threats	A Special				National Authorities specified
B Mild steel core projectiles	4.6 x30	B2	2.0 ± 0.1	40	2.0 ± 0.1	RUAG AP SX
	5.56x45	B3	4.0 ± 0.1	40	0.4 ± 0.1	According to STANAG 4172
	7.62x39	B4	7.9 ± 0.2	40	3.6 ± 0.1	7.62x39 M43 PS
	7.62x51	B5	9.6 ± 0.1	40		
	Emerging threats	B Special				National Authorities specified
C Hardened steel core projectiles	7.62x39	C4	8.0 ± 0.1	60	4.0 ± 0.1	7.62x39 API BZ
	7.62x51	C5	8.0 ± 0.1	60	4.6 ± 0.1	FN P80
	7.62x54	C6	8.0 ± 0.1	60	5.3 ± 0.1	7.62x54R B32 API
	7.62x63	C7	10.7 ± 0.1	60	5.2 ± 0.1	M2 AP US Arsenal
	Emerging threats	C Special				National Authorities specified
D Tungsten cobalt (WC) core projectiles	9x19	D1	5.7 ± 0.1	70		MEN 9x19 AP
	5.56x45	D3	3.4 ± 0.1	70	2.2	M995 MEN AP DM 31
	7.62x51	D5	8.2 ± 0.1	70	5.9	M993 Nammo AP8
	Emerging threats	D Special				National Authorities specified

3.5.3 Vereinigung der Prüfstellen für Angriffshemmende Materialien und Konstruktionen (VPAM) - APR 2006

The Durchschusshemmender Helm mit Visier und Nackenschutz (HVN) 2009 standard [VPAM, 2017] specifies that the energy transferred to the head during impact must not exceed 25 J. The last revision of this standard was done in 2017. The test is carried out with a measuring head, which consists of a soap device which facilitates determination of residual energy for bulging/deformation This standard is valid in combination

with the Allgemeine Prüf Richtlinie (APR) 2006 standard, which is the general basis for ballistic material, construction and product tests [VPAM, 2014]. This last standard is a guideline developed by the Association of Test Laboratories for bullet resistance material and constructions (VPAM), created in 2006 with the latest version dated 2014. These guidelines ensure reproducible results on the one hand, and more transparency from the manufacturer for customers and users on the other hand. Normally, this guideline is used by German speaking and Scandinavian communities. Table 3.6 lists the classification of the different test levels.

Table 3.5: Ballistic Requirements Penetrations / Back Face Signature NIJ 0101.06 [Mukasey et al., 2008].

Test variables						Performance requirements	
Threat Level	Caliber	Bullet Mass [g]	Bullet Manufacturer	Conditioned Armour Test Velocity [m/s]	New Armour Test Velocity [m/s]	Hits Per Panel at 0 Angle	Maximum BFS Depth [mm]
IIA	9 mm FMJ RN	8.0	Remington 23558	355 ± 9.1	373 ± 9.1	4	44
	.40 S&W FMJ	11.7	Remington 23686	325 ± 9.1	352 ± 9.1	4	44
II	9 mm FMJ RN	8.0	Remington 23558	379 ± 9.1	398 ± 9.1	4	44
	.357 Magnum JSP	10.2	Remington 22847	408 ± 9.1	436 ± 9.1	4	44
IIIA	.357 SIG FMJ FN	8.1	Speer 4362	430 ± 9.1	448 ±9.1	4	44
	.44 Magnum SJHP	15.6	Speer 4453 or 473	408 ± 9.1	436 ± 9.1	4	44
III	7.62 mm NATO FMJ	9.6	US/NATO M80 ammunition	847± 9.1	847± 9.1	6	44
IV	.30 Caliber M2 AP	10.8	US Military	878 ± 9.1	878 ± 9.1	1 to 6	44

Abbreviations: RN - Round Nose; FMJ - Full Metal Jacketed; AP - Armour Piercing; SJHP - Semi Jacketed Hollow Point.
Notes:
Backing is conditioned Roma Plastilina No 1.
For certification Level IIA, II and IIIA, 28 complete vests must be provided.
For Level III certification, nine armour inserts are required.
For Level IV certification, 7 to 37 armour inserts are required.
All new vests and hard armour plates will be immersed for 30 minutes before testing starts. As per section 7.8.2 NIJ STD 0101.06.
Bullet manufacturer is specified.

Table 3.6: Classification of VPAM test levels [VPAM, 2014].

Test Level	Type of weapon	Calibre	Ammunition and projectile			Test conditions	
			Type	Bullet mass [g]	Bullet Manufacturer	Shot distance [m]	Bullet velocity [m/s]
1	K/L	.22 Long Rifle	L/RN	2.6	Winchester	10±0.5	360± 10
2	K	9 mm Luger	FMJ/RN/SC, tinned	8.0	DAG, DM 41	5±0.5	360±10
3	K	9 mm Luger	FMJ/RN/SC, tinned	8.0	DAG, DM 41	5±0.5	415±10
4	K	.357 Magnum	FMJ/CB/SC	10.2	Geco	5± 0.5	430±10
		.44 Rem. Mag.	FMJ /FN/SC	15.6	Speer	5±0.5	440±10
5	K	.357 Magnum	FMs/CB	7.1	DAG, Spezial	5±0.5	580±10
6	L	7.62 × 39	FMJ/PB/FeC	8.0	PS	10±0.5	720±10
7	L	223 Rem.[2)]	FMJ/PB/SCP	4.0	MEN, SS 109	10±0.5	950±10
		.308 Win	FMJ/PB/SC	9.55	MEN, DM 111	10±0.5	830±10
8	L	7.62 x 39	FMJ/PB/HCI	7.7	BZ	10±0.5	740±10
9	L	.308 Win.)	FMJ/PB/HC	9.6	MEN/CBC, FNB, P 80	10±0.5	820±10
10	L	7.62 × 54 R	FMJ/PB/HCI	10.4	B32	10±0.5	860±10
The rates of twist can be gathered from the dimension sheets (TDCC) of the C.I.P.							

For more information about the abbreviations please see the standard.

3.5.4 Home Office Scientific Development Branch (HOSDB) - Body Armour Standard (2017)

The Home Office Scientific Development Branch (HOSDB), integrated in the Centre for Applied Science and Technology (CAST) since April 2018, is the organisation responsible for testing and standardisation for body armour material in the United Kingdom.

In 1993 and 1995, the HOSDB published a stab resistant body armour test specification and the Police Scientific Development Branch (PSDB) the Ballistic Body Armour Standard (1995), respectively. These two documents describe a test methodology for assessing the protection afforded by commercial body armour systems against typical ballistic and edged weapons judged to be a threat in the United Kingdom. In 1999 the HOSDB completed a major revision to the 1993 stab specification and published the PSDB stab resistance standard for body armour. In 2003, the HOSDB revised the 1999 stab standard and produced a three part standard divided in three parts: General Requirements; Ballistic Resistance; and Knife and Spike Resistance. The major revision done in 2007 of the 2003 standard included increased protection levels to address more powerful handgun (HG3) and rifle (RF2) weaponry, in-production manufacturers quality testing (MQT), and an increased number of knife, spike and ballistic compliance tests.

More recently, in 2017, the Home Office Body Armour Standard published the outlines for the minimum performance requirements and test methods for body armour intended for UK law enforcement agencies. The Home Office Body Armour Standard (2017) supersedes all previous Home Office Body Armour standards. These requirements provide direction for a body of work to produce a test standard that better represents the needs of end-users. The key requirement for body armour is to reduce the risk of death or serious injury to the wearer from ballistic or stab attack to the torso in normal operational usage. Table 3.7 lists the different classifications of the test levels for handguns, shotguns and rifles.

3.6 Thesis objectives

The main idea behind the research here presented is to create a new helmet concept able to defeat high velocity rifle bullets using already available ballistic materials. To design and produce an effective combat helmet, developers must consider a wide range of factors. These include overall helmet size and mass, acoustic protection, ballistic qualities of the construction material, comfort, preservation of field of vision and hearing, compatibility with weapons and other equipment (communications gear, for example), ease of maintenance and modification in the field, durability, availability of raw materials and manufacturing techniques, ease of decontamination from nuclear, biological and chemical threats, cost and disposability after use [Carey et al., 2000].

In the last few decades, non-metallic materials, such as composites and ceramics, have been increasingly incorporated into more efficient lightweight armours. In particular, mostly due to their low density, high hardness, high stiffness and strength in compression, ceramics have become widely used. The proposed helmet design will hence be composed of a hard ceramic outer shell (silicon carbide, since this material combines excellent ballistic properties with near net-shape casting possibilities, which are important for a one-piece integral design), a polyethylene composite material used in a cross-ply (0°/90°) lay-up with a thermoplastic resin, a ductile metal to limit the back face deflection of the

Table 3.7: HOSDB Ballistic Standard for different test levels for handguns, shotguns and rifles [Croft and Longhurst, 2007].

Performance level	Calibre	Test round designation	Bullet mass [g]	Range [min] [m]	Single shot BFS [mm]	Velocity [m/s]
H01	9 mm FMJ	MEN 9mm FMJ DM11A1B2	8.0	5	44	365 ± 10
	9 mm JHP	Federal Premium 9 mm JHP P9HST1	8.0	5	44	365 ± 10
H02	9mm FMJ	MEN 9mm FMJ DM11A1B2	8.0	5	44	430 ± 10
	9 mm JHP	Federal Premium 9 mm JHP P9HST1	8.0	5	44	430 ± 10
H03	Rifle 7.62 calibre	Radway Green 7.62 mm NATO Ball L44A1 or L2A2	9.3	10	30	830 ± 15
	Rifle 7.62 calibre	7.62 x 39 mm surrogate	7.9	10	30	705 ± 15
H04	Rifle 7.62 calibre	SAKO .308 Win 480A Powerhead or Barnes .308 TSX BT	10.7	10	30	820 ± 15
SG1	Shotgun 12 Gauge True Cylinder	Winchester 1oz. Rifled 12RSE	28.4	10	30	435 ± 25

first two layers, and finally a fourth layer able to absorb the shock wave of the initial impact and the following helmet deflection.

Nowadays military soldiers are engaged in more law enforcement and anti-terrorist operations and the most commonly found small caliber threat is the 7.62×39 mm M43 ammunition employed with the AK-47 assault rifle (known as Kalashnikov). Figure 3.5 shows the ubiquitous Kalashnikov ammunition, projectile and weapon. Also, for safety reasons, soldiers must be protected from their own ammunition in the case of accidentally being hit by their own troops. The Belgian Army uses a standard cartridge for NATO forces namely the 5.56×45 mm NATO Ball ammunition used with, among others the M16 weapon (see Figure 3.6).

For this reason, the most important goal of this work is to create a new helmet concept able to stop the 7.62×39 mm round at nominal velocity in the first step. In addition, two other goals are included: the optimisation of the total weight of the helmet and the reduction of the risk on skull fracture.

The head can only support a limited weight and the threshold value depends on several factors such as how long the user has to wear the helmet [Arbogast et al., 2003]. A typical military helmet, which is used extensively during operations, normally weighs an

(a) 7.62×39 mm ammunition.

(b) 7.62×39 mm projectile (left) and steel core (right).

(c) Kalashnikov rifle.

Figure 3.5: Kalashnikov 7.62×39 mm (a) ammunition, (b) projectile and (c) rifle.

average of 1.5 kg [Military, 2017b]. For titanium helmets, normally used by special police forces in high-risk interventions, the typical weight is approximately 3.0 kg (without the visor). Titanium helmets used during the latter type of operations offer protection against pistol (handguns with one or more stationary chambers) and revolver (handguns that use multiple rotating chambers) threats, while the military helmets generally only offer protection against fragmentation. The total helmet shell mass for different types of ballistic helmets as a function of the VPAM protection levels is shown in Figure 3.7, where the ballistic helmets are divided in two categories: the titanium helmets (higher mass) and the composite material helmets (lower mass). The goal of this work is to have a helmet concept with a mass that is acceptable to the user (around 2.5 kg) and comparable to what exists in the market with a VPAM protection level of 6.

For this thesis the goal for risk on skull fracture is having a force lower then 5 kN and for brain injury is to have a HIC threshold value of maximum 900. There are no criteria to measure brain injury and skull fracture simultaneously, so each criterion should be measured individually. Skull fracture is related to the impact force, and brain injury is related to the acceleration.

In terms of body armour standards, the projectile 7.62×39 mm fits in different levels according to the standard. For STANAG 2920 standard the referred projectile fits in class 4 of category B for mild steel core projectiles. For the NIJ 0101.06 standard the typical 7.62×39 mm M43 ammunition employed with the AK-47 assault rifle has a projectile that falls between two typical classes: it has a mild steel core enveloped in a steel jacket with a lead filler in the voids in between. As there is no level for the 7.62×39

(a) 5.56 × 45 mm ammunition.

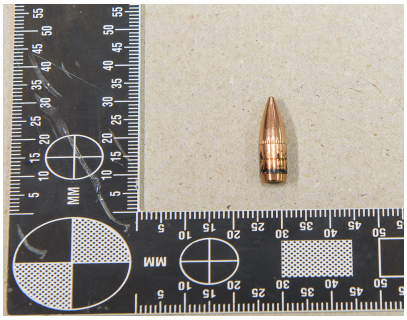

(b) 5.56 × 45mm NATO Ball projectile.

(c) M16 rifle.

Figure 3.6: M16 5.56 × 45 mm (a) ammunition, (b) projectile and (c) rifle.

mm M43 projectile in this standard, it should likely be placed between levels III-A and IV, but is often put between levels III and IV using the unofficial level indication III+. For the VPAM standard the projectile corresponds to level 6 of the APR 2006 VPAM Standard in combination with the HVN 2009. For the HOSDB standard the projectile 7.62 × 39 mm studied in this thesis falls between two different levels of protection, the H03 and the H04 levels.

To conclude this chapter the main goals of this thesis are:

- Stop the incoming projectile, in order to avoid direct penetrating injuries;
- Avoid contact between the inner helmet shell and the head, in order to reduce the risk on skull fracture and traumatic brain injury (TBI);
- Determine the biomedical constraints acceptable for the load and momentum transfer of the helmet shell to the human head, to avoid unacceptable injury;
- Absorb the shock of the load on the helmet using an adapted shock-absorbing structure and within the previously determined biomedical constraints;
- Development of a new helmet concept (protection) including material implementation;
- Development of numerical procedures using finite element tools to model different materials of the helmet concept;

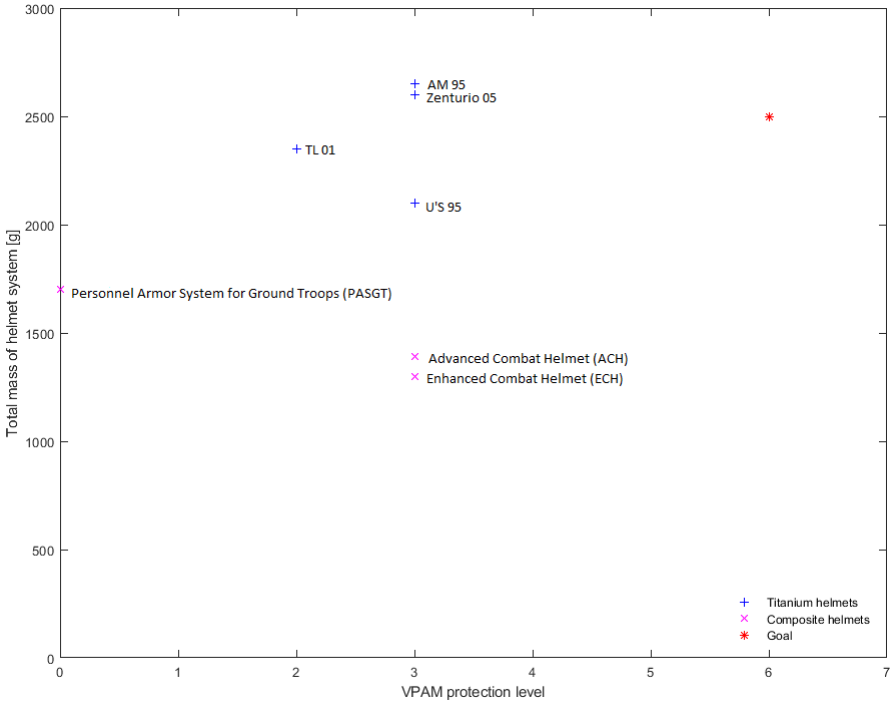

Figure 3.7: VPAM protection level vs helmet mass [Ulbrichts Witwe GmbH, 2009, Zebra Armour, 2018].

- Implement and validate the numerical models with experimental results;
- Evaluation of numerical analysis and validation of the behaviour of the ballistic helmet concept using finite element techniques;
- Assess of the proposed design in comparison to the design goals.

Chapter 4

Materials and geometry

A comprehensive review of the ammunition and armour materials used in this thesis is presented in this chapter.

4.1 Ammunition

This section will cover the relevant ballistic threats, small arms projectiles and fragments. The threat may vary depending on the scenario encountered. Ammunition should be referred to as a type of material fired, scattered, dropped or detonated from weapons, such as bombs or rockets, and especially shot, shrapnel, bullets, or shells fired by guns. Almost all mechanical weapons require some form of ammunition to work. The term ammunition can be traced back to the mid-17th century. The purpose of the ammunition is to project a force against a selected target to have an effect.

Ammunition comes in a range of sizes and types and is often designed to work only in specific weapon systems. There are however, internationally recognised standards for certain ammunition types that enable their use across different weapons and by different users. There are also specific types of ammunition that are designed to have a specific effect on a target or during flight, such as armour-piercing shells, used only in specific circumstances. Ammunition design has evolved throughout history together with weapons and different effects. Ammunition has been of relatively simple design and build (e.g. sling-shot, stones hurled by catapults), but along the years with the development of weapon design the requirement for more specialised ammunition increased [Office, 1936]. There are four main different components of rifle ammunition:

- Cartridge casing or case;
- Fuse or primer;
- Powder and/or propellant; and
- Projectile or bullet.

The cartridge case is the container that holds the other ammunition components. However, not all ammunition types have a cartridge case. In its place, a wide range of materials can be used to contain the ammunition components. In some large weapons, the ammunition components are stored separately until loaded into the weapon system

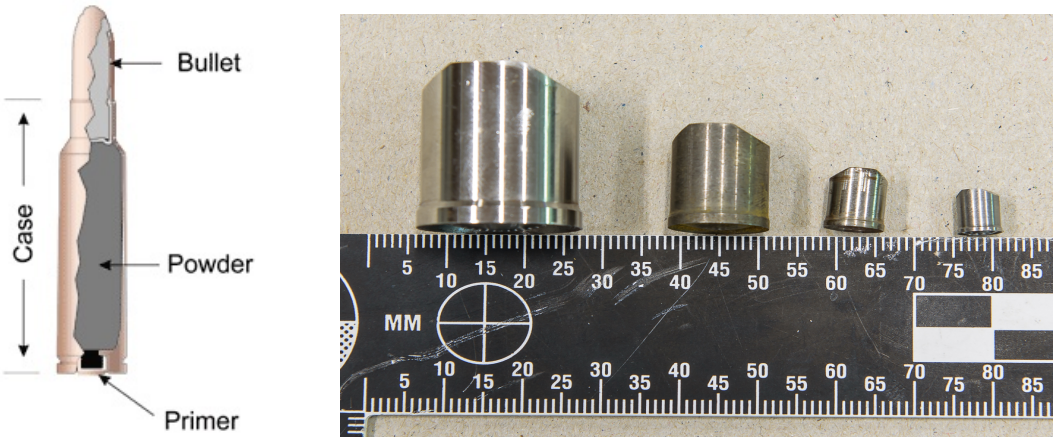

(a) (b)

Figure 4.1: (a) Schematic representation of ammunition components [**?**]; (b) FSP projectile (from left to right): 20 mm, .50 in, .30 in and .22 in.

for firing. In small arms, caseless ammunition can reduce its weight and cost, and simplify the firing process for increased firing rate. The cartridge case can be made of brass, steel, copper, plastic or even paper. The projectile is the part of the ammunition that leaves the weapon and hits the target.

Different components of an ammunition are shown in Figure 4.1 (a). The specific projectiles used in this work are described in the following paragraphs.

Bullets only made with lead deform on impact, resulting in high levels of neutralising capacity. Full metal jacketed projectiles are more stable than lead bullets and therefore more suitable for longer ranges, but they do not deform significantly on impact.

4.1.1 Fragment Simulating Projectiles

Fragment simulating projectiles (FSPs) are used in laboratory tests to study the effect of fragment impacts. FSPs are made of steel and standard FSP sizes include .22 in (1.1 g), .30 in (2.84 g), .50 in (13.39 g), and 20 mm (52.73 g) caliber. Figure 4.1 (b) shows the four different standard FSP projectiles. Fragmentation is a process by which, for example, the casing of bombs and grenades is broken up by the detonation of an internal explosive. The fragments may have various predefined shapes such as spherical, cubical, cylindrical, or maybe formed by natural fragmentation. In order to standardise the impact effects of fragments, standards have been created to produce these types of projectiles. The MIL-DTL-46593 standard [MIL-DTL-46593B, 2006] is currently used by the US military for the production of FSP projectiles. Tests carried out with these types of projectiles usually focus on the verification of the response of body armour materials in protective vests [Wambua et al., 2007] and military helmets [van Hoof and Worswick, 2000]. The above US standard specifies the dimensions, mass and material used in the construction of these projectiles (Table 4.1). In this work, the FSP .30 projectile is used to validate the composite layer with 5 and 7 mm thickness and the FSP .22 was used to validate the combination of silicon carbide and the composite layer.

Table 4.1: FSP characteristics according to MIL-DTL-46593 standard.

Caliber	Diameter [mm]	Length [mm]	Mass [g]
.22 in	5.0	6.4	1.1
.30 in	7.4	8.6	2.8
.50 in	12.6	14.7	13.4
20 mm	19.9	22.8	53.7

4.1.2 7.62 × 39 mm M43 steel core round

The 7.62 × 39 mm round, also known as 7.62 Soviet, is a rifle cartridge of Soviet origin that was designed during World War II. This is the cartridge of the well known AK-47 rifle (or simply AK). Design work on the AK-47 began in the last year of World War II (1945), developed in the Soviet Union by Mikhail Kalashnikov. In 1946, the AK-47 was presented for official military trials, and in 1948, the fixed-stock version was introduced into active service with selected units of the Soviet Army [Walsh, 2003].

The 7.62 × 39 mm M43 was first used in the RPD (Degtyaryov hand-held machine gun). The design of the 7.62 × 39 mm cartridge was influenced by a variety of foreign developments, including the German Mkb 42(H) and the US M1 carabine [Monetchikov, 2005]. This cartridge was designed by Nickolay Elizarov and Boris Semin [Bolotion, 1995, Long, 1988].

In the 21st century the 7.62 × 39 mm remains a common service rifle chambers, including for newly developed rifles.

The original Soviet M43 bullets weighs 7.9 g with a copper-plated steel jacket, a lead filler and a large steel core [Bolotion, 1995, Long, 1988]. While the bullet design has gone through a number of redesigns, the cartridge itself remains largely unchanged.

The popular AK-47 has been produced in various forms by at least 31 countries and has been the standard service weapon of 55 nations [Studies, 2011]. An estimated 100 million AK-47 type rifles have been produced as of 2013, and it has proliferated extensively around the world, both in legal and in illegal circuits [Pauker, 2007]. Due to this, it has often been encountered by both military and police forces. It seems that wherever there is conflict, one party or another will be utilising the AK-47. Figure 4.2 shows the 7.62 × 39 mm with cartridge, the projectile and the steel core.

4.2 Armour

This section focuses on armour materials. Composite or steel helmets are designed to defeat soft core projectiles at relatively low velocities. However, hard core projectiles at high impact velocities require different materials to stop the projectile.

After a thorough search in the literature to find a single material able to stop a hard core projectile at high impact velocities no single material that could meet these requirements within the given design constraints was found. For that reason, it was necessary to make a combination of different materials to stop the bullet. Following the structure of a bullet resistant vest, the armour is composed of two parts, although the whole armour works together in stopping the projectile. The first material is responsible

Figure 4.2: 7.62 × 39mm (from left to the right): ammunition cartridge, projectile and steel core.

of deforming/breaking the projectile and the second to absorb the energy of the impact. Otherwise, the deformation of the full armour caused by the deformation can cause severe injury to the user.

For the new helmet concept, however, two materials were not sufficient to avoid BHBT because the BFD and the shock wave is still high, it was necessary adding a third layer to reduce the back face deformation due to the combined movement of the outer layers and the projectile. Finally, a fourth and last layer able to absorb the shock wave of the initial impact and the following helmet deflection was also added. Figure 4.3 shows the sketch of the different layers for the new helmet concept.

4.2.1 Ultra-high-molecular-weight polyethylene (UHMWPE)

Ultra-high molecular weight polyethylene (UHMWPE) is a thermoplastic characterised by having an extremely long molecular chain. Through a gel spinning process, the molecular chains are aligned and fibres are produced with very high specific strength and stiffness. Chains are bonded through van der Waals bonds. This provides the superior physical properties attractive for a number of military and industrial applications. As a result, these fibres are increasingly being used to produce flexible fabrics for ballistic vests or as reinforcement in fibre-reinforced composites to produce vest inserts or helmets. UHMWPE composites are also used as contact spall liners in vehicles to protect occupants from internal fragmentation from the initial ballistic threat or from secondary fragmentation of the base armour of the vehicle. As such, UHMWPE composites are becoming an increasingly important part of modern armour systems as there is a signific-

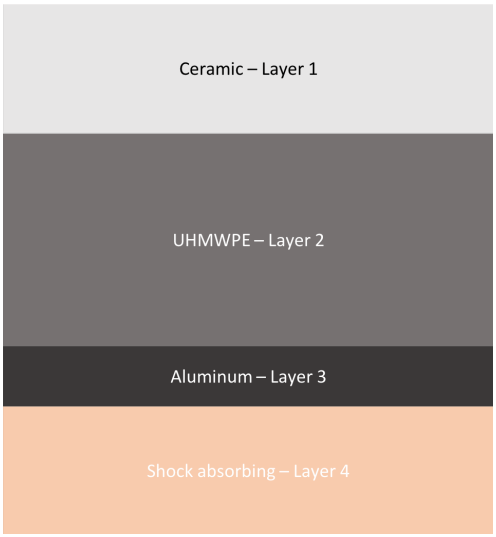

Figure 4.3: Sketch of the different layers for the new helmet concept.

ant need for lighter armour solutions for protection against both existing and emerging ballistic threats. Nowadays, the application of UHMWPE composites in personal ballistic protection is almost imperative due to the need for lower weight compared to other ballistic materials.

UHMWPE composites can have variations in fibre grade, composition (fibre-resin content, woven or uni-directional and stacking sequence), processing conditions (temperature, pressure and time) and laminate thickness. The weak bonding between olefin (also called an alkene) molecules allows local thermal excitations to disrupt the crystalline structure and therefore UHMWPE fibres have lower heat resistance than other high-strength fibres [Bhatnagar, 2016]. The melting point of UHMWPE fibres is around $144 - 152°C$ but UHMWPE fibres are generally not used at temperatures exceeding $100°C$ for long periods of time. UHMWPE fibres however maintain their performance temperatures at below $-50°C$ [Bhatnagar, 2016]. Owing to the molecular structure of UHMWPE fibres, they exhibit surface and chemical properties that are rare in high-performance polymers and do not absorb water readily. UHMWPE fibres are resistant to water, moisture, most chemicals, ultraviolet (UV) radiation and microorganisms. The density of gel-spun UHMWPE fibres is $0.97\ g/cm^3$ [Bhatnagar, 2016].

The fibre architecture in composites used for ballistic protection has been influenced by the fabric structure used in "soft" body armour design for over 40 years. Thus, many of the composites used for ballistic protection contain woven fabrics similar to those used in body armour. In modern combat helmets, for example, multiple layers of woven para-aramid fabrics are typically used to provide protection from fragments [Fejdy et al., 2015]. UHMWPE are widely used in ballistic applications due to their low density, high tenacity and high specific modulus. These materials have a unidirectional construction in which the fibres lie parallel to each other. A thermoplastic resin is used as the matrix. The two most popular examples of UHMWPE materials are Spectra manufactured by Honeywell [Bhatnagar, 2016] and Dyneema manufactured by DSM Dyneema [DSM Dyneema, 2016].

DSM Dyneema has been focusing on research and development of a new UHMWPE

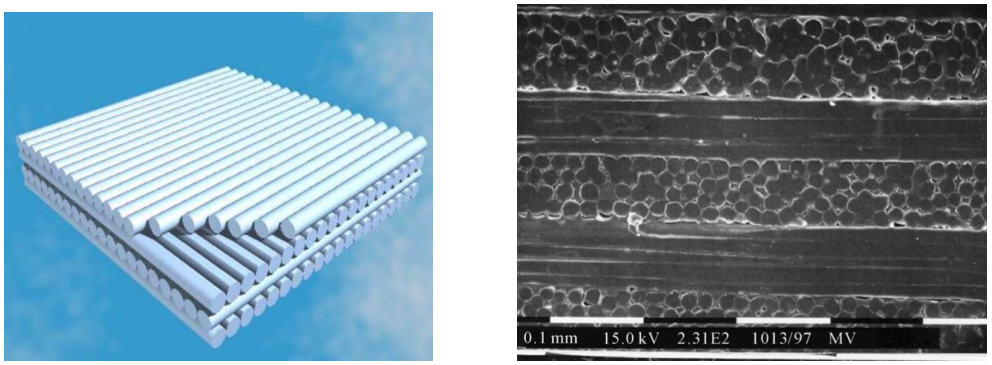

(a) (b)

Figure 4.4: Illustration of fibre cross plies of a UHMWPE for armour systems: (a) schematic picture of build up sequence and (b) SEM micrograph of a cross section of a UHMWPE composite.[Marissen, 2011].

series of materials to substantially lighten the load for military and law enforcement personnel. The company develops new unidirectional (UD) materials suitable for the next generation improved combat helmet, offering superior ballistic performance at lower weight. DSM Dyneema launched the HB80 in June 2009. Initially known as Prototype Dyneema X31, this UD composite material has undergone extensive ballistic and secondary property testing, demonstrating the potential to significantly lighten the load carried by soldiers, providing greater comfort and mobility for soldiers wearing protective gear. This material has now been selected for both body and vehicle armour applications where ultra-light weight and enhanced performance are required [Eshel, 2010].

Polyethylene fibres such as Dyneema or Spectra are capable of stopping a projectile at relatively low areal densities. Polyethylene fibres are very important in body-armour design in general and specifically for ballistic helmets. These fibres can ensure a good protection against fragments, bullets or other projectiles. However, the big disadvantage is the typical increased back face deformation of the composite material [Bhatnagar, 2016]. Even in the case of an impact from a small calibre projectile, the material can cause significant BABT. Composite materials like Dyneema often have very low shear and compressive strength, while the tensile strength and strain to failure are excellent for a polymer. Polyethylene fibres have very high strength and low density, which are essential properties for stopping high energy projectiles.

One other significant disadvantage of this material is the higher cost compared to more traditional armour materials. Polyethylene fibres are delivered by the manufacturer in large rolls and is cut in the appropriate size before pressing. Polyethylene sheets are then pressed together under elevated pressure and temperature to produce composite products such as plates, helmets or panels. The obtained layer often has $0°/90°/0°/90°$ orientation, with two perpendicular fibre directions, as can be seen from the schematic representation in Figure 4.4a and the SEM micrograph in Figure 4.4b. This disposition reduces splitting between fibres that would allow projectiles to pass through effortlessly. The in-plane strength and stiffness properties of the final laminate are almost exclusively determined by the properties of the composite filaments.

Delamination, fibre failure and fibre sliding are the most important phenomena that

occur when a projectile impacts a composite armour panel. These phenomena, and the interaction between them, determine the actual ballistic strength of a composite plate [Eshel, 2010]. Table 4.2 lists some mechanical properties of Dyneema HB80 composite material.

Table 4.2: Mechanical properties of Dyneema HB80 composite material [Kulkarni et al., 2013, Attwood et al., 2014].

Property	Dyneema HB80	Units
Density	980	kg/m^3
Elastic modulus	1200	GPa
Shear strength	2	MPa
Strain to fracture	3.5-3.7	%
Tensile strength	2500	MPa
Elastic modulus	1200	GPa
Shear strength	2	MPa
Strain to fracture	3.5-3.7	%

Due to the excellent tensile strength and the very low shear and compressive strength this material is a very good candidate to absorb the kinetic energy of the impacting projectile.

For this work, Dyneema HB80 is used as the second layer for the development of a new ballistic helmet concept since it is a composite laminate for low weight hard armour applications.

4.2.2 Ceramic

Ceramic materials can be defined as compound materials (made up of two different elements) with metallic and non-metallic element having interatomic bonds that range from purely ionic to totally covalent, having a hard but brittle character. The most ordinary and well-known ceramic materials are traditional ceramics. They primarily consist of raw materials such as clay, cement or glass. The raw material for ceramic production is extracted from natural raw materials and then processed.

Advanced ceramics are used for a broad range of applications, like artificial bioceramics, engine components or integrated circuit packages.

Ceramic products that use naturally occurring minerals must first undergo special processing in order to control purity, particle size and homogeneity, before going to production. This is an important part of the manufacturing process, since the material structure greatly influences the final properties of the finished material.

Ceramic materials are also important within the context of this research. In ballistic protection of military personnel and vehicles it is common to use ceramic materials. Ceramic backed by composite armours (like polyaramid or polyethylene fibres) are the subject of many investigations because their performance against small and medium caliber projectiles is outstanding when the weight is a design condition, for instance in light weight vehicles, airplane and helicopter protection or body armours. The main role of the ceramic is the erosion and rupture of the projectile. The composite backing then absorbs the kinetic energy of the fragments, finally stopping them. The design of these

armours is complex. The great advantage of ceramics is the low density in comparison to metal armour protection and an equal or higher ballistic performance can be achieved with a reduced areal density.

In armour vests with a higher level of protection the combined armour is constituted from two different materials: a ceramic front plate and a high-performance polyaramid or polyethylene fibres reinforced backing. In armoured vehicles, a metal backing of steel or aluminium can also be used. The thickness of the ceramic tiles varies according to the ballistic performance required and is usually between 5 and 15 mm for small calibre threats. The most important ceramic materials that currently fill the requirements for ballistic applications are:

- Boron carbide (B_4C);
- Silicon carbide (SiC);
- Silicon nitride (SiN);
- Alumina (Al_2O_3); and
- Aluminium nitride (AlN).

Chabera et al. [Chabera et al., 2015] studied the ballistic behaviour of two composite armour systems using different ceramics. The composite armour systems consisted of a front layer made of Al_2O_3 or SiC and high strength steel as the backing material. The ballistic performance of the proposed protective structures were tested with a 7.62 × 54R B32 mm Armour Piercing (AP) projectile. The authors concluded that the application of SiC ceramic instead of Al_2O_3 decreases a probability of steel plate perforation. This is caused by the use of a high isostatic pressure method to improve the mechanical properties of silicon carbide making this material better than alumina.

Kaufmann et al. [Kaufmann et al., 2003] conducted experimental tests on four different ceramic materials including alumina, modified alumina, silicon carbide and boron carbide when impacted by a 12.7 mm (0.50 in) AP projectile. The authors conclude that silicon carbide has the best ballistic performance at the tested range of velocities. In many cases, however, the performance of boron carbide and silicon carbide were similar. The modified alumina did not appear to have increased ballistic properties relative to unmodified alumina. Both alumina compounds were outperformed by silicon carbide and boron carbide.

Alumina emerged as today's most widely used ceramic armour, combining good mechanical behaviour at relatively low cost. Alumina is less expensive than either SiC or, especially, B_4C. The densities of B_4C (2.52 g/cm^3) and SiC (3.29 g/cm^3) are considerably lower than that of Al_2O_3 (3.98 g/cm^3). However, because of its easy sinterability and the lower cost of the raw powders, alumina is still preferred for use in vehicle applications, where the extra weight can be tolerated, while the lighter B_4C and SiC ceramics are now used in body armour [Council, 2011].

Compared to boron carbide (B_4C), silicon carbide (SiC) has a higher fracture toughness (minimum of 14 MPa.m$^{1/2}$ against 2.5 MPa.m$^{1/2}$). The low fracture toughness of ceramics in general and, consequently, their predisposition to fracture when subjected to high tensile stresses has led to the development of composite armours in which a ceramic plate is backed by a more ductile material, such as a composite or metal material, that

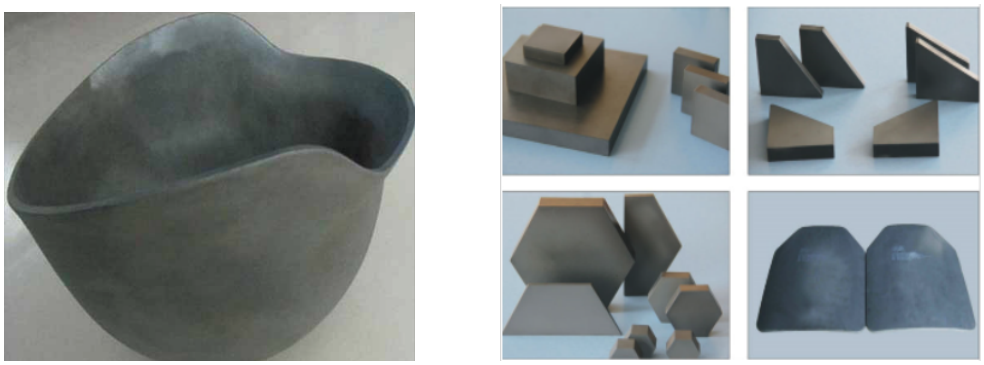

(a) SiC helmet sheel. (b) SiC tiles.

Figure 4.5: Examples of SiC shapes used for ballistic protection [Pingxiang, 2017].

can better resist in tensile failure. However, at the moment of this research it was not possible to produce complex shapes (curved shapes, like helmet shells) with B_4C.

Figure 4.5 shows different examples of SiC tiles (square, hexagonal, cylindrical) and a helmet shell.

Due to the good properties of silicon carbide in breaking and eroding the impacting projectile (especially the steel core) this material is used in this project as the first layer for the development of a new ballistic helmet concept.

4.2.3 Aluminium alloys

Metallic materials, such as steel, aluminium and titanium, have always taken a special position in the development of protective armour, considering their availability, machinability and cost. One of the most common examples are the first ballistic helmets, made from steel [Council, 2011].

Aluminium is the third most abundant element (after oxygen and silicon) in the crust of the earth and is used in a considerable diversity of industries due to its properties, in particular its low density (2.68 g/cm^3).

Its good formability ensures that this material can be used in the manufacturing of various metal products, and can be deformed and shaped with relative ease.

Alloying, heat treatment and various mechanical working procedures, can be used to obtain special characteristics (hardness, strength, toughness) enabling the fulfilment of different ballistic protection requirements. Owing to their strength-to-weight ratio, plasticity, fracture toughness and corrosion resistance, aluminium alloys are widely applied in the military industry. As high mobility is essential for a modern army, aluminium alloys can be used to reduce the weight of the equipment and contribute towards this objective.

Aluminium alloys are classified into seven main classes according to the chemical composition. Due to the requirement for a stiff back face to limit the back face deflection of the first two layers, aluminium alloy 5754-H22 is used as the third layer in the optimised ballistic helmet solution. The class 5xxx, or class of aluminum-magnesium alloys, is suitable for the manufacturing of sheet products, which are applied in naval structures, transport and structural processes, and has been used since the 1950s in

military applications, due to its low cost, weldability, and mechanical and corrosion resistance properties [Davis, 2001].

The aluminium alloy 5754-H22 has high fatigue strength and fair machinability making it highly suited to containers, boilers or ship building. The chemical composition of the 5754-H22 alloy is listed in Table 4.3.

Table 4.3: Chemical composition of alloy Al5754-H22 (% weight) [Rodriguez Millan et al., 2014].

Mn	Si	Cr	Cu	Zn	Fe	Ti	Mg
0.26	0.29	0.03	0.04	0.02	0.32	0.03	2.80

4.3 Penetration mechanisms

Penetration mechanisms are an interdisciplinary subject. As the materials involved in an impact behave differently, the different materials have to be treated separately. This large difference in behaviour due to an impact, and also associated mechanical properties, makes the selection of a material for ballistic protection an important one.

In this thesis the penetration mechanisms for composites, ceramics and metals are presented. In all cases, the techniques for analysing and modelling these materials are progressing daily, especially in the area of numerical methods.

4.3.1 Penetration and failure of metal targets

Models for penetration and perforation are based on laws of conservation and compatibility. As an impact occurs, the kinetic energy of the projectile is transferred to the plate. Some of the energy is used to deform the plate and will finally also be turned into heat. Another part of the energy is given off as light and heat, the remainder of the energy is imparted to the fragments as kinetic energy. Measuring or determining each of these energies is complex and dependent of the target and the projectile. For penetration and perforation analysis, the most important aspect is to predict the kinetic energy (i.e. mass and velocity) of the fragments. Once this kinetic energy is determined, conservation of mass, and momentum energy, is applied to the projectile/target system. The analysis is complex because the events that occur at the projectile/target interface are unknown. Although many studies have been performed, only cases for projectiles with highly controlled velocities, shapes, sizes and trajectories have been examined [Hatzenbichler and Buchmayr, 2009]. As a result, numerous approximations and assumptions must be made in order to apply these analyses to fragments. Ballistic impact in metals is a very localised phenomenon. The stress and strain effects are usually limited to within 3-6 projectile diameters of the impacted zone [Zook, 1977]. Impacted target materials may fail by a combination of several modes including spalling, plugging, petaling, ductile or brittle fracture, and adiabatic shearing.

The basic mechanisms for the penetration behaviour depending on the material characteristics are shown in Figure 4.6 [Hatzenbichler and Buchmayr, 2009]. Brittle fracture (a), radial cracks at the projectile exit side (b) and fragmentation (c) only occur on

brittle materials or thick specimens. Thinner metal sheets (i.e. sheet thickness smaller than the projectile's calibre) or ductile sheets tend to show ductile hole growth (d) and plugging (e). The latter is typical a consequence from adiabatic shear band formation at very high strain rates. This softening mechanism is a result of a temperature increase which occurs faster than the local hardening of the material [Hu et al., 2002]. The impact on thin ductile sheets leads to petaling at the back of the plate, as shown in Figure 4.6 (f).

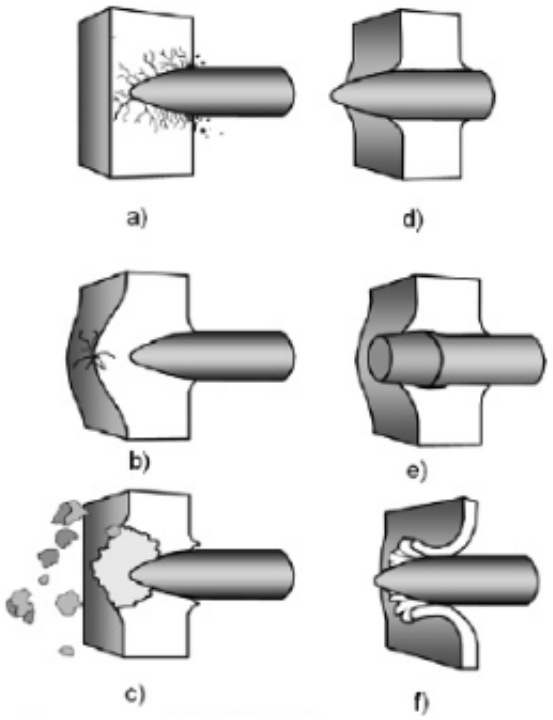

Figure 4.6: Perforation mechanisms in metals: (a) brittle fracture (cracking); (b) radial fracture; (c) fragmentation; (d) ductile hole growth; (e) plugging; and (f) petaling [Hatzenbichler and Buchmayr, 2009].

4.3.2 Composite damage and failure

Fibre reinforced composites are generally orthotropic materials i.e., having different properties in perpendicular directions. Parameters which significantly affect the properties of a composite are shape, size, orientation and distribution of the reinforcement and various other features such as matrix in case of polymer matrix composites. These, together with volume fraction, constitute what is called the microstructure of the composite. The orientation of the reinforcement within the matrix affects the isotropy of the system. When the reinforcement is in the form of equiaxial particles, the composite behaves essentially as an isotropic material whose elastic properties are independent of direction. The manufacturing process may result in different orientations of the reinforcement and hence the loss of isotropy; thus the composite becomes anisotropic in nature. High velocity impacts will cause localized compression of the composite and

subsequently shearing of the fibres and spalling of the resin during impact. Once the projectile has slowed down, the composite deforms causing fibre stretching, pullout, and delamination of the composite layers (plies) and thus reducing the load carrying ability.

It is extremely difficult to obtain an analytical model for the penetration of continuous fibre composites. This is due to the change of energy dissipation as the composite is damaged.

A range of mechanisms has been proposed for the penetration/failure of fibre composite beams and plates impacted by a nominally rigid projectile. These include (Figure 4.7): (a) tensile stretching failure in a string-like mode as first modelled by Phoenix and Porwal [Leigh Phoenix and Porwal, 2003] and used to rationalise the Cunniff [Cunniff, 1999] scaling relationship; (b) shear plugging [Cheeseman and Bogetti, 2003] resulting in the formation of a plug; and (c) tensile fibre failure by the generation of indirect tension due to the compressive loading under the projectile [Woodward et al., 1994].

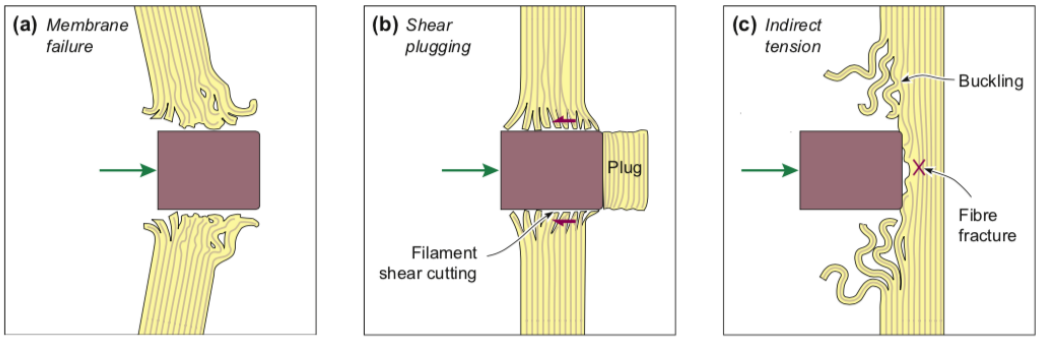

Figure 4.7: Illustrations of three penetration mechanisms for fibre reinforced composites: (a) Failure by tensile stretching in a string-like mode; (b) shear plugging at the edges of the projectile and the consequent formation of a shear plug; and (c) progressive tensile ply failure by indirect tension developed due to compressive stresses under the projectile [Attwood et al., 2016].

4.3.3 Ceramic fracture

Ceramic fracture under impact has different physical characteristics compared to other armour materials because of the inherent brittleness. Most of ceramics have a high compressive strength but low tensile strength. For these reasons, they can easily resist the compressive shock wave after the impact, but on the other hand, they may crack because of the tensile shock wave generated by rarefaction. When the stress is higher than the strength limit of the ceramic tile, the tile is broken into pieces by spalling. To reduce the danger from spalling, ceramic armour has to be supported by a backing sheet, made out of steel and/or fibres. The fracture behaviour of ceramic armour with a backing plate is different from the phenomena previously described. The ceramic receives the initial impact of the projectile and its function is to destroy the tip of the projectile progressively as it tries to penetrate the composite material. In this initial stage a major part of the impact energy is dissipated. Then in the second stage, the base layer made of ductile material absorbs the residual impact energy caused by the fragmented parts of the projectile and ceramic as they come to a complete halt, thus

resulting in plastic deformation of the ductile material.

A fracture conoid is formed in the ceramic and this 'pushes' against the support/ backing plate with a force that is governed by the deceleration of the projectile, absorbing energy. The interest of the conoid is that it increases the area transferring kinetic energy from the projectile to the backing plate. For a larger area, the impact energy can be better distributed over the rear plate as shown in Figure 4.8. In general, the time that the fracture conoid develops can be calculated by Equation 4.1 [Carlucci and Sidney, 2007].

$$t_{\text{conoid}} = \frac{h_{\text{c}}}{C_L} + \frac{h_{\text{c}}}{V_{\text{rad.crack}}} \tag{4.1}$$

where h_{c} is the thickness of the ceramic as illustrated in Figure 4.8. C_{L} is the longitudinal wave speed in the material and $V_{\text{rad.crack}}$ is the radial crack growth speed.

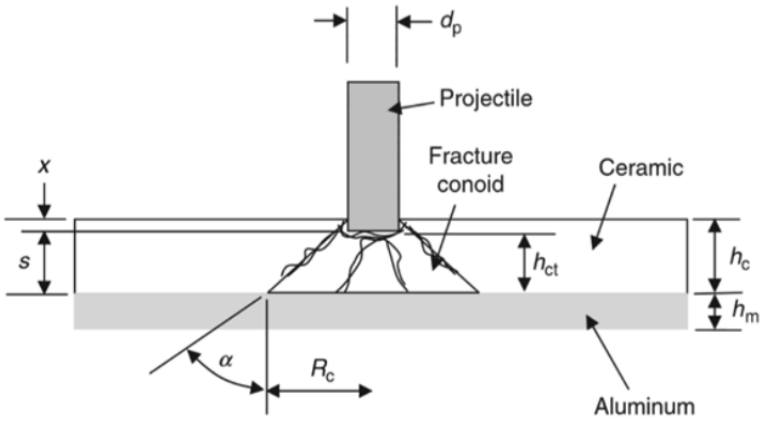

Figure 4.8: Fracture conoid formation in ceramic material [Carlucci and Sidney, 2007].

However, it is essential to note that this equation does not take into account the material properties of the ceramic, the impact velocity nor the tile boundary conditions.

Chapter 5

Material behaviour

Finite Element (FE) models extend the spectrum of physical parameters that can be investigated for a better understanding of the dynamic phenomenon being analysed in this work. The development of these models has been made possible thanks to the development of numerical techniques and powerful computing systems. The increasing knowledge on materials science has led to the development of material models that better describe dynamic material behaviour, paving the way for a better assessment of the effects of ballistic impacts. Common to most mechanical analyses of engineering materials and their structural behaviour is the need for constitutive models that link the states of stress and strain. From a mathematical viewpoint, the constitutive equations that define the constitutive model are complementary to the balance and kinematic equations. Taken together with the loading and boundary conditions, these are the sufficient, but not always the necessary, equations that formulate a complete boundary value problem, from which the behaviour of a given body can be calculated [Runesson, 2006]. Constitutive models may be very different for the various materials used in engineering practice, such as metals and alloys, polymers, fibre composites, concrete and wood, etc. However, to a large extent it is possible to employ the same principles and concepts (and even the same terminology) in establishing constitutive relations for different materials. It is emphasised that constitutive models are just mathematical simplifications of complex physical behaviour. For example, it is appropriate to claim that the behaviour of steel can be represented by an elastic-plastic model, but it does not make sense to claim that steel is elastic-plastic. In fact, it is appropriate to model steel (and any other engineering material) in a number of ways depending on the purpose, conditions and the required precision of the model predictions [Runesson, 2006]. The next section presents an introduction to the finite element analysis in order to better understand the numerical material models that are needed in this work.

5.1 Material models

The material strength, material failure and the equation of state (EOS) used to model the behaviour of the materials investigated in this work will now be reviewed in detail.

5.1.1 Dyneema HB80

An orthotropic material constitutive model was required to account for different material properties along each of the three principal directions.

Several material models are implemented in LS-Dyna^{TM} to describe the behaviour of composite materials. However, many of these are not suitable to model an Ultra High Molecular Weight Polyethylene Composite (UHMWPE) like Dyneema HB80 in the way this work needs, due to the layup used for the numerical model. However, the orthotropic simplified damage material model can be adopted for the UHMWPE, since, as the name implies, it is used in orthotropic materials. This material model is an orthotropic material with simplified damage and failure. The material input data consist of material properties such as Young's modulus, Poisson's ratio and shear modulus in the various directions. In addition, nine failure criteria on strains are available. This material model needs several material parameters as input, such as:

- The material density: ρ;
- Young's moduli in xx, yy-direction and zz-direction: E_{xx}, E_{yy}, and E_{zz} respectively;
- Poisson's ratios: ν_{yx}, ν_{zx} and ν_{zy};
- The shear moduli: G_{xy}, G_{yz} and G_{zx};
- Failure strain in tension along the xx, yy- and zz-directions.

The material model used in this dissertation is an orthotropic, or orthogonally anisotropic constitutive material model. The model is general enough to model a large majority of long fibre-reinforced composite materials with three mutually perpendicular material planes. The orthotropic material model is a simplification of the most general anisotropic formulation relating the stresses and strains as:

$$\{\sigma\} = [C]\,\{\varepsilon\} \tag{5.1}$$

$$\begin{Bmatrix} \sigma_{xx} \\ \sigma_{yy} \\ \sigma_{zz} \\ \sigma_{xy} \\ \sigma_{xz} \\ \sigma_{yz} \end{Bmatrix} = \begin{bmatrix} C_{11} & C_{12} & C_{13} & C_{14} & C_{15} & C_{16} \\ & C_{22} & C_{23} & C_{24} & C_{25} & C_{26} \\ & & C_{33} & C_{34} & C_{35} & C_{36} \\ & & & C_{44} & C_{45} & C_{46} \\ & \text{Sym} & & & C_{55} & C_{56} \\ & & & & & C_{66} \end{bmatrix} \begin{Bmatrix} \varepsilon_{xx} \\ \varepsilon_{yy} \\ \varepsilon_{zz} \\ \gamma_{xy} \\ \gamma_{xz} \\ \gamma_{yz} \end{Bmatrix} \tag{5.2}$$

where the stiffness matrix, C, is symmetric due to energy considerations, requiring 21 independent elastic constants [de Moura et al., 2011].

An orthotropic material is one which has three orthogonal planes of microstructural symmetry. Three mutually perpendicular planes of symmetry can be passed through each point in the continuum model. The x, y and z axes forming these planes are called the material directions. The material symmetry inherent in the orthotropic material reduces the number of independent elastic constants that consider an element of orthotropic material subjected to a shear strain ε_{yz} and also a strain $-\varepsilon_{yz}$.

From Equation 5.2, the stresses induced by a strain γ_{yz} only are

$$\sigma_{xx} = C_{16}\gamma_{yz}, \sigma_{yy} = C_{26}\gamma_{yz}, \sigma_{zz} = C_{36}\gamma_{yz}$$
$$\sigma_{xy} = C_{46}\gamma_{yz}, \sigma_{xz} = C_{56}\gamma_{yz}, \sigma_{yz} = C_{66}\gamma_{yz}$$

The stresses induced by a strain $-\gamma_{yz}$ only are (the prime is added to distinguish these stresses from those of Equation 5.2

$$\sigma_{xx}^{'} = -C_{16}\gamma_{yz}, \sigma_{yy}^{'} = -C_{26}\gamma_{yz}, \sigma_{zz}^{'} = -C_{36}\gamma_{yz}$$
$$\sigma_{xy}^{'} = -C_{46}\gamma_{yz}, \sigma_{xz}^{'} = -C_{56}\gamma_{yz}, \sigma_{yz}^{'} = -C_{66}\gamma_{yz}$$

These stresses, together with the strain, are shown in Figure 5.1.

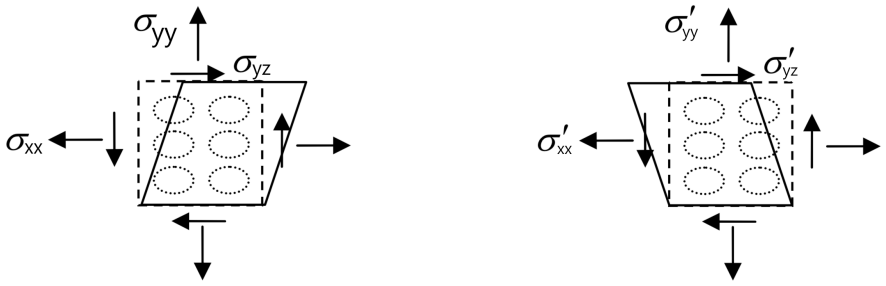

(a) (b)

Figure 5.1: An element of orthotropic material undergoing shear strain: (a) positive strain and (b) negative strain [Kelly, 2013].

Due to the material symmetry the normal stresses in Figure 5.1 are the same, $\sigma_{xx} = \sigma_{xx}^{'}$, and $\sigma_{yy} = \sigma_{yy}^{'}$, but the shear stresses has the opposite sign, $\sigma_{yz} = -\sigma_{yz}^{'}$. From the Equations of the stresses induced by a strain it is implicit that

$$C_{16} = C_{26} = C_{36} = C_{46} = C_{56} = 0 \tag{5.3}$$

Similar conclusions follow from considering shear strains in the other two planes:

$$\varepsilon_{xz} : C_{15} = C_{25} = C_{35} = C_{45} = 0$$
$$\varepsilon_{xy} : C_{14} = C_{24} = C_{34} = 0$$

The elastic stiffness matrix, C is thus reduced, and there are only nine independent elastic constants:

$$\begin{Bmatrix} \sigma_{xx} \\ \sigma_{yy} \\ \sigma_{zz} \\ \sigma_{xy} \\ \sigma_{xz} \\ \sigma_{yz} \end{Bmatrix} = \begin{bmatrix} C_{11} & C_{12} & C_{13} & 0 & 0 & 0 \\ & C_{22} & C_{23} & 0 & 0 & 0 \\ & & C_{33} & 0 & 0 & 0 \\ & & & C_{44} & 0 & 0 \\ & \text{Sym} & & & C_{55} & 0 \\ & & & & & C_{66} \end{bmatrix} \begin{Bmatrix} \varepsilon_{xx} \\ \varepsilon_{yy} \\ \varepsilon_{zz} \\ \gamma_{xy} \\ \gamma_{xz} \\ \gamma_{yz} \end{Bmatrix} \tag{5.4}$$

These equations can be inverted to introducing elastic constants E, υ and G in place of the compliance matrix S_{ij}:

$$\begin{Bmatrix} \varepsilon_{xx} \\ \varepsilon_{yy} \\ \varepsilon_{zz} \\ \gamma_{xy} \\ \gamma_{xz} \\ \gamma_{yz} \end{Bmatrix} = \begin{bmatrix} \frac{1}{E_{xx}} & -\frac{\upsilon_{21}}{E_{yy}} & -\frac{\upsilon_{zx}}{E_{zz}} & 0 & 0 & 0 \\ & \frac{1}{E_{yy}} & -\frac{\upsilon_{zy}}{E_{zz}} & 0 & 0 & 0 \\ & & \frac{1}{E_{zz}} & 0 & 0 & 0 \\ & & & \frac{1}{2G_{yz}} & 0 & 0 \\ & \text{Sym} & & & \frac{1}{2G_{xz}} & 0 \\ & & & & & \frac{1}{2G_{xy}} \end{bmatrix} \begin{Bmatrix} \sigma_{xx} \\ \sigma_{yy} \\ \sigma_{zz} \\ \sigma_{xy} \\ \sigma_{xz} \\ \sigma_{yz} \end{Bmatrix} \tag{5.5}$$

where E_{ii} are the elastic moduli in the principal material directions, G_{ij} are the elastic shear moduli representing the shear stiffness in the corresponding plate and υ_{ij} are the elastic Poisson's ratios.

In this constitutive model, failure is based on a strain criterion and is initiated when a specific failure strain value is reached. Failure can occur along the three orthotropic directions, in tension, in compression or shear. For this work, failure can occur along the plane directions (xx and yy) and only occur in tension. The failure in compression or shear was not considered as during real ballistic tests these types of failure were not observed.

The pressure is defined by the negative of the mean stress:

$$p = -\frac{1}{3}(\sigma_{xx} + \sigma_{yy} + \sigma_{zz}) \tag{5.6}$$

So that the pressure for a linear orthotropic material is given by:

$$p = -\frac{1}{9}[C_{11} + C_{22} + C_{33} + 2(C_{12} + C_{23} + C_{31})]\varepsilon_{vol} \tag{5.7}$$

The equation in the above describes the pressure contribution from the volumetric component (linear EOS).

5.1.2 Steel

The Johnson-Cook constitutive relation is used in this work to describe thermo-mechanical deformations of the steel jacket and the steel core. The Johnson-Cook material model is based on empirical equations, which relate the stress, strain, strain rate and temperature for an isotropic material [Johnson and Cook, 1983]. This model describes the strength of metals at large non-linear strains, high strain rates and high temperatures. The effective stress σ is given by:

$$\sigma = (A + B\varepsilon_{\text{eff}}^{n})\,(1 + C\ln\dot{\varepsilon}^{*})\,(1 - (T^{*})^{m}) \tag{5.8}$$

where ε_{eff} is the effective plastic strain; ε^{*} is the effective plastic strain rate, normalised with respect to a strain rate of 1.0 s^{-1}; n is the work hardening exponent; A is the initial yield stress; B is the strain hardening coefficient; C is the strain rate coefficient and m is the thermal softening exponent. The values of A, B, C, n and m can be determined from an empirical fit of stress-strain curves. The first term in equation 5.8 represents the influence of plastic strain (strain hardening), the second term represents the influence of

strain rate (viscous behaviour) and the third term represents the influence of temperature (thermal softening). The homologous temperature T^* is:

$$T^* = \frac{T - 298\text{K}}{T_{\text{melt}} - 298\text{K}} \tag{5.9}$$

where T_{melt} is the melting temperature and T is the current temperature.

The failure strain criterion is given by the following empirically-based equation, also known as the Johnson-Cook failure model:

$$\varepsilon_{\text{f}} = [D_1 + D_2^{(D_3\sigma^*)}][1 + D_4 \ln \dot{\varepsilon}^*][1 + D_5 T^*] \tag{5.10}$$

where σ^* is the mean stress normalised by the effective stress, and the parameters D_1, D_2, D_3, D_4 and D_5 are material constants. The Johnson-Cook damage model is a cumulative- damage fracture model that takes into account the loading history, which is represented by the strain to fracture. The strain to fracture is expressed as a function of the strain rate, temperature, and pressure. The D_1, D_2 and D_3 parameters are predominant compared with the two others. In other words, the strain to fracture is mostly dependent of the stress state. To determine the damage model's constants, the strain to failure is established in function of the triaxial state of stresses. This step gives the D_1, D_2 and D_3 constants. After that, strain rate parameter, D_4, and temperature parameter, D_5, can be found. Failure is assumed to occur when the damage parameter $D = 1$ [Hallquist, 2012] with D defined as:

$$D = \sum \frac{\Delta\varepsilon_{\text{eff}}}{\varepsilon_{\text{f}}} \tag{5.11}$$

An equation of state (EOS) is a relation between state variables (e.g. the internal energy, pressure, temperature and volume) [Winterbone, 1997]. More specifically, an equation of state is a thermodynamic equation describing the state of matter under a given set of physical conditions. The thermodynamic state of a homogeneous material that does not suffer any chemical reaction or phase changes can be defined by two state variables [Serway and Jewett, 2003]. Some numerical modelling problems need the definition of an EOS in addition to the constitutive model.

5.1.2.1 Equation of state

Materials subjected to high strain rates or even the propagation of shock waves, are often modelled by additionally using an EOS in the definition of the material behaviour. Two EOS were used with Johnson-Cook constitutive model in this work for the description of the projectile jacket and core. The particularities of these two EOS are described in the following paragraphs.

The linear polynomial EOS is a polynomial equation of state, linear in the specific (volumetric) internal energy, e. This equation definition of the initial thermodynamic state of the material and the pressure, is given by [Hallquist, 2012]:

$$p = C_0 + C_1\mu + C_2\mu^2 + C_3\mu^3 + (C_4 + C_5\mu + C_6\mu^2)e \tag{5.12}$$

Parameters C_0 to C_6 are user-defined constants determined experimentally and $\mu = \frac{1}{V} - 1$ where V is the relative volume.

The Gruneisen EOS equation of state is commonly used in shock physics as a function of particle-velocity $u_s(u_p)$. It accurately represents the behaviour of the Hugoniot relationships under modest compressions. Classically, the Mie-Gruneisen EOS considers only the effects of the lattice and zero-temperature contributions. Pressure and energy are determined from a given reference state; this could be room temperature, zero temperature, the Hugoniot, or other relationships [Hallquist, 2012], and is commonly presented as:

$$p = \frac{\rho_0 C^2 \mu [1 + (1 - \frac{\gamma_0}{2})\mu - \frac{a}{2}\mu^2]}{[1 - (S_1 - 1)\mu - S_2 \frac{\mu^2}{\mu+1} - S_3 \frac{\mu^3}{(\mu+1)^2}]} + (\gamma_0 + \alpha\mu)e \tag{5.13}$$

where, e is the internal energy, C is the interception of the $u_s(u_p)$ curve (in velocity units), S_1, S_2, and S_3 are the coefficients of the slope of the $u_s(u_p)$ curve, γ_0 is the Gruneisen gamma and a is the firs order volume correction to γ_0. The compression is defined in terms of the relative volume V as

$$\mu = \frac{1}{V} - 1 \tag{5.14}$$

The difference between both EOS is shown in Figure 5.2, showing that the hydrostatic pressure is higher for the Gruneisen EOS than for the Linear Polynomial EOS [Olleak and El-Hofy, 2015].

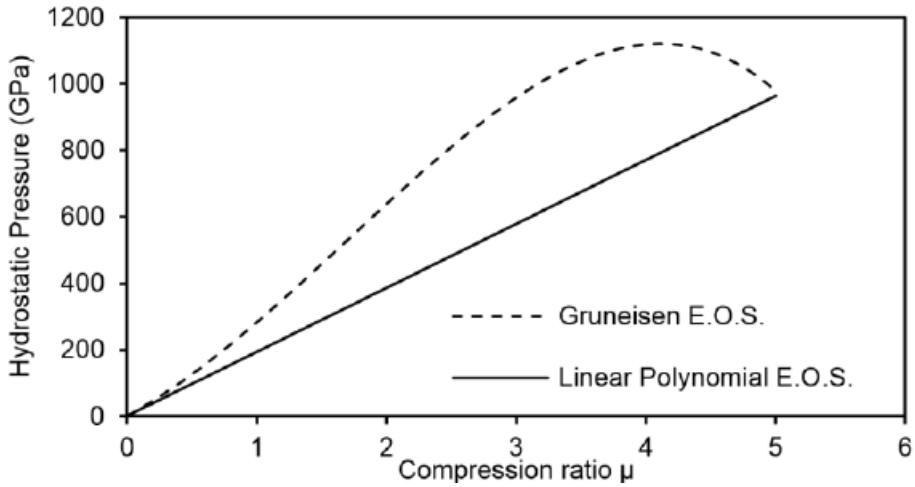

Figure 5.2: Difference in the hydrostatic pressure values for the Gruneisen and Linear Polynomial equations of state [Olleak and El-Hofy, 2015].

5.1.3 Aluminium, lead and steel 4340

The isotropic elastic-plastic constitutive relation was employed to simulate mechanical deformations of the aluminium plate representing the third layer, the lead in the Kalashnikov projectile and also to simulate steel in the Fragment Simulating Projectiles (FSP). The input parameters for the elastic-plastic material type are its density ρ, shear modulus G, initial yield stress σ_0, plastic hardening modulus E_t and bulk modulus K.

The von Mises yield condition is given by:

$$\phi = J_2 - \frac{\sigma_y^2}{3} \tag{5.15}$$

where the second stress invariant, $J_2 = \frac{1}{2} s_{ij} s_{ij}$, defined in terms of the deviatoric stress components, and the yield stress σ_y, are a function of the effective plastic strain, ε_{eff}, and the plastic hardening modulus, E_{p}:

$$\sigma_y = \sigma_0 + E_p \varepsilon_{\text{eff}} \tag{5.16}$$

In isotropic hardening, it is assumed that the evolution of the yield surface is, at any state of hardening, a uniform (isotropic) expansion without translation of the initial yield surface, that is, the centre of the new updated surface remains invariant in the (σ_1, σ_2, σ_3) space.

A proper relation between stress and plastic strain is defined. To obtain a suitable scalar measure of the effective plastic stain, the magnitude of the accumulated plastic strain can be defined as [Neto et al., 2008]:

$$\varepsilon_{\text{eff}}^{\text{p}} = \int_0^t \sqrt{\left(\frac{2}{3} \dot{\varepsilon}_{ij}^{\text{p}} \dot{\varepsilon}_{ij}^{\text{p}} \right)} \mathrm{d}t \tag{5.17}$$

and the plastic tangent modulus is defined in terms of the tangent modulus, E_{t}, as:

$$E_{\text{p}} = \frac{E E_{\text{t}}}{E - E_{\text{t}}} \tag{5.18}$$

The next step is to define the yield stress, σ_y, as a function of the effective plastic strain, ε_{eff}. There are several hardening functions that can represent real and elastic-plastic behaviour. The most common forms are the linear strain-hardening relations, for the one dimensional case, generally defined as:

$$\sigma_y(\varepsilon_{\text{eff}}) = \sigma_0 + h \varepsilon_{\text{eff}}, \tag{5.19}$$

or the power-law hardening relations, generically defined as:

$$\sigma_y(\varepsilon_{\text{eff}}) = \sigma_0 + h {\varepsilon_{\text{eff}}}^{1/k}. \tag{5.20}$$

where σ_0 is the initial stress and h and k are material parameters that can be obtained experimentally.

The pressure is given by the expression

$$p^{n+1} = K \left(\frac{1}{V^{n+1}} - 1 \right) \tag{5.21}$$

where K is the bulk modulus. In this constitutive model, failure is based on an effective plastic strain criterion and is initiated when the failure strain is reached (and the element is deleted from the calculation).

5.1.4 Silicon carbide

Ceramic materials are commonly used in protective armour applications where they may be subjected to high-energy ballistic impacts. Under simple loading conditions, ceramics may be regarded as elastic-brittle materials. When considering ballistic impacts the post-yield response of the ceramic becomes significant. One of the most widely used constitutive models for simulating the post-yield response of ceramic materials is the Johnson-Holmquist constitutive model. This constitutive equation, developed by Johnson and Holmquist [McIntosh, 1998], incorporates the effect of damage on residual material strength and bulking (shear induced dilatancy) during failure in compression [McIntosh, 1998]. The relevant equations describing the response of the material are summarised in the following paragraphs. The Johnson-Holmquist Damage Model (JH-2) is used to model silicon carbide, as the ceramic material is subjected to loading conditions that include high pressures, high strain rates and large deformations [Azevedo et al., 2016].

This constitutive model includes a representation of the intact and fractured strength, a pressure-volume relation that can include bulking and a damage model that transitions the material strength from an intact state to a fully damaged state.

The intact ceramic material strength and the fractured material strength are defined as a non-linear function of the normalised pressure (P^*), the tensile strength (S^*) and the normalised total incremental strain rate ($\dot{\varepsilon}^* = \dot{\varepsilon}/\dot{\varepsilon_0}$), by:

$$\sigma_\mathrm{i} = A_\mathrm{JH}(P^* + S^*)^{N_\mathrm{JH}}(1 + C_\mathrm{JH} \ln \dot{\varepsilon}^*) \tag{5.22}$$

$$\sigma_\mathrm{f} = B_\mathrm{JH}(P^*)^{M_\mathrm{JH}}(1 + C_\mathrm{JH} \ln \dot{\varepsilon}^*) \tag{5.23}$$

where σ_i and σ_f are the intact and fractured ceramic strength respectively. A_JH, B_JH, C_JH, N_JH and M_JH are the Johnson-Holmquist [Johnson and Holmquist, 1994] parameters. The stresses are normalised in respect to the equivalent stress at the Hugoniot elastic limit (HEL) that is defined as follows,

$$\sigma_\mathrm{HEL} = \frac{3}{2}(\mathrm{HEL} - P_\mathrm{HEL}) \tag{5.24}$$

in which, HEL is the Hugoniot elastic limit and P_HEL is the pressure component of the HEL. Then, the normalised pressure P^*_HEL, is given by:

$$P^*_\mathrm{HEL} = P/P_\mathrm{HEL} \tag{5.25}$$

where P is the real pressure. Any normalised stress, σ^*, is given by:

$$\sigma^* = \sigma/\sigma_{HEL} \tag{5.26}$$

where σ is the real stress. The description of the model is explained below.

For any given state of the material where it is neither intact nor fully fractured, the damaged material equivalent strength is given by the combination of these two material strengths as:

$$\sigma = \sigma_\mathrm{i} - D(\sigma_\mathrm{i} - \sigma_\mathrm{f}) \tag{5.27}$$

The current increment (ΔD) in damage (D) can be determined by:

$$\Delta D = \frac{\Delta \varepsilon_{\mathrm{P}}}{\Delta \varepsilon_{\mathrm{p}}^{\mathrm{f}}} \Rightarrow D = \sum \frac{\Delta \varepsilon_P}{\Delta \varepsilon_{\mathrm{p}}^{\mathrm{f}}} \tag{5.28}$$

where $\Delta \varepsilon_{\mathrm{P}}$ is the plastic strain increment and $\Delta \varepsilon_{\mathrm{p}}^{\mathrm{f}}$ is the plastic strain at fracture, which is a function of the actual pressure,

$$\varepsilon_{\mathrm{p}}^{\mathrm{f}} = D_1 (P^* + T^*)^{D_2} \tag{5.29}$$

which is evaluated as a function of the normalised pressure, the tensile strength and the two material damage constants D_1 and D_2 [Johnson and Holmquist, 1994]. These equations summarise the framework of the JH-2 constitutive model.

Initially the material response is considered to be elastic, with the stress state completely described by the elastic material properties (shear modulus) and equation of state. Based on the current material deformation, μ (equation 5.30) and the corresponding pressure (equations 5.31 and 5.32) can be calculated.

The hydrostatic pressure p before fracture is given by the polynomial equation of state:

$$\mu = \frac{\rho}{\rho_0} - 1 = \frac{V_0}{V} - 1 \tag{5.30}$$

$$p = K_1 \mu + K_2 \mu^2 + K_3 \mu^3 \quad \text{(compression)} \tag{5.31}$$

$$p = K_1 \mu \quad \text{(tension)} \tag{5.32}$$

where ρ_0 and V_0 are respectively the initial specific density and specific volume, and ρ and V are the specific density and relative volume during impact loading. K_1, K_2 and K_3 are constants.

5.2 Methodology for modelling the thesis work

Modelling impact problems requires the understanding of the complexity of real impact events. This complexity is due to the time scale of the event, the non-linearities (geometrical, material, contact) involved and the difficulty of obtaining continuous measurements of the impact event effectively and efficiently. In the case of a new helmet design in which the idea is to obtain the best combination of different materials (also taking into account the thickness) to stop a rifle specific ammunition, the finite element method has a great advantage. The FE analysis is more cost effective than experimental testing and also, as one of the major objectives, in addition to stopping the projectile, is taking into account the possible types of head injuries, using FE is the only possibility of extracting data which otherwise would be impossible to obtain.

The problem becomes more complex when it comes to deformable projectiles, as is the case for this work (both bodies are deformable bodies). To simulate an advanced ballistic helmet concept against a rifle ammunition it is necessary:

- To numerically build the ballistic helmet layered concept as well as the projectile models. The FE model requires the geometry, the mesh and the material properties via specific experimental tests to supply the material models;
- To validate, each model (armour and ammunition) individually based on experimental results;
- To assess measurable physical parameters of interest, i.e., relevant for the risk assessment;

Before numerically impacting the projectile on the new helmet design it was necessary to validated the ammunition and targets models individually. All numerical models and validations are present in Chapter 7.

Part II

Numerical modelling and validation

Chapter 6

Finite element analysis

This chapter presents a generic overview on the material behaviour laws and the presentation and overview of the finite element analyses that may be used to study the effects of impact problems. Also in this chapter, the state-of-the-art of numerical simulations applied to impact problems are presented. The last section of this chapter introduces how the pre-processing phase of the model input is required to solve the problem.

6.1 Material behaviour laws

The Finite Element (FE) method is based on conservation equations that describe the motion and deformation of a given continuum in solid mechanics. These differential equations established through the principles of conservation of momentum, mass and energy from a macroscopic point of view can be summarised as follow:

- Conservation of mass:

$$\frac{D\rho}{Dt} + \rho\frac{\partial v_i}{\partial x_i} = 0 \tag{6.1}$$

- Conservation of energy:

$$\frac{DI}{Dt} = -\frac{p}{\rho}\frac{\partial v_i}{\partial x_i} + \frac{1}{\rho}\Pi_{ij}\dot{\epsilon}'_{ij} \tag{6.2}$$

- Balance of momentum (linear and angular):

$$\frac{Dv_i}{Dt} = f_i + \frac{1}{\rho}\frac{\partial \sigma_{ji}}{\partial x_j} \tag{6.3}$$

where ρ is the material density, v_i is the velocity, I is the specific internal energy, σ_{ij} is the stress tensor, which is composed of a hydrostatic part, the pressure p, and a deviatoric part, Π_{ij}. f_i are the external body forces per unit mass, and $\dot{\epsilon}'_{ij}$ is the deviatoric strain rate tensor. The subscripts represent the standard tensorial notation, and summation is implied by repeated indices [Pierazzo and Collins, 2004].

The equation of state relates the pressure to the density and the internal energy,

$$\text{Equation of state} p = p(\rho, I) \tag{6.4}$$

It thereby can account for compressibility effects thatis, changes in density and irreversible thermodynamic processes such as shock induced heating.

A material when subjected to an external mechanical loading must have a proper mathematical model that describes the mechanical behaviour of the continuous medium. Within the material, the behaviour can be different depending on the loading conditions. To take into account all theses considerations, a suitable set of equations, in which it is ensured that the medium remains continuous and that it relates to different representative variables, must be defined. These equations generally relating stress and strain, represent the material strength model.

These constitutive equations (or material model) describe the intrinsic behaviours of materials. Different models have been developed to describe the wide variety of solid material (like elastic, hyperelastic or viscoelastic or material with damage) behaviour [Rohani, 1977].

The constitutive model that describes the effect of deformation or strength properties, relates the stress to a combination of strain ϵ_{ij}, strain rate effects $\dot{\epsilon}_{ij}$, internal energy I, and damage D,

$$\text{Constitutive model} \sigma_{ij} = g(\epsilon_{ij}, \dot{\epsilon}_{ij}, I, D) \tag{6.5}$$

Analytical solutions [Anderson et al., 1995] to equations 6.1 to 6.5 are only obtainable for circumstances where simplifications can be made, reducing the number of variables to be considered [Anderson et al., 1995]. Numerical techniques, using digital computers, provide the only amenable method to achieve the number of mathematical operations required for obtaining the solution.

Hydrocodes are computational tools for modelling the behaviour of continuous media. All hydrocodes utilise some form of the conservation equations; however, the usefulness of a hydrocode depends on the sophistication of the equations of state and the constitutive models.

6.2 Finite element method

Nowadays, computational methods are highly developed and used in many areas of studies. Computational mechanics plays an important role nowadays since it is an extremely important discipline in the development of new and innovative structures and applications. One of the major factors that puts computational mechanics on such a level is that it complements the experimental part of an investigation and, therefore, it makes it possible to avoid unnecessary experimental work, reducing costs. Not only the reduced costs (compared to experimental analyses) are an advantage of the numerical methods. In situations where non-linearity of the behaviour of the material and complexity of the analytical analysis is high numerical tools are highly relevant. One of the most commonly used methods is the finite element method, which is implemented in the majority of software products for nonlinear dynamic analysis. Users of computational programs have access to libraries containing a wide range of material models, which allow researchers to describe the mechanical response of traditional materials as well as modern

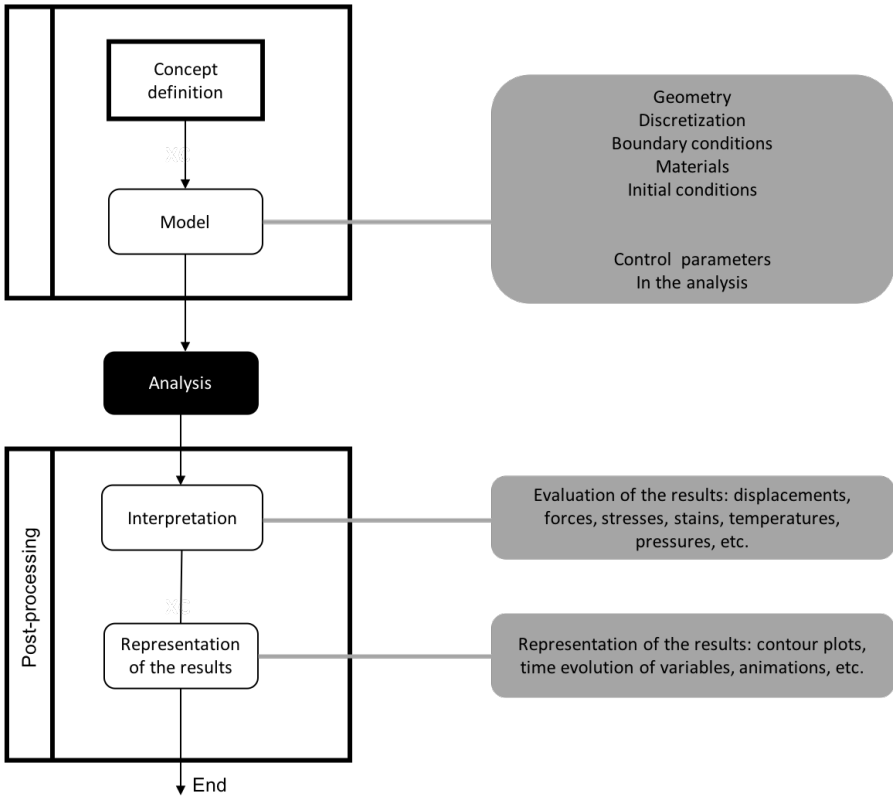

Figure 6.1: Methodology used when solving a FE model (adapted from [Teixeira-Dias et al., 2010]).

and advanced ones. There are plenty of sophisticated models, which take into account a lot of parameters such as deformation, strain rate, temperature, anisotropy, etc. Part of these enable failure of material to be modelled. The above mentioned advantages makes it possible for computational methods to be applied in studies of ballistic resistance.

FEA may be divided into different steps, shown in Figure 6.1 (see, for example, [Belytschko et al., 2014, Zienkiewicz et al., 2013]), of which the main ones are:

1. Pre-processing;
2. Analysis;
3. Post-processing.

In the first step, pre-processing, the spatial domain is divided (discretised) in smaller elements. Each element has nodes associated to it in which physical properties can be determined. Physical properties can also be obtained within elements by means of interpolation. All this information collected in the first stage is computed in the Analysis stage. The problem can, for example, involve obtaining the temporal solution of non-differential equations (this can be achieved through time integration). Two different types of algorithms can be used in the integration: implicit or explicit. The explicit and implicit methods are numerical analysis methods used to solve a time-dependent differential equations. The explicit method calculates the system status at a future

time from the currently known system status and the implicit method calculates the system status at a future time from the system statuses at present and future times [Belytschko et al., 2014].

Finally, the last stage of the finite element method corresponds to Post-Processing where the obtained output from the analysis stage is presented. The information can be presented, for example, by contour plots, tables, history plots, animations and videos, etc. Nowadays, there are several commercial software packages available for FE analysis for solving non-linear structural problems. Several of these packages are already prepared for solving problems either implicitly or explicitly.

6.3 The finite element method applied to impact problems

Predictive numerical tools can be extremely useful for enhancing our understanding of ballistic impact events. Models that are able to capture the key mechanical and thermodynamic processes can significantly improve our understanding of the phenomena by allowing time-resolved investigations of virtually every aspect of an impact event. Impact events are dynamic phenomena characterised by high strain rates, inertial effects and wave propagation effects. These events are often localised but can also manifest large displacements and large strains, and failure or damage to structures. For a better understanding of these phenomena and the different mechanisms involved in the finite element method, numerical tools are increasingly used.

LS-Dyna^{TM} is a general -purpose finite element program developed at the Livermore Software Technology Corporation (LSTC) [LSTC, 2011] capable of simulating complex real world problems. It is used in many fields: automotive, aerospace, civil engineering, military, manufacturing, and bioengineering industries.

6.3.1 Numerical simulations

Generally speaking, the study of ballistic impact on textile reinforced composites can be achieved by three methods, experimental, analytical and numerical methods.

For the experimental methods, the composite ballistic performance, including the ballistic limit, backface signature and depth of penetration need to be measured. This method is considered effective when there are only small numbers of parametric variables to be studied. Although the process of the experimental methods is often time and money consuming, it is still essential for practically evaluating and validating the impact responses of composites. Unlike the experimental method that gives results only according to specific testing conditions, both the analytical and the numerical methods enable the tailoring of predefined parameters for a more comprehensive understanding of the problem. Parameters related to stress and strain, which are difficult to measure during experiments, can be obtained through these methods.

Benefitting from the developments in computer sciences, the numerical methods have become more effective in the prediction and analyses. The numerical analyses are often conducted on commercial finite element packages, including ABAQUS [Barbero, 2013], ANSYS [Barbero, 2013] and LS-Dyna^{TM}.

Numerical methods become increasingly popular when it comes to the simulation and analysis of the ballistic impact on composite structures. In a ballistic impact scenario, the complex interaction between the projectile and the composite, deformation and

failure of the composites can all be simulated by these finite element (FE) packages at a relatively low cost. Also, they allow user-defined material models to be imported when the materials models are not included in the standard material library.

Computational modelling and simulation has since long been considered an invaluable tool for analysing engineering systems in a wide range of technology areas. Significant effort has been devoted in the last few decades to the development of fundamental science, algorithms, simulation software, and hardware infrastructure to assess system's performance and inform potential improvements [Council, 2012]. One main value of computational modelling and simulation in human injury biomechanics is its ability to obtain information in situations in which it is fundamentally impossible to conduct *in vivo* tests on humans. In the particular case of military helmets, evaluation and acceptance protocols are based exclusively on tests that use head surrogates with limited biofidelity. It is therefore clear that modelling and simulation can play a significant role in both improving the understanding of injury biomechanics and guiding the design of protective systems with enhanced injury mitigation performance.

A snapshot of the current state-of-the-art on finite element simulations for impacts on ballistic helmets is presented in the following paragraphs based on a literature review.

Hoof and Worswick [van Hoof and Worswick, 2000] simulated the impact on a Kevlar composite helmet fitted on a simple head model. They used LS-Dyna^{TM} software and the Chang-Chang composite failure model [van Hoof and Worswick, 2000] to consider the failure of the helmet during the impact. Also, Baumgartner et al. considered a head model, including its main anatomic components, and studied the contact between the helmet interior and the skull surface [Daniel and Remy, 2005]. They modelled an aluminium helmet and subjected it to an impact by a steel bullet.

Lee et al. [Tham et al., 2008] conducted experiments where a spherical projectile was launched from a gas gun striking the helmet at 205 m/s. The helmet-projectile interaction was then compared to the AUTODYN-3D simulation conducted with conditions similar to the experments. Results show that the simulations were consistent with the ballistic impact experiments.

Tham et al. [Lee and Gong, 2010] studied, the ballistic impact of a 9 mm full metal jacket (FMJ) projectile using the finite element method, and of an FSP on the PASGT helmet with interior cushioning. In terms of overall protection to the head, the authors concluded that the helmet together with its interior straps offer good protection against small fragments but fared poorly against larger projectiles.

Li et al. [Li et al., 2015] developed a finite element computational model for simulating the ballistic performance of the ACH helmet against a 9 mm full metal jacket projectile, which was validated against experimental data obtained at the Army Research Laboratory (USA) [Li et al., 2015]. The authors present numerical results for the helmet BFD as recorded by the clay in a head form, which match experimental data well. Figure 6.2 shows the numerical results of the deformation pattern at the impact area from inside the helmet shell, the BFD as a function of time and the velocity profile of the impact point with the maximum BFD. The time history of the BFD and the velocity agrees well with the experimental data obtained by Hisley et al. [Hisley et al., 2011], as shown in Figures 6.2(b) and (c).

Aare and Kleiven [Aare and Kleiven, 2007] studied an effect not previously analysed: how different impact angles affects the load levels in the human head. These authors also studied the influence of the helmet shell stiffness on eventual injury levels during

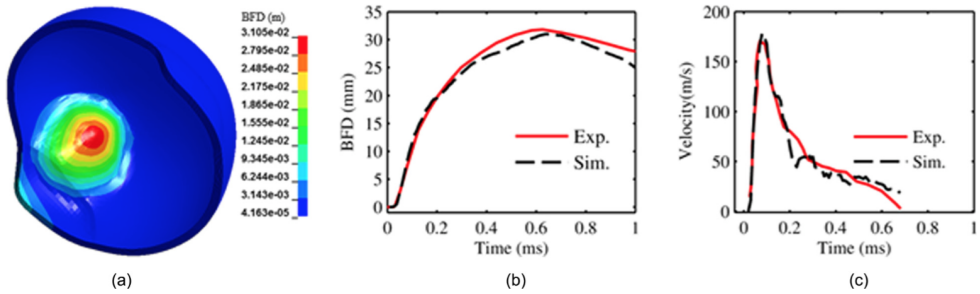

Figure 6.2: (a) BFD seen from inside the helmet shell, (b) BFD time-history, and (c) velocity profile for a 9 mm projectile impact, as obtained by Li et al. [Li et al., 2015].

impacts at different angles, using a 9 mm Parabellum projectile at an impact velocity of 360 m/s. An expected conclusion was that this stiffness is another factor that strongly affects injury levels. These authors state that oblique impacts may cause higher strains in the brain tissue than pure radial ones. Angles close to 45° are the ones leading to higher strains in the brain tissue causing serious lesions [Kleiven, 2006, Kleiven, 2007].

In 2015, Oukara in his PhD thesis [Oukara, 2015] proposed the development of three different approaches allowing the assessment of non-lethal head impacts. In this study, the Force Wall (FW) method links the maximum head impact force to the maximum impact force; a mechanical surrogate and respectively a finite element head model in order to predict the maximum impact head force and injuries were used [Oukara, 2015]. The results show a very good agreement for six different Kinetic Energy Non-Lethal projectiles between the Strasbourg University Finite Element Head Model (SUFEHM) and the mechanical surrogate Ballistic Load Sensing Headform (BLSH) in terms of maximum head impact force.

6.4 FE model pre-processing

As said before the pre-processing phase of the model input is required to solve the problem. Input data includes domain geometry, initial and boundary conditions, coefficients and constants for the particular problem. The overall quality of a finite element analysis depends on how the user approaches this pre-processing stage, including possible simplifications to consider in modelling and in choosing the type of elements and the mesh to be used. Finally, all the loads and constraints that the model submitted to are defined [Teixeira-Dias et al., 2010]. Details about element types and motion description of continuum that can be involved in the application of an FE model are described in this section.

6.4.1 Types of elements

Different types of elements can be used [Hallquist, 2012]. The most frequently used solid elements [Belytschko et al., 2014] are the 4-node tetrahedron and the 8-node hexahedron.

Tetrahedral elements, when compared with the hexahedral, offer obvious advantages in the discretization phase, that is, finite element mesh construction, problems with com-

plex geometry, or even in re-meshing procedures. The usual criticism toward them is that they yield much more unknowns than the quadrilateral and hexahedral edge elements when a similar mesh size is considered. Consequently, tetrahedral element tends to be less accurate in complex problems, thus requiring finer finite element meshes. For this reason, hexahedral elements are more used when the main concern is to obtain reliable results in problems involving loads, boundary conditions and materials with complex mechanical properties, although at the expense of more elaborate meshing mechanisms [Teixeira-Dias et al., 2010]. However, this crude comparison, which is only based on the mesh size, is apparently not justified since different element types produce different accuracies in the solutions, even though the same mesh size is considered.

Hexahedral elements with a single integration point have been known to be efficient in terms of stability and computational cost. They are, however, difficult to generate and meshing can represent a significant part of a model development time [Bourdin et al., 2007]. In recent years, computing power has become affordable and new formulations of tetrahedral elements that can be generated automatically, even for complex shapes, have been introduced in explicit finite element codes. In the present study, only hexahedral elements are used.

6.4.2 Formulation description

In this section the principles of the different formulations used in computational ballistics are discussed as well as the advantages and disadvantages. The Lagrangian formulation, also known as material coordinates, is best suited for solid materials and allows an accurate material interface tracking but suffers from severe distortions under large deformations. This formulation defines that the grid points on a body are unique, i.e. each grid point has different material coordinates. It makes it easy to keep track of material and material flow during a simulation. Contact between different parts is also handled more easily in the Lagrangian formulation as it can be determined as contact between parts with distinct nodes and element edges. As a body undergoes a deformation the nodes are forced to move and the element will be distorted. Severe mesh distortions (e.g. material elements which pass through each other) are a typical difficulty with a classical Lagrangian formulation for example in penetration problems. Remeshing is necessary to obtain a certain level of reliability. The great advantage of the Lagrangian formulation is that small displacements/deformations and material interfaces can be described with high accuracy.

An Eulerian mesh is a“fixed frame of reference” in which material moves from one element to the other and so does mass, momentum and energy. The Eulerian mesh must be large enough in order to model existing as well as future regions where material may flow into. The Eulerian formulation is most frequently used for analyses of fluids or materials undergoing very large deformations. Target and threat materials can undergo such deformations which can make an Eulerian formulation more suitable. In an Eulerian formulation the grid points are fixed in space and elements are also created by connecting these points.

There are other types of formulations besides these two. The Arbitrary Lagrangian Eulerian (ALE) formulation is a generalisation of the Lagrangian and Eulerian approaches. It combines the advantages of both approaches while trying to minimise their respective drawbacks. The computational domain is not attached to the material

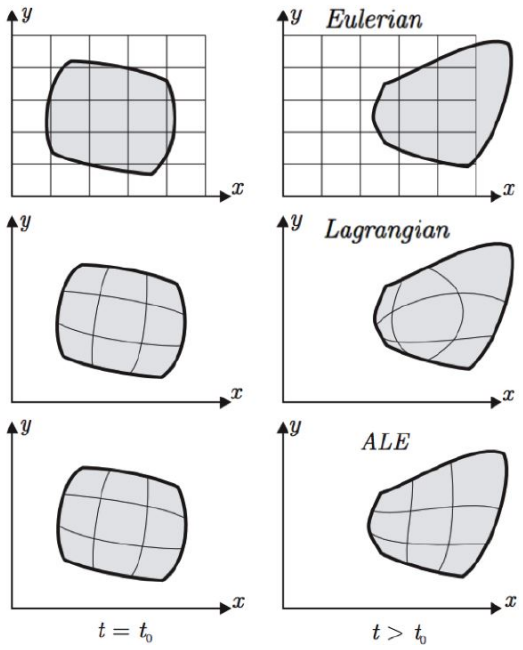

Figure 6.3: Eulerian, Lagrangian and ALE formulation configuration (left) and the deformed (or current) configuration (right) (adapted from [Boman, 2010]).

(Lagrangian) or fixed (Eulerian), but attached to a reference configuration which has an arbitrary motion. The Lagrangian and Eulerian descriptions are therefore special cases of ALE. It is best suited for fluid structure interaction (FSI) [Donea et al., 2004]. Figure 6.3 shows the difference between Eulerian, Lagrangian and the ALE formulations.

It is worth mentioning that depending on the problem, one formulation might be more appropriate than another. In this research Lagrangian formulation was used, since Lagrangian formulation is most appropriate for impact of solid bodies (used in this work) since the surfaces of the bodies will always coincide with the discretisation and are therefore well defined.

Chapter 7

Numerical validation of ammunition and armour models

This chapter describes the validation of the ammunition models and armour materials used in this work. A finite element model with a well developed material model is indispensable in understanding the various nuances of projectile-armour interaction and finding light-weight solutions. To validate the models, numerical and experimental results are compared. To build finite element (FE) models it is necessary to get the correct geometry and the material models of all parts should be obtained, in most cases the most challenging problem.

7.1 Ammunition materials

The goal of the numerical simulation was to validate a finite element model for the FSP 0.22 in, FSP 0.30 in and for the 7.62 × 39 mm projectile using experimental results.

All parts, steel jacket, lead filler, steel core and FSP projectile, were modelled using a Lagrangian approach. Only one quarter of the model was sufficient to simulate the impact process as all simulations had two symmetry planes because only perpendicular impacts were considered. The following sections describe the FSP 0.22 in and FSP 0.30 in and also the validation of the 7.62 × 39 mm projectile against a rigid wall (RW).

7.1.1 Fragment Simulating Projectile 0.22 in and 0.30 in

The material model selected to describe the behaviour of the FSP 0.22 in and 0.30 in projectiles is an elastic-plastic material model with isotropic hardening from the LS-Dyna^{TM} library since this is a very low cost isotropic plasticity model. The model parameters for AISI 4340 steel [Warren et al., 2004] used in the simulation for both FSP are shown in Table 7.1.

The definition drawings and dimensions of the FSP projectiles used in this work are illustrated, in Figures 7.1 and 7.2

Since the properties of AISI 4340 steel are well known [van Hoof and Worswick, 2000] and the projectile is assumed to not deform significantly for the considered impacts cases [Yen, 2002], it was not necessary to validate the FSPs projectiles separately.

Table 7.1: Mechanical properties of AISI 4340 steel for the FSP 0.22 and 0.30 [van Hoof, 1999].

Material	Density [kg/m^3]	Shear modulus [GPa]	Yield stress [MPa]	Plastic hardening modulus [MPa]	Bulk modulus [GPa]
AISI 4340	7860	80	792	685	140

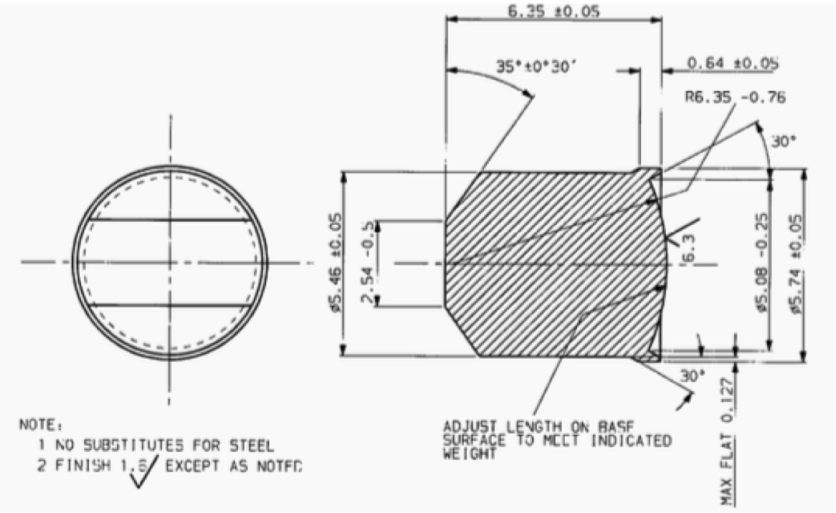

Figure 7.1: Schematic representation of FSP 0.22 in.

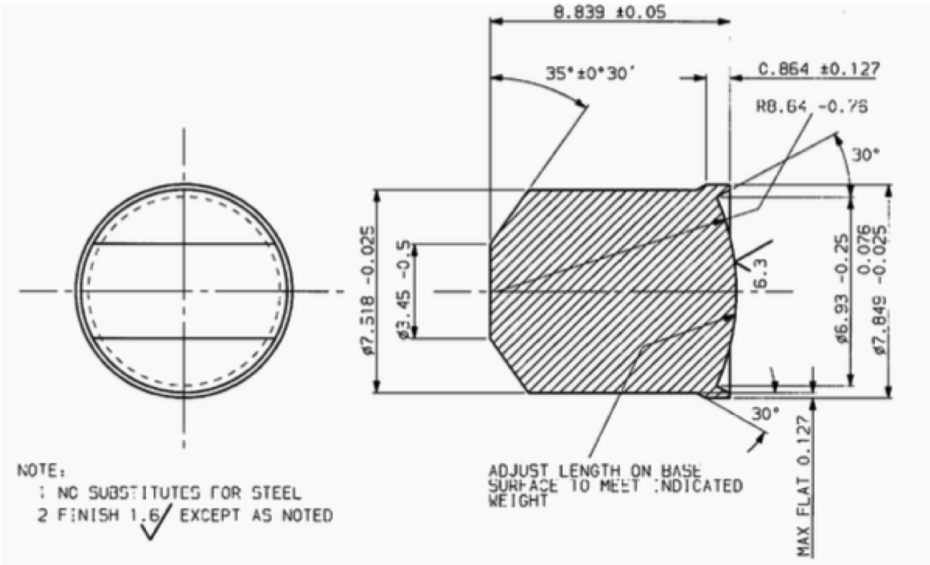

Figure 7.2: Schematic representation of FSP 0.30 in.

7.1.2 7.62 × 39 M43 steel core

The projectile model of the 7.62 × 39 mm ammunition consists of three different parts: a steel jacket, a lead filler and a steel core. The CAD model of the projectile was developed using the commercial package SolidWorks^{TM} and exported to the commercial HyperMesh^{TM} software to create a hexahedral mesh. After creation of the mesh, the model was imported into LS-Dyna^{TM}.

7.1.2.1 Numerical model description

The Johnson-Cook constitutive relation was employed to simulate thermo-mechanical deformations of the steel jacket and the steel core. The lead filler of the projectile was modelled with an elastic-plastic material model with isotropic hardening material model available in LS-Dyna^{TM}.

The Johnson-Cook material constants for the steel jacket and the steel core are listed in Table 7.2 [Karim and Fatt, 2005]. Table 7.3 shows the mechanical properties of the lead material.

Table 7.2: Johnson-Cook material constants for the steel used to model the 7.62 × 39 mm projectile jacket and core [Karim and Fatt, 2005].

Material	Density [kg/m^3]	Shear modulus [GPa]	A [MPa]	B [MPa]	C[-]	m[-]	n[-]
Steel	7800	81	1100	275	0.022	1	0.36
T_{melt} [K]	Specific heat [J.g.K]	D_1	D_2	D_3	D_4	D_5	–
1811	0.452	0.05	3.44	-2.12	0.002	0.61	–

Table 7.3: Material properties of lead [Krishnan et al., 2008].

Material	Density [kg/m^3]	Shear modulus [GPa]	Yield stress [GPa]	Plastic hardening modulus [GPa]	Bulk modulus [GPa]
Lead	11340	5	0.012	0.06	29

As explained previously in Section 5.1.2, two different EOS were used in this work. The linear polynomial EOS is the first polynomial equation coefficient (the elastic bulk modulus) with a value of 140 GPa. The bulk modulus gives a linear relation between hydrostatic stress and change in volume, and does not take temperature into account. The Mie-Gruneisen EOS is a relation between the pressure and the volume of a solid at a given temperature. The used parameters for the Mie-Gruneisen EOS are: the bulk

sound speed equal to 4570 m/s, the Hugoniot linear slope coefficient equal a 1.49, and the Gruneisen coefficient $\gamma = 1.93$, which relates energy and volume to pressure.

Figure 7.3 shows the individual meshed parts of the projectile and Figure 7.4 shows the cross section of the assembly of the three parts. Other characteristics are given on Table 7.4. One of the most common and important criterion for validating a numerical method is convergence. The convergence criterion states that as the model is discretised progressively, the solution should converge on a fixed value. In order to make sure that a given numerical code converges, a mesh convergence study was performed in order to optimise the numerical model. A detailed comparison of different results was carried out using convergence test based on ballistic limit.

Table 7.4: 7.62 × 39 mm projectile characteristics.

Properties	
Diameter [mm]	7.89
Length [mm]	26.78
Mass [g]	7.97
Material type	
Jacket	steel
Filler	lead
Core	steel

For the numerical validation of the projectile, experimental impact tests of the projectile against a rigid wall have been performed. Six velocities were considered for the validation process, between 200 to 700 m/s.

An eroding single surface contact available in LS-Dyna^{TM}[Hallquist, 2012] is defined between all parts of the projectile to prevent interpenetrations between elements in the initial configuration.

7.1.2.2 Experimental setup and tests

As in most scientific projects, the theoretical component should be, whenever possible, accompanied by experimental tests that validate the theoretical models. All the experimental tests were carried out at the Department of Weapon Systems and Ballistics at the Royal Military Academy (Belgium). All numerical models were validated based on experimental tests. In order to study the deformation of the core, often the projectiles were fired with a universal receiver with interchangeable barrel (BMCI) against a rigid target. The velocity of the projectiles was varied by adapting the propellant mass. The distance between the muzzle and the target was sufficient to eliminate the influence of the intermediate ballistics. The experimental setup is shown in Figure 7.5.

A rigid wall was used to focus on the deformation behaviour of the projectile core. The rigid target consisted of an 12 mm thickness SSAB Armox 500T [SSAB, 2016] steel armour plate. No significant bulging or damage to the armour plate was observed after the testing.

The projectile core is the only part that can be recovered as the jacket and the filler part are destroyed. The residual length and mass of the recovered cores were measured.

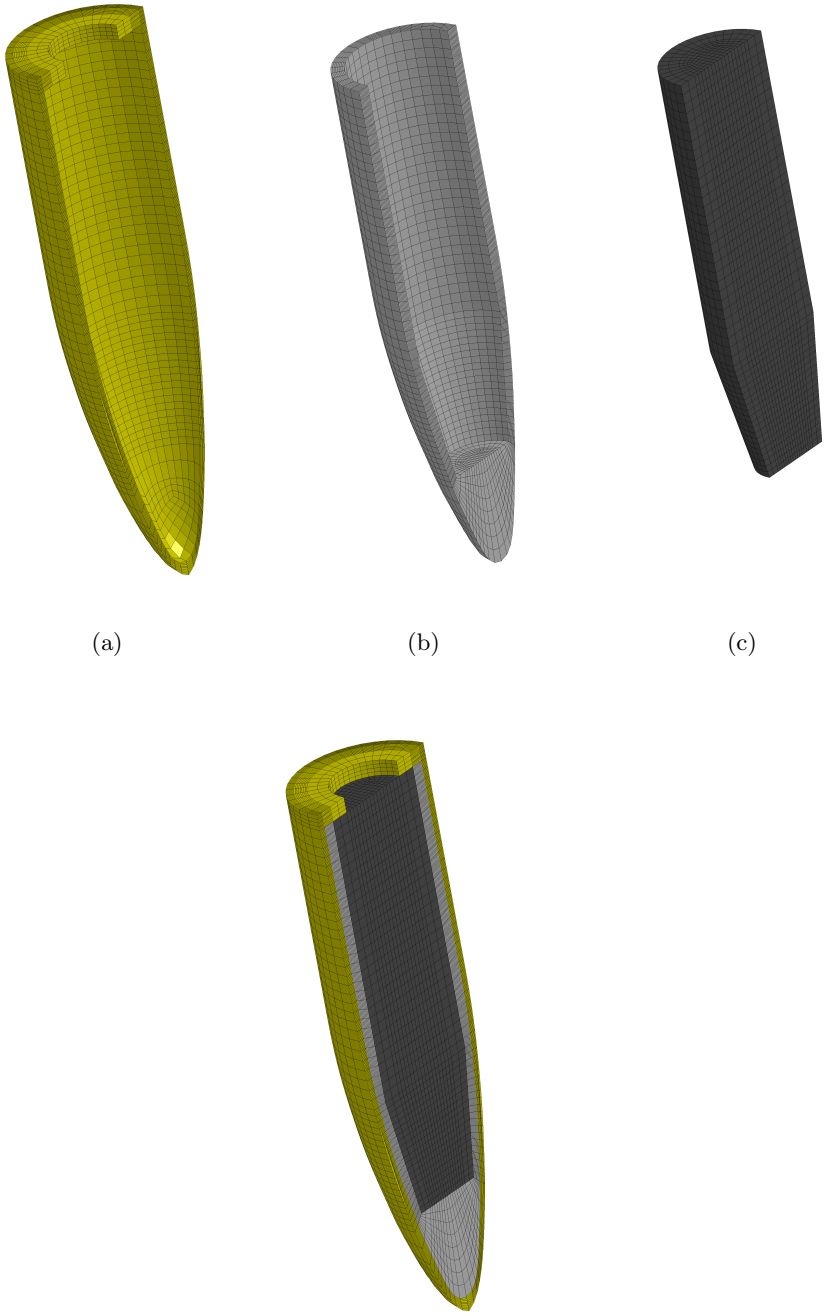

(a) (b) (c)

(d)

Figure 7.3: Numerical model of the 7.62 × 39 mm projectile: (a) steel jacket; (b) lead filler; (c) steel core and (d) assembly.

Consequently, the validation of the numerical results are based on the projectile core.

When impacting on the rigid wall, the core of the projectile suffers deformation

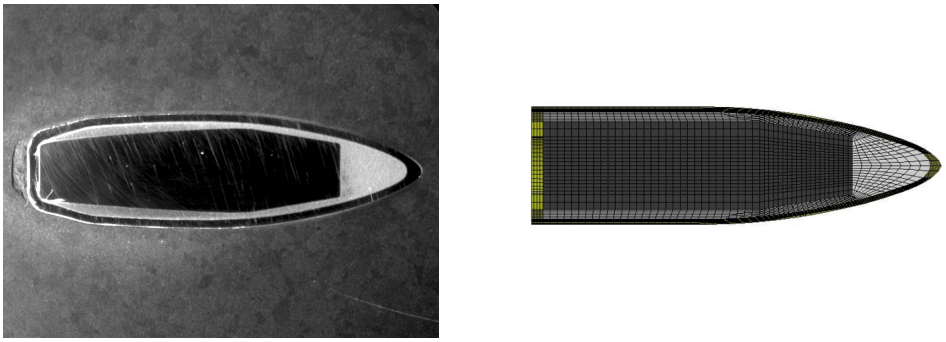

(a) (b)

Figure 7.4: Cross section of 7.62 × 39 mm projectile: (a) real; (b) numerical.

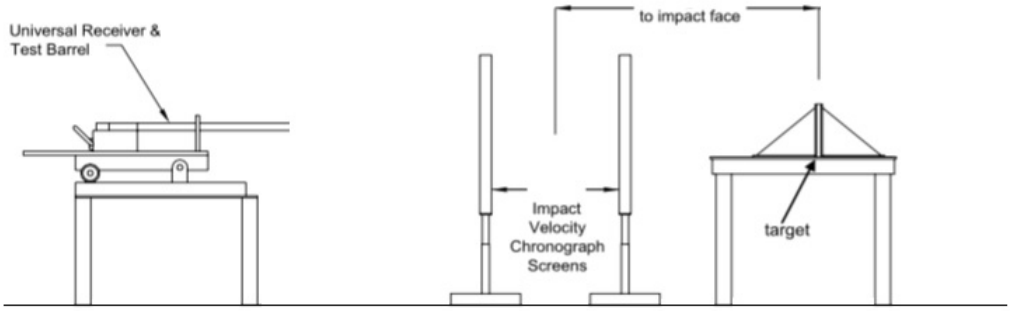

Figure 7.5: Schematic representation of the experimental setup for the ballistic impact tests.

and loss of mass, depending on its impact velocity. The core deforms into a flat shape following the flat geometry of the surface of the steel plate. Almost all the energy is used in deforming the projectile and increasing its temperature [Meyers, 1994].

7.1.2.3 Results and validation

A parametric study of the core model has been carried out to find the optimal model parameters that fit the experimental results. In order to evaluate the possibility to reduce the simulation time, two different approaches were followed. A first approach consisted of taking into account the thermal part of the Johnson-Cook material model, while a second one neglected the thermal effects, reducing the computational cost of the simulations.

Figure 7.6 shows the numerical projectile core length results for the two different approaches (with and without thermal effects), together with the experimental results. Both numerical approaches follow the same tendency as the experimental results.

Figure 7.7 shows the relative difference between the experimental and numerical results for the residual length of the projectile core after impact as a function of initial velocity. The results are shown for both numerical approaches (with and without thermal effects) and compared to the experimental results. As can be seen, both numerical approaches follow the same tendency as the experimental results. Accordingly,

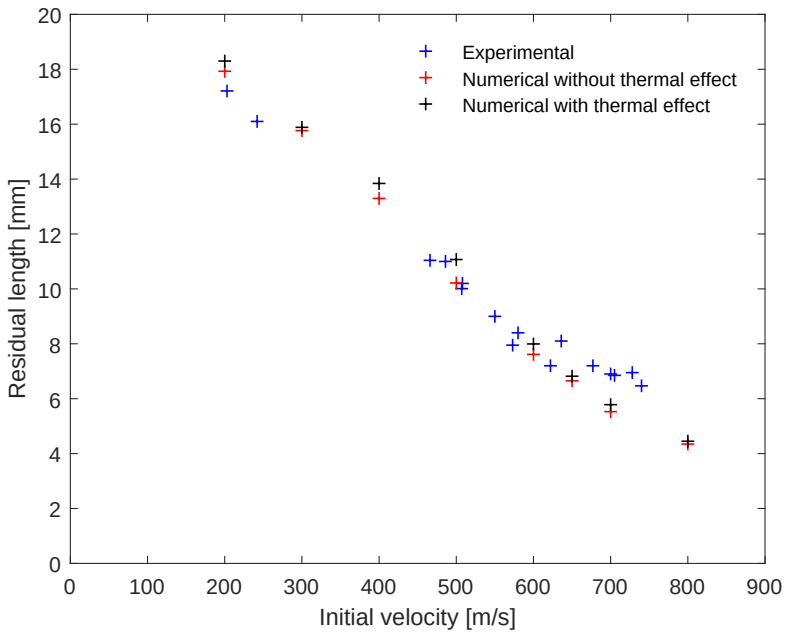

Figure 7.6: Residual length (numerical), with and without thermal effects, as a function of impact velocity.

the simulations were done neglecting the thermal effects. A simulation considering the thermal effects needs 3 times more time than without the thermal effects. For impact velocities outside the regular ordnance velocities of the considered projectile (see Figure 7.7 for an impact velocity of 800 m/s), the error rapidly increases to large values (more than 20%), showing the importance of not using the aforementioned material models outside the regular projectile velocity range without additional validation.

A comparative study about the effect of the choice of EOS on the results was also conducted. Figure 7.8 shows the numerical and experimental results in terms of residual mass as a function of the impact velocity and Figure 7.9 shows the numerical and experimental results in terms of residual length as a function of the impact velocity. In terms of residual mass the relative error between the two EOS were calculated. A quadratic trend was found to fit well to the experimental results (Figure 7.8). The relative error was smaller for the Gruneisen EOS in terms of residual mass. For the residual length (for both numerical simulation) the relative error was also estimated. In this case, results are identical, as can be seen in Figure 7.9.

The deformation of the projectile core is shown in Figure 7.10 for different impact velocities against a rigid wall for experimental and numerical tests, respectively. The numerical results are again very similar to the experimental results. For this study, the numerical simulations were done without thermal effects and using the Gruneisen EOS.

Modelling results were found to be in good agreement in terms of residual core length and mass and also the core projectile shape with the experimental tests. In all cases the relative error compared with the experimental tests is less than 12%. The validated projectile finite element model can now be used to study more complex impact problems where experimental measurements are complex or impossible.

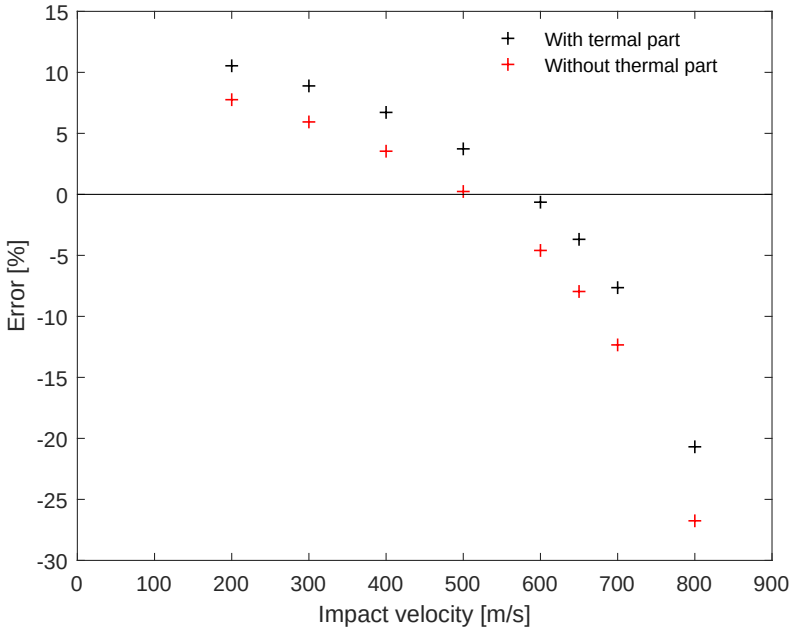

Figure 7.7: Relative diference of the numerical simulations (with and without thermal effects) in comparison with the experimental results as a function of impact velocity.

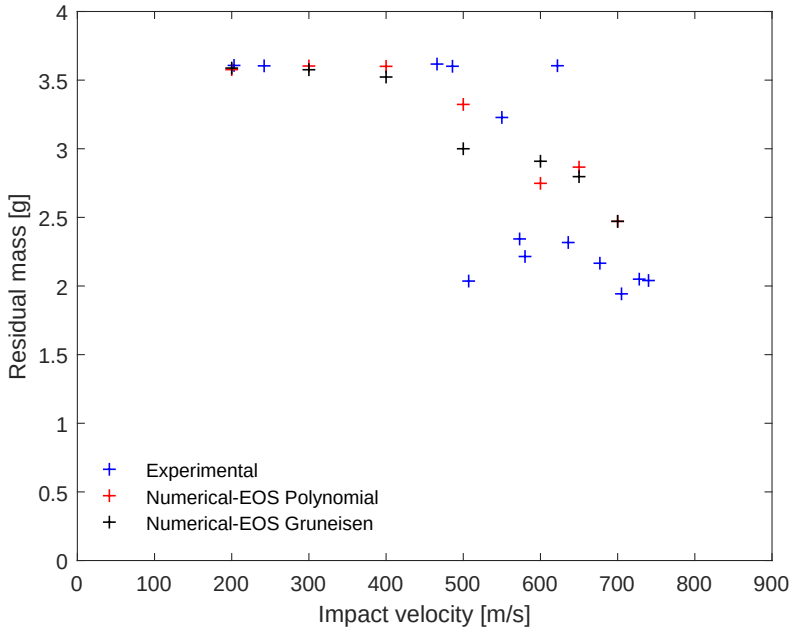

Figure 7.8: Residual mass for numerical simulations (Polynomial EOS and Gruneisen EOS) and the experimental results as a function of impact velocity.

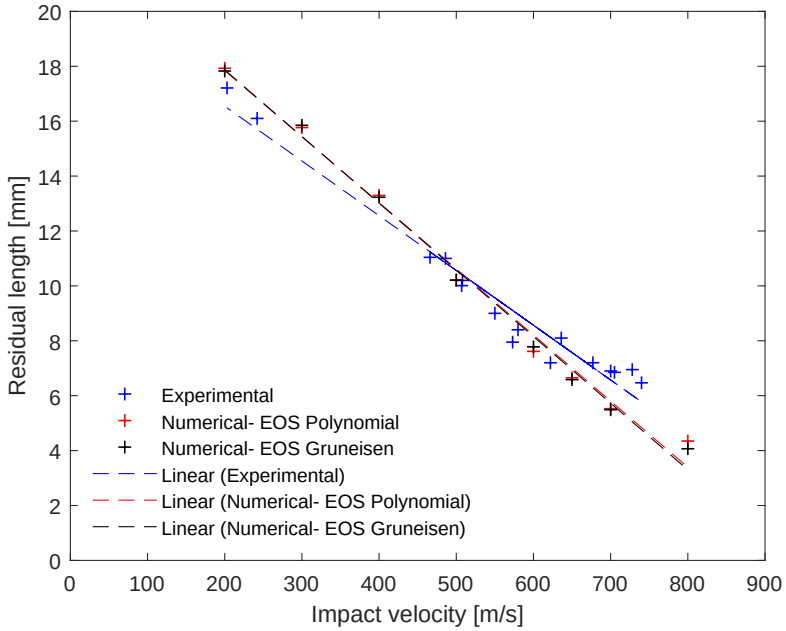

Figure 7.9: Residual length for numerical simulations (Polynomial EOS and Gruneisen EOS) and the experimental results as a function of impact velocity.

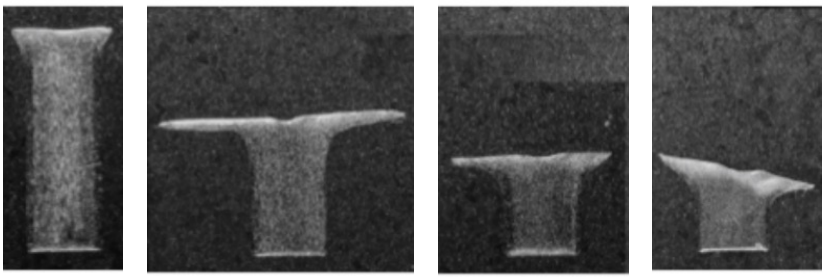

(a) 203 m/s (b) 466 m/s (c) 622 m/s (d) 740 m/s

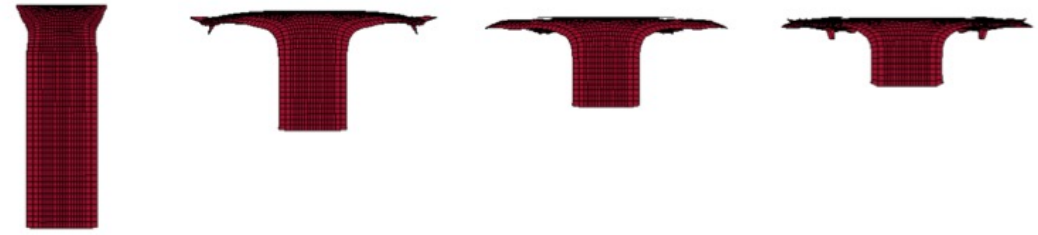

(e) 200 m/s (f) 500 m/s (g) 600 m/s (h) 700 m/s

Figure 7.10: Deformed projectile core after impact against a rigid wall at different impact velocities: (a) to (d) experimental and (e) to (h) numerical.

7.2 Numerical model of armour materials

In this section the numerical simulations of the armour materials are described.

7.2.1 Dyneema HB80

Modelling the response of fibre-reinforced composites under impact loading is challenging because of the complexity of the material composition and the many failure modes it exhibits at different scales (fibrillation, intra- and inter-laminar failure, etc.) and different impact regimes. For this reason numerical simulation of impacts using hydrocodes was exclusively performed on isotropic materials until the late 1990s [Ramezani and Rothe, 2017]. Since then, there have been many advances in modelling composites brought about by the introduction of more accurate constitutive models and modelling techniques. In general, fibre-reinforced composites can be modelled at three different scales, as shown in Figure 7.11 [Meyer and Mayer, 2011].

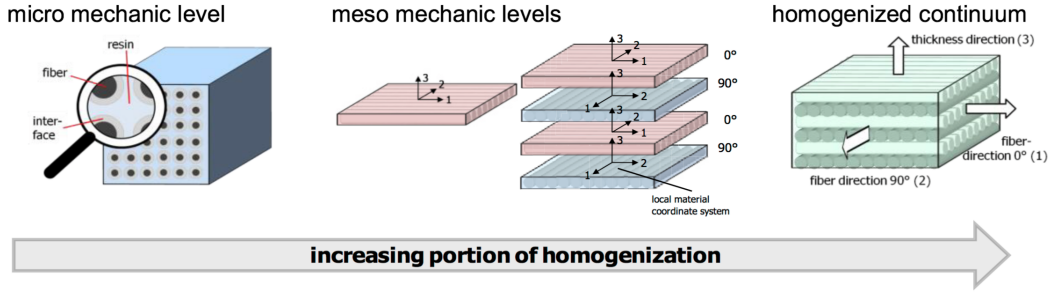

Figure 7.11: Different scales of modelling for fibre reinforced composites (FRC) (adapted from [Meyer and Mayer, 2011]).

- Micro-scale, where the individual fibre, matrix and (in some cases) the fibre-matrix interface is explicitly modelled;
- Meso-scale, where the properties of the individual plies that are homogenised in the fibre directions are modelled and stacked together to produce a laminate;
- Macro-scale, where the laminate is modelled as a continuum and the properties of the laminate are homogenised in the principal directions.

Modelling of fibre-reinforced composites at the micro-scale has several important advantages. This includes increased model fidelity, relatively simpler constitutive equations to describe the fibre, matrix and the interface, and characterisation tests that are relatively easy to perform [Ramezani and Rothe, 2017]. However, at this scale models require explicit modelling of every single fibre, matrix and the interface, which is computationally extremely expensive and not practical for typical engineering problems. While the meso-scale approach is far more computationally tractable compared to the micro-scale, models at this scale are still not practical for thick targets, which is the focus of this thesis. With the increasing development of high speed computers however, some researchers have modelled UHMWPE composite plates under ballistic impact at the micro- and meso-scale levels very recently [Segala and Cavallaro, 2014, Chocron et al., 2014].

Segala and Cavallaro [Segala and Cavallaro, 2014] used a micro-scale approach to model UHMWPE composite under blast and ballistic loading. The fibre and matrix were modelled explicitly for two plies, but the scale of the fibres was increased and the overall model dimensions were small due to the size of the computational model. Chocron et al. [Chocron et al., 2014] used a micro-meso scale approach where the fibres were bundled into strips which were connected to strips of matrix material. These fibre and matrix strips were arranged into a ply and multiple plies were generated to form a laminate. This approach is more computationally tractable, but increased scaling of the fibre bundle strips was still required in the thickness direction to make the model solvable within a reasonable period of time for a moderate target thickness ($\sim$11 mm). Although valuable to understand the mechanisms of penetration at the micro- and meso-scale, these approaches are still impractical for modelling thick UHMWPE composite. Approaches based on macro-scale modelling present a more practical alternative to solve typical engineering problems. However, the complexity of the constitutive equations and characterisation tests necessary to describe an anisotropic material at a macro or continuum level increases significantly. Nonetheless, this approach has historically been a more feasible and widely adopted method for modelling UHMWPE composites under impact. Iannucci et al.[Iannucci et al., 2009] proposed in 2009 a plane stress material model that includes separate matrix and fibre failure and a polynomial description of the non-linear in-plane shear behaviour. The model showed good global deformation behaviour for thin targets impacted at approximately 350 m/s. Burger et al. [Burger et al., 2012] proposed a progressive failure model to predict the structural response of Dyneema composite. The model included a description of fibre failure in tension/compression, inter-fibre failure, and in-plane shear failure. The lack of a delamination model however, led to poor predictions of deformation. Grujicic et al. [Grujicic et al., 2008] proposed a multi-scale approach to model composite laminates. In this approach, a unit cell model was coupled to a continuum model for which the continuum model was used to update the deformation state of the unit cell, which in turn was used to compute the material stress state. Validations against ballistic experiments from Iremonger [Iremonger, 1999] showed good agreement with the target deformation. Other continuum models for composites have also been reported by Gama et al. [Gama and Gillespie Jr., 2011] and Beissel [Beissel, 2014], although these models have yet to be applied to UHMWPE composite.

7.2.1.1 Numerical model description

The goal of the numerical simulations was to validate a material model for the Dyneema HB80 composite material using results from experimental tests. The experimental setup consisted of a universal receiver with an interchangeable barrel (BMCI) system. The calibre used is the FSP 0.30 as defined in STANAG 2920 standard. As the goal was only to validate the numerical behaviour of the composite panel, the geometry of the FSP 0.30 projectile was simplified into a right circular cylinder (RCC) keeping the same mass and the same diameter. All tests were conducted in accordance with STANAG 2920 [NATO Standardization Agency, 2016], as shown in Figure 7.12. Figure 7.13 shows an example of a Dyneema plate (real and numerical model) used in this work. A sideview of the numerical model is shown in Figure 7.14. All parts (i.e. projectile and targets) were modelled using a Lagrangian meshes. One quarter of the model was

sufficient to simulate the impact process as all simulations had two symmetry planes. In all cases, the different layers of the armour package were simulated with fixed edges on all four sides, corresponding to the clamping condition in the STANAG 2920 support.

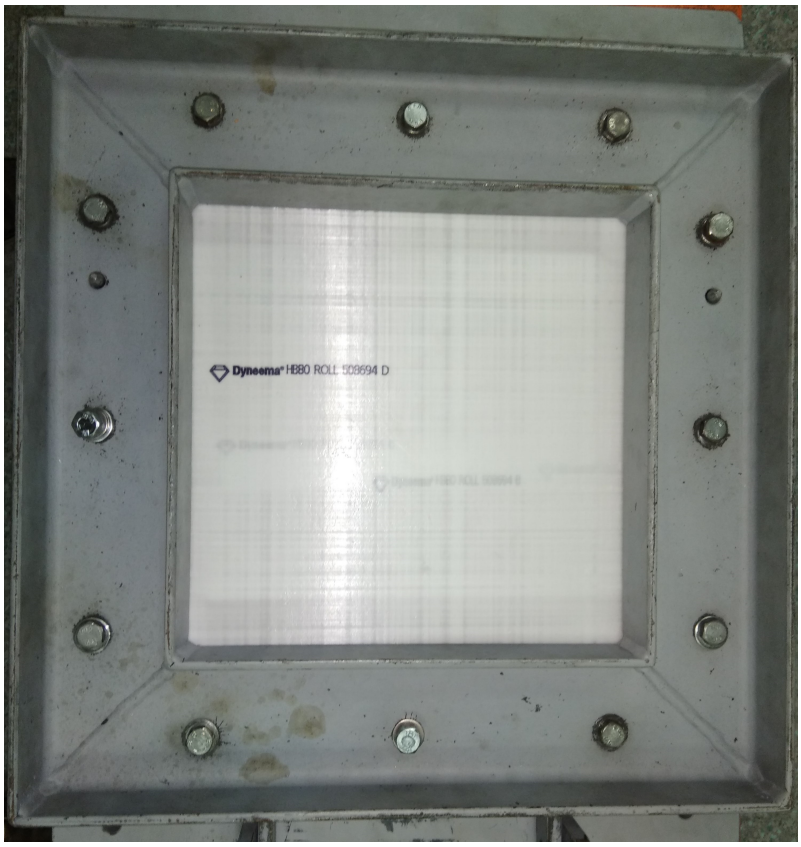

Figure 7.12: Experimental front view setup of Dyneema plate attached to a STANAG 2920 support.

The simulated Dyneema HB80 composite plates had thicknesses of 5 and 7 mm according to the modelled configuration. The given thicknesses are approximate, as in the simulations the plates were modelled as a layup of the individual plies, as is the case for the real panel. The thickness of an individual ply (typical thickness 0.148 mm) was hence used instead of the nominal thickness of the plate. By multiplying the ply thickness with the number of plies for each panel thickness (34 and 49 plies) one retrieves approximately 5 and 7 mm, respectively. Although in the real material, each ply consists of four unidirectional laminate sheets arranged in a 0°/90°/0°/90° configuration, the simulated plies were modelled as orthotropic laminates using the orthotropic simplified damage material model. Cross-plies have been homogenised to represent the composite layup as a sub-laminate, and these sub-laminates are then stacked and separated by a tied contact. Figure 7.15 shows a schematic representation of sub-laminate homogenisation.

The main parameters of this material model are presented in Table 7.5. The selected failure criteria was tensile strain in the plane of the plate.

One main problem with Lagrange formulation is the large distortions once the grid distorts with the material, leading to the reduction of the element size. When the element

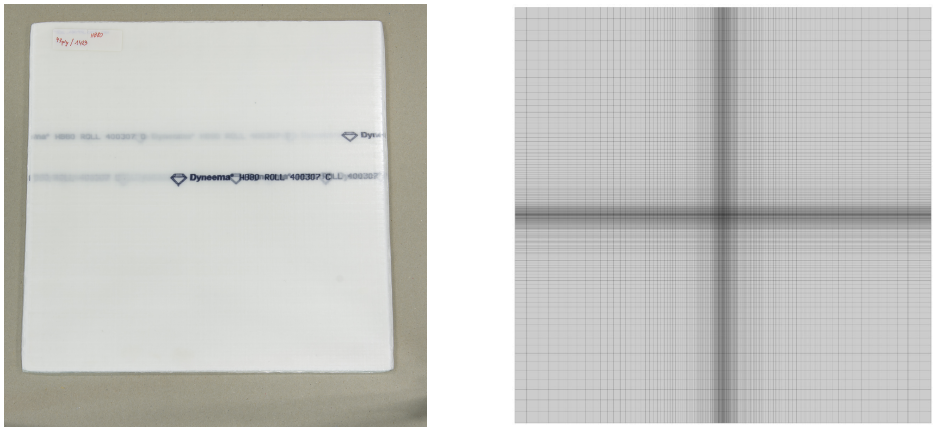

(a) Experimental (b) Numerical

Figure 7.13: Example of the 400 x 400 [mm^2] Dyneema plate: (a) experimental and (b) numerical.

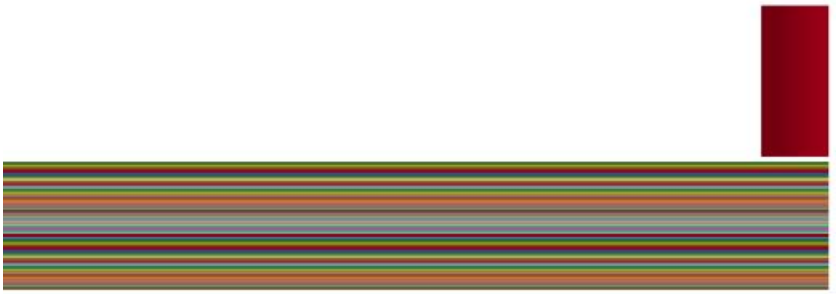

Figure 7.14: Sideview of the numerical model of Dyneema with the projectile.

Table 7.5: Mechanical properties of Dyneema HB80 [Heisserer, 2011a, Heisserer, 2011b].

Properties	
Young's modulus x- and y- direction [GPa]	56.32
Young's modulus z- direction [GPa]	5.99
Poisson's ratio xz- and yz- direction	0.5183
Poisson's ratio yx- direction	0.0269
Shear modulus zx- and yz- direction [GPa]	0.4
Shear modulus xy- direction [GPa]	0.89
Tensile strain at failure x- and y- direction	0.06

size tends to zero, the time step also tends to zero, due to which, little progress is made

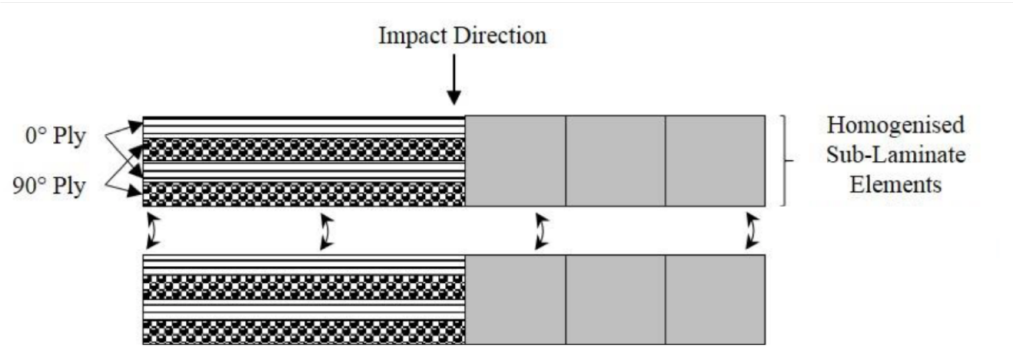

Figure 7.15: Schematic representation of sub-laminate homogenisation: left part is a sketch of the real situation with orthogonally oriented uni-directional layers and the right part is the concept used for finite element modelling (adapted from [Hazzard et al., 2018]).

with each time step leading to excessive use of computational resources what can lead to numerical instabilities. In order to delete the elements that can cause these instabilities, erosion algorithms are used.

An erosion algorithm is available in LS-Dyna^{TM}, which allows for penetration and perforation by eroding elements from the projectile surface as well as the target structure. Numerical erosion is a possible solution for both compressive and tensile failure. In this numerical model, the erosion criterion was only applied to the composite part. The erosion is modelled based on the criterion that elements do not contribute to the physics of penetration if their effective plastic strain and the equivalent stress reaches a critical value (which is defined as erosion strain and erosion stress in LS-Dyna^{TM}). If an element shares nodes with another element at the surface and satisfies the criterion, then the stresses in it are brought to zero and the element is eroded away and eliminated from the mesh. However, using this algorithm there are no conservation of energy or mass. The mass and energy of the deleted element is either removed or distributed to the corner nodes of the adjacent element. The default option of the software is deletion of mass upon erosion and is used in this study. Upon erosion, the sliding interface between the projectile and the target is re-defined dynamically due to total element failure. In other words, computation can be carried out without the need for re-zoning distorted regions of the mesh during the penetration process.

During impact, contacts occur between the different Dyneema layers, influencing the whole dynamics of the composite part. As in the material model, it is important to choose the correct contact model in order to determine the forces developed at the body interfaces to adequately capture the deformations.

The definition of how each layer of Dyneema HB80 interacts with one another is very important and is done by defining material (part) contacts. There are several contact models available in the library of the LS-Dyna^{TM} software that may be used to describe the interaction between the different plies of the composite plate. The contact automatic surface to surface was selected from the LS-Dyna^{TM} contact library and is well suited for nodes that are initially in contact through an adhesive layer. The normal failure stress and the shear failure stress were the two criteria chosen for this contact, introducing the delamination of the composite plates due to through-thickness tensile and in-plane shear

loads. The possible delamination between adjacent plies (layer) of the UHMWPE fibre layers has been modelled using the interface strength-based cohesive zone mode given below. The delamination ensues at the point when:

$$\left(\frac{|\sigma_{\mathrm{n}}|}{S_{\mathrm{n}}}\right)^2 + \left(\frac{|\sigma_{\mathrm{s}}|}{S_{\mathrm{s}}}\right)^2 \geq 1 \tag{7.1}$$

where σ_{n} and σ_{s} are the current normal and shear stresses, respectively, and S_n and S_s the interlaminar normal and shear strengths. In the cohesive zone mode, when the relative displacement either in the normal or in the tangential direction reaches a critical value, complete separation/sliding occurs there. The interlaminar normal strength of Dyneema HB80 is S_n =0.015 GPa and the shear strength is S_s= 0.05 GPa.

7.2.1.2 Results and comparison

The numerical models were correlated with experimental data reported by Miranda-Vicario [Miranda-Vicario et al., 2014]. The material types and dimensions as well as the boundary conditions used in the computational models were the same as those reported in the aforementioned experimental studies. A well known criterion in ballistics was used to validate all armour materials using numerical simulations and to compare then with the experimental results, based on the experimental tests is the ballistic limit, typically denoted as the V_{50}, which is the velocity of the bullet at which 50% of the shots are expected to perforate and 50% are stopped by the armour. There are different methods to calculate the ballistic limit. The most well know are the STANAG 2920 Ed. 1 method [NATO Standardization Agency, 2016], the Probit method [Hahn and Soyer, 2005] and the Kneubuehl method [Kneubuehl, 1996].

The experimental and numerical V_{50} was determined for single Dyneema HB80 panels with thicknesses of 5 and 7 mm. The numerical V_{50} was obtained by taking the average velocity of the highest non-perforating impact velocity and the lowest completely perforating impact velocity in a 10 m/s velocity interval. Good agreement (less then 10% difference) was obtained between the numerical and experimental data, although the numerical V_{50} values were below the experimental values and outside a 95% confidence interval (CI) determined using the Probit method. This is however, deemed acceptable for the future helmet concept as it leads to a conservative design and the error is less than 6%.

Table 7.6: Ballistic resistance of the single Dyneema HB80 plates.

Armour thickness [mm]	V_{50} STANAG experimental [m/s]	V_{50} Probit (IC 95%) experimental [m/s]	V_{BL} numerical [m/s]
5	506	495 (481-509)	475
7	636	628 (626-646)	610

7.2.2 Silicon Carbide

The impact of a projectile on the surface of the ceramic material generates compressive shock waves that propagate through the ceramic plate [Kaufmann et al., 2003]. The ceramic material fractures if the magnitude of the reflected tensile wave exceeds the dynamic tensile strength of the material. Radial cracks are formed at the bottom of the ceramic material due to the initial impact and travel from the bottom to the top of the ceramic plate, as can be seen in Figure 7.16.

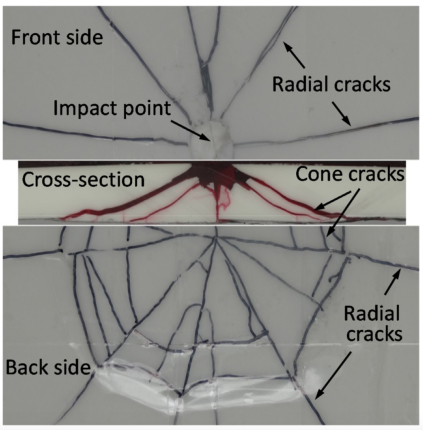

Figure 7.16: Three views of a ceramic material with different damage mechanisms [Rahbek et al., 2017].

In the case of a composite armour system where the ceramic tile is backed by a ductile material, part of the compressive wave may be transmitted into the ductile backing and part is reflected back into the ceramic plate. The magnitude of the stress waves that are transmitted depends on the mechanical impedance of the materials.

The particular importance of the impact response of ceramics is the low/negligible ductility exhibited under both quasi-static and dynamic loading, and the influence of hydrostatic pressure on the strength of the material [Johnson and Holmquist, 1994]. Two distinct responses can be identified when a ceramic material is subjected to a dynamic impact. The first phase begins upon impact where a compressive stress wave initiates at the impact side and travels radially outwards from this point [Den Reijer, 1991, Kaufmann et al., 2003]. The compressive stress wave velocity, determined by the shock response of the material, may greatly exceed the elastic wave velocity for a given impact. If the magnitude of the compressive stress wave exceeds the local dynamic strength of the material, damage begins to accumulate through the formation of cracks. This fracture front travels at the elastic wave speed in the material and forms a conoid of comminuted or pulverised material under the impact location. When the compressive stress wave reaches a free surface of the ceramic it reflects as a tensile wave and may lead to the formation of spall (tensile cracking) damage if the dynamic tensile strength of the ceramic material is exceeded. The second phase of impact corresponds to large scale deformation and erosion of the ceramic and/or projectile. This phase occurs over much larger time scales (typically milliseconds) and terminates when the projectile penetrates or is arrested by the ceramic.

Material models should be able to represent the evolving macro-mechanical material

properties which result from the detailed and complex micro-mechanical structure.

7.2.2.1 Numerical model description

In order to validate the ceramic plate a numerical model was prepared. Due to the brittle properties of the ceramic, a multi-component armour target such as a hard faced ceramic armour with a composite backing was used. For the ammunition, a FSP 0.22 projectile was used. The target consisted of a 4.2 mm thick tile of silicon carbide (SiC) supported by a 5 mm plate of Dyneema HB80.

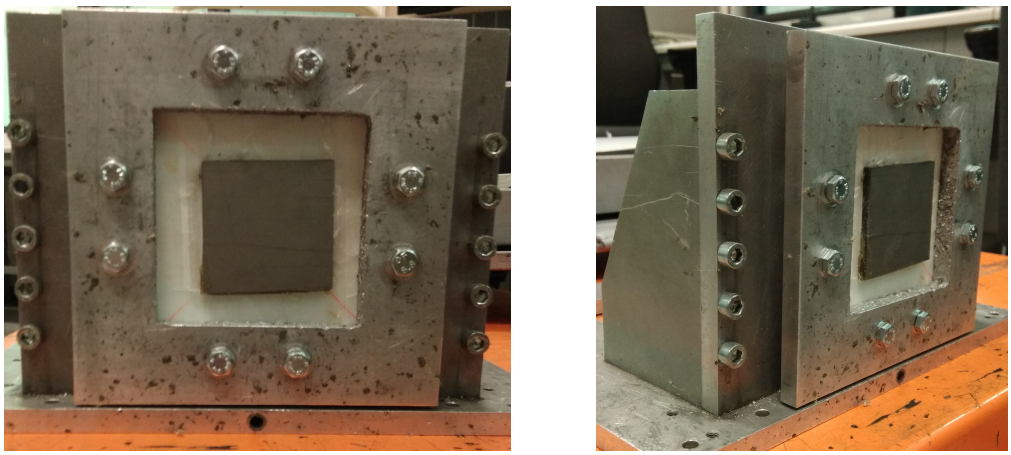

(a) (b)

Figure 7.17: Experimental setup of a SiC tile supported by a Dyneema plate attached to a support rig.

One of the most widely used models for ceramic materials in the ballistic research field is the Johnson-Holmquist model because of its relatively easy implementation. In this work the Johnson-Holmquist-2 (JH-2) model was used to simulate the ceramic material. The JH-2 model has intact and failed material curves, but the model is gradually softened as damage accumulates and it gradually increases the bulking pressure as the damage accumulates [Johnson et al., 2003, Anderson et al., 1995].

The composite material (Dyneema HB80) was modelled with the same material model used in section 7.2.1. The relevant material properties of SiC are listed in Table 7.7.

For the numerical analysis, the Lagrangian approach is used to simulate the projectile impact on the target. Both plates composing the armour system and also the projectile are modelled with eight-nodes hexahedron solid elements. Due to the symmetric nature of the problem, only one quarter of the projectile-armour system is modelled in the present research. The ceramic material is modelled using an element size of 0.21 mm along all three directions in order to reproduce in a constant and progressive way the possible damage. In the case of the composite material there is no such problem, therefore a progressive mesh in the plane direction was used. Figure 7.18 shows the numerical discretisation of SiC and Dyneema target.

The modelled SiC plate had dimensions of 50×50×4.2 $[mm^3]$, and the composite plate had 100×100×5$[mm^3]$. Figure 7.19 represents the experimental and numerical

Table 7.7: Mechanical properties of silicon carbide (SiC) [Cronin et al., 2003].

Properties	
Density ρ [kg/m^3]	3163
Shear modulus [GPa]	183
Strength constant A	0.96
Strength constant B	0.35
Strength constant C	0.0
Strength constant M	1.0
Strength constant N	0.65
Reference strain rate $\dot{\varepsilon}^*$ (EPSI) [1/s]	1
Tensile strength (T^*) [GPa]	0.37
Hugoniot elastic limit (HEL) [GPa]	14.57
P_{HEL} [GPa]	5.9
Damage constant D_1	0.48
Damage constant D_2	0.48
Bulk modulus K [GPa]	204

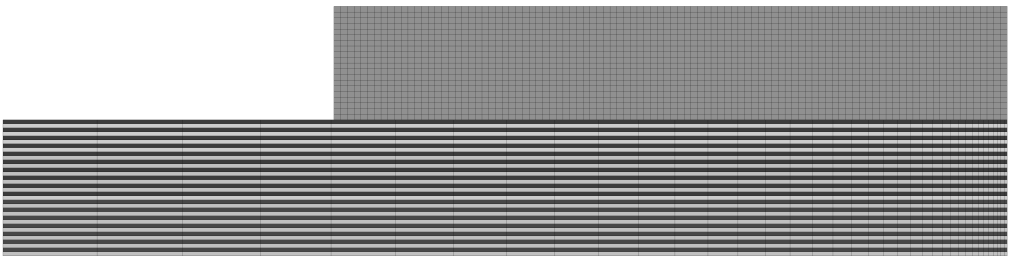

Figure 7.18: Discretisation of SiC and Dyneema target.

target. As can be seen on the real sample, an adhesive was used to connect the ceramic to the Dyneema plate. In the numerical model, a contact tied surface-to-surface is used to connect the ceramic and the composite layer. The interface between the projectile and armour material is defined with a eroding surface-to-surface contact.

7.2.2.2 Results and comparison

The material dimensions as well as the boundary conditions used in the computational models were the same as reported by Ernotte and Colens done at the Royal Military Academy of Belgium [Ernotte and Colens, 2011]. In this master thesis a set of experimental tests using different materials and configurations were done in order to improve (based on the ballistic limit values) the ballistic helmets. To validate the numerical model of silicon carbide the aforementioned experimental study was used. The material properties used in the analysis for the projectile and for the composite material were presented in the previous sections. The experimental ballistic limit was calculated using two different methods: the STANAG 2920 and the Kneubuehl [Kneubuehl, 1996] methods. In the latter, a minimum number of 12 shots are required. The difference

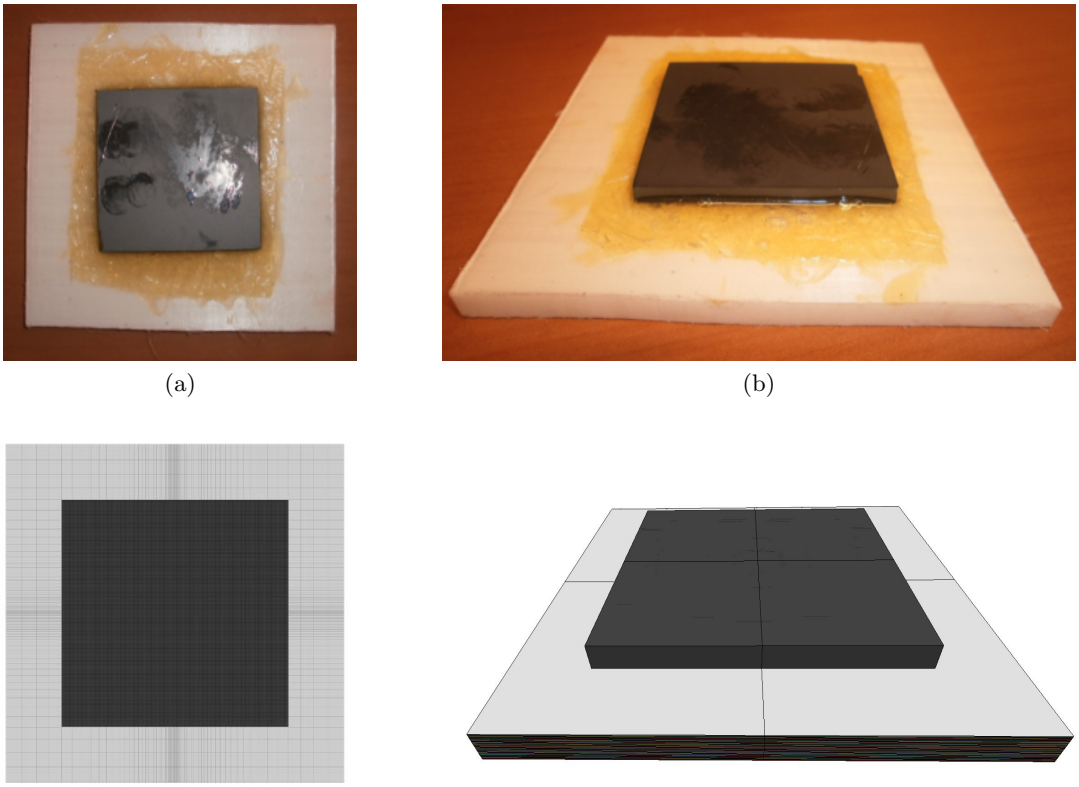

(a) (b)

(c) (d)

Figure 7.19: Experimental (top) and numerical (bottom) SiC and Dyneema HB80 target.

between this method and the V_{50} determination according to STANAG 2920 is that the Kneubuehl method takes the standard deviation into account. By doing so, the threshold velocity is determined as a function of the impact velocity instead of determining only one specific threshold velocity V_{50}. By using the Kneubuehl method, not only the V_{50} is established but also the sensitivity for decreasing or increasing the impact velocity (shooting distance). Table 7.8 lists the experimental and numerical ballistic limit of SiC and Dyneema HB80 target against FSP 0.22.

Table 7.8: Ballistic resistance of SiC and Dyneema HB80 target against FSP 0.22.

V_{50} STANAG experimental [m/s]	V_{50} Kneubuehl experimental [m/s]	V_{BL} numerical [m/s]
1296	1286	1248

The simulation results in terms of ballistic limit were in good agreement with the experimental values. When comparing the numerical ballistic limit with both experimental values there is a difference of less than 4%. Figures 7.20 and 7.21 show snapshots of the numerical simulation of the projectile impacting against a SiC tile and Dyneema HB80 backing without and with complete perforation, respectively.

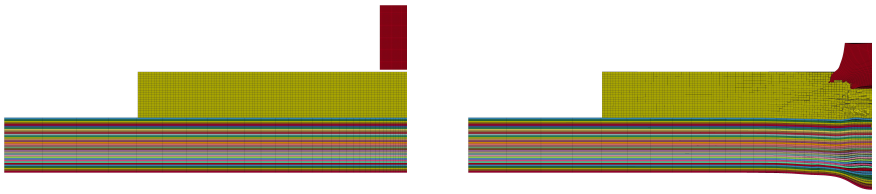

(a) t=0.0 ms

(b) t=0.003 ms

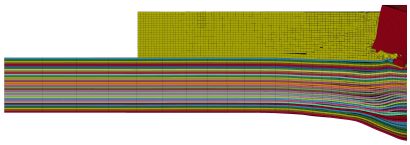

(c) t=0.006 ms

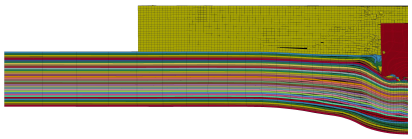

(d) t=0.009 ms

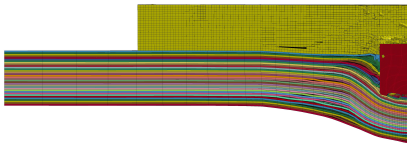

(e) t=0.012 ms

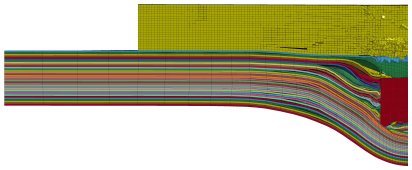

(f) t=0.018 ms

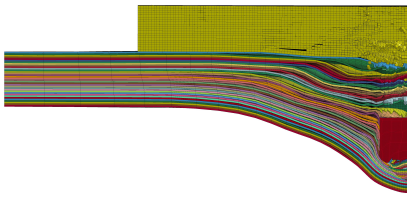

(g) t=0.030 ms

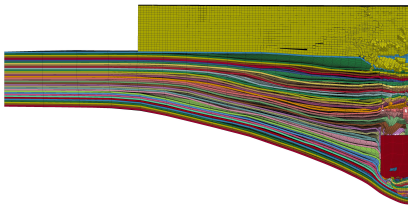

(h) t=0.046 ms

Figure 7.20: Non-perforating impact on SiC and Dyneema plate at 1245 m/s.

The residual mass of the projectile after the impact was used to validate the numerical model. Figure 7.22 shows the residual mass as a function of the impact velocity of the projectile for both the experimental and the numerical tests. The numerical results follow as expected the same trend of the experimental tests, that when the impact velocity increases, the residual mass decreases. The experimental and numerical trends

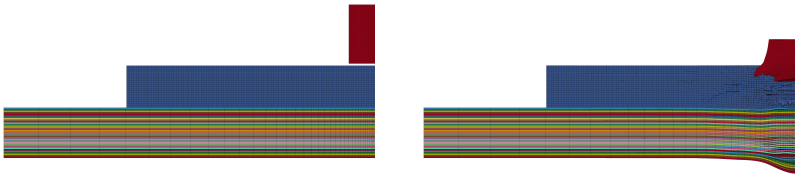

(a) t=0.0 ms

(b) t=0.003 ms

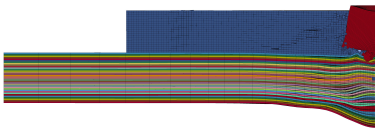

(c) t=0.006 ms

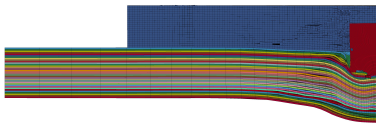

(d) t=0.009 ms

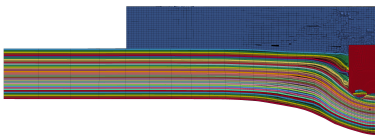

(e) t=0.012 ms

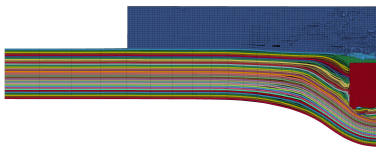

(f) t=0.018 ms

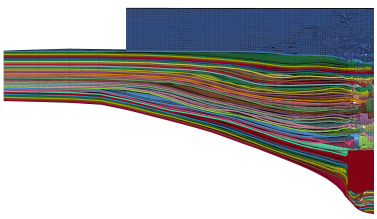

(g) t=0.050 ms

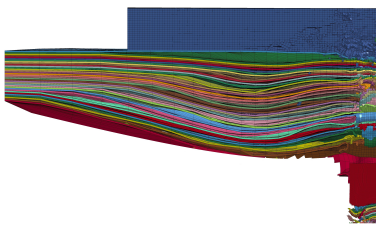

(h) t=0.067 ms

Figure 7.21: Perforating impact on SiC and Dyneema plate at 1250 m/s.

are also presented in the graph and as can be seen the tendency of the curves are different the slopes are very similar (difference around 20%). The numerical results shows less residual mass when compared to the experimental tests. This is thought to be related to the use of the numerical feature used in the numerical simulations (element erosion) that allows to remove/delete elements and contributes in reducing the residual mass of

the projectile.

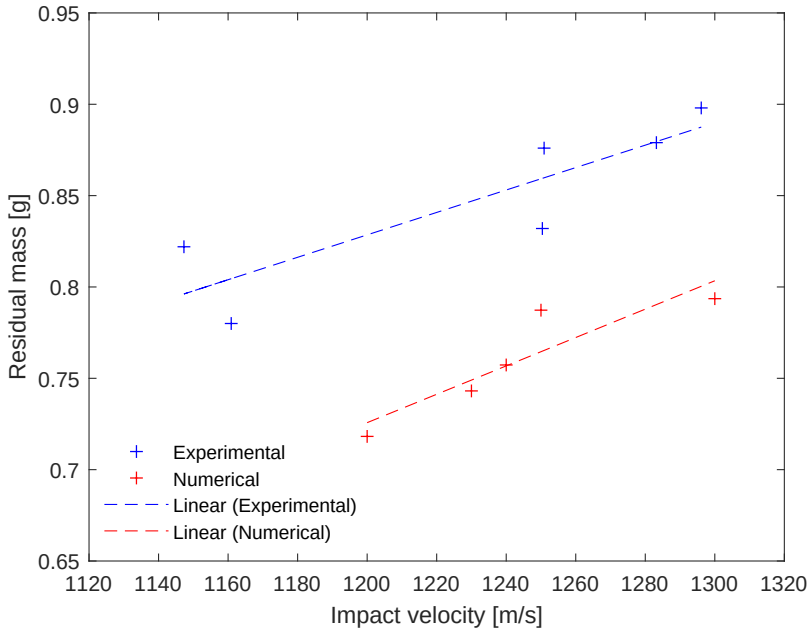

Figure 7.22: Residual mass of experimental and numerical tests as a function of the impact velocity.

7.2.3 Aluminium

Aluminium is widely used in numerical simulations as well as in experimental tests. The mechanical properties used are listed in Table 7.9 and the material model used to model this material was the isotropic-elastic-plastic, available in the LS-Dyna^{TM} library.

Table 7.9: Mechanical properties of aluminium 5754 - H22 [Aalco, 2018].

Material	Density ρ [kg/m^3]	Shear modulus G [GPa]	Yield stress σ_y [MPa]	Plastic hardening modulus [MPa]	Bulk modulus K [GPa]
Al 5754	2650	26	185	0.3	75

7.3 Verification of results

After validating all the parts individually used in this work, other validation tests were done using different combinations of the target materials with the different projectiles. In this section three different tests were done in order to understand the influence of a backing plate in terms of ballistic limit and also in terms of maximum deflection. The main goal of this thesis is to stop the incoming projectile at nominal velocity and avoid contact between the inner helmet shell and the head. As such, it is important to know which is the best material (taking into account market availability) for a backing plate but also the minimum distance between the two plates in order to minimise the back face deformation (BFD).

7.3.1 Dyneeema HB80 and aluminium backing against FSP 0.30 for different distances

Numerical and experimental tests were done using a composite armour system consisting of a Dyneema HB80 panel with a thickness of 5 mm, and a 5754 - H22 aluminium backing plate with a thickness of 3 mm (dimensions 400 $\times$ 400 [mm^2]). This backing plate was put at different distances (0, 2.5, 5, 7.5, 12.5 and 50 mm) from the Dyneema HB80 panel. Figure 7.23 shows the schematics of the experimental and numerical setup. The main idea of this test was to determine the influence of the distance between both layers, composite layer and aluminium, on the ballistic resistance and the BFD. The numerical tests were validated based on experimental results done by [Miranda-Vicario et al., 2014].

7.3.1.1 Numerical models

All material models for the Dyneema HB80, aluminium and FSP 0.30 projectile were already described in the previous sections. The mechanical properties used were the same as shown before. The correct interaction between the projectile, the layers of Dyneema HB80 and the backing plate was ensured through different contact algorithms from the LS-Dyna^{TM} contact library and that are active when the surface of different

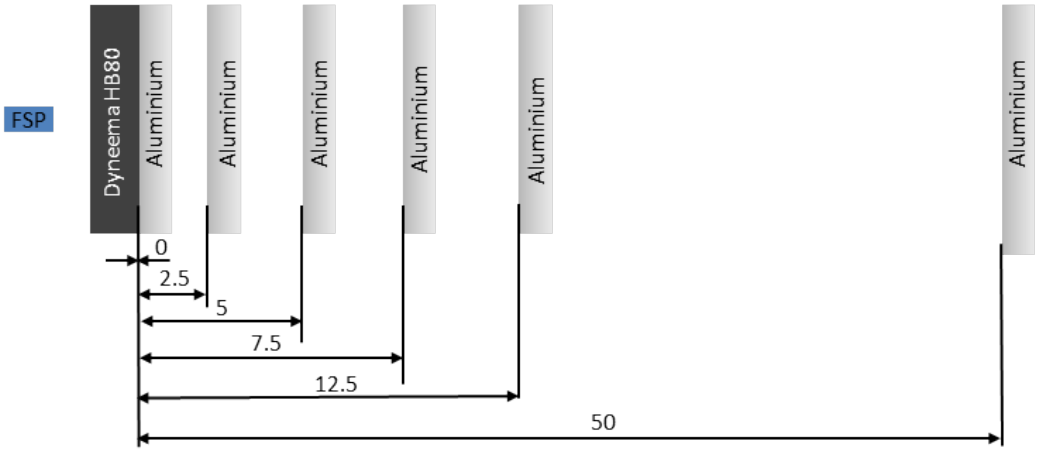

Figure 7.23: Experimental and numerical setup for Dyneema HB80 with aluminium backing plate at different distances.

parts have contact. An eroding contact was used between the target and the projectile and an automatic surface-to-surface contact was used between the composite plate and the aluminium plate since in this contact is commonly used for bodies that have large contact areas and the contact surfaces are known.

7.3.1.2 Results

Both the experimental and the numerical results (see Figure 7.24) show that for a distance varying from 0 to 12.5 mm, the ballistic resistance increases, as expected, due to the fact that the degree of liberty of movement of the fibre-reinforced composite material is increased. Interestingly, there is however a synergetic effect between the aluminium backing plate and the HB80 composite material. When the backing plate is put at such a distance that during the penetration process contact between the composite plate and the backing plate is avoided (e.g. for a standoff of 50 mm), the ballistic resistance decreases again (see Figure 7.24). This trend can be observed for both the experimental as well as the numerical results, even if the simulation results generally underpredict the ballistic resistance again. The experimental error bars show the confidence interval at 95%. Once more, the numerical results have a good agreement when compared with the experimental results. As an illustration of this experiment Figure 7.26 shows the numerical simulation of an impact at 510 m/s for a distance of 12.5 mm between the Dyneema HB80 and the aluminium plate. The simulation was performed just below the ballistic limit.

An important conclusion of this test is that compared to the configuration with a distance of 50 mm (no contact between the composite plate and the aluminium backing plate during penetration) there is no significant drop in ballistic resistance when the backing plate is put against the back side of the composite layer. Intuitively, it could have been expected for the ballistic resistance to decrease significantly as the movement of the fibre-composite is severely restricted in the impact direction. This is however not

the case. A possible explanation for this is that the aluminium backing is thin enough to sufficiently deform in order to allow the composite layer to absorb the impact energy of the projectile effectively.

Finally, a study on the permanent BFD of the aluminium backing plate was done for the different distances. For this, all the experimental plates were scanned to measure the maximum deflection of the impact. A plot of the experimental and numerical results is given in Figure 7.25, showing the maximum deflection of the backing plate and the minimum total thickness for each configuration. This minimum total thickness is calculated by adding the maximum deflection to the total initial thickness of each configuration (e.g. for a distance of 5 mm the minimum total thickness is 5 mm for Dyneema thickness, plus 5 mm gap, plus 3 mm of aluminium and finally 7.5 mm of deformation, making a total of 20.5 mm). Configurations with high initial thickness but very low BFD are compared on an equal basis to configurations with low initial thickness but high BFD. The maximum BFD occurs when there is no gap. As the gap is increased, the deformation decreases. There is however, only a very limited influence of the distance between the composite panel and the backing plate. No change in deformation mode was observed for the different configurations. These observations lead to the conclusion that the BFD is most likely largely determined by the properties of the material and the thickness chosen for the backing layer. The simulation results systematically underestimate the BFD compared to the experimental value. A first partial explanation for this phenomenon is due to the fact that the experimental maximum value for the BFD is generally obtained for an impact velocity above the ballistic limit. This effect can not be reproduced in finite element modelling due to the deterministic nature of the simulations. Secondly, the finite element model generally underestimates the ballistic resistance of the material. This further increases the observed differences between the experimental and the numerical results, as the simulations required an impact velocity below the numerically obtained ballistic limit in order to avoid complete perforation of the backing plate. Last but not least, the failure strain of the aluminium alloy is likely underestimated, as it was derived from a regular tensile test.

7.3.2 Multilayered armour of Dyneema HB80 and aluminium backing plate against FSP 0.30

The test presented here consisted of testing a multilayered armour assembly of sequential layers of Dyneema HB80 sheets (nominal thickness of 1 mm times 5 layers) with 10 mm gap between layers, followed by a 3 mm thick aluminium backing plate. Figure 7.27 shows the two different configurations tested in these experiments. The rationale behind the splitting up the Dyneema layer was that in that case the different layers would absorb more energy since they would be deformed more under tensile loading conditions due to the improved freedom of movement in the out-of-plane direction, increasing the ballistic resistance.

7.3.2.1 Numerical models

Materials models for the Dyneema HB80, aluminium and FSP 0.30 projectile were already described in the previous sections. The correct interaction between the projectile, the layers of Dyneema HB80 and the backing plate was assured through an automatic contact algorithm, which and is active when the surface of different parts contact.

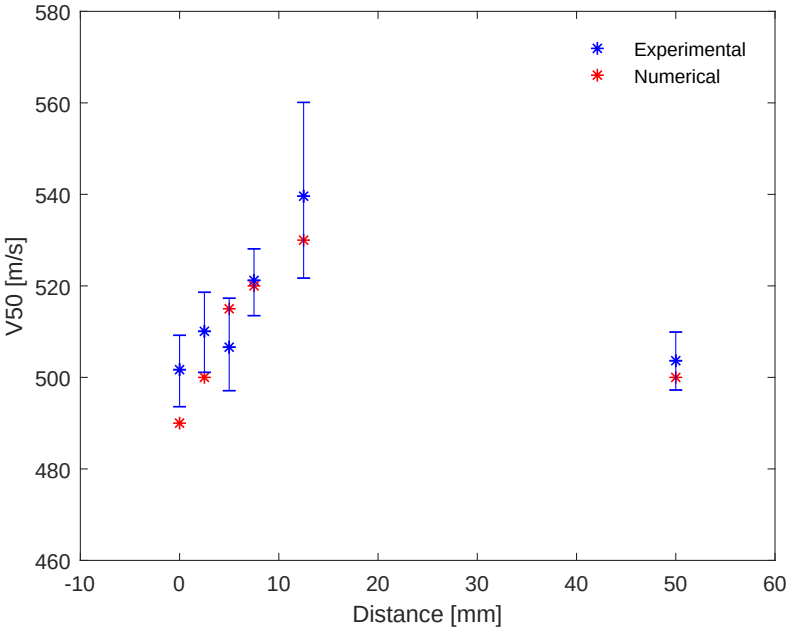

Figure 7.24: Experimental and numerical ballistic limit (V_{50}) as a function of the distance.

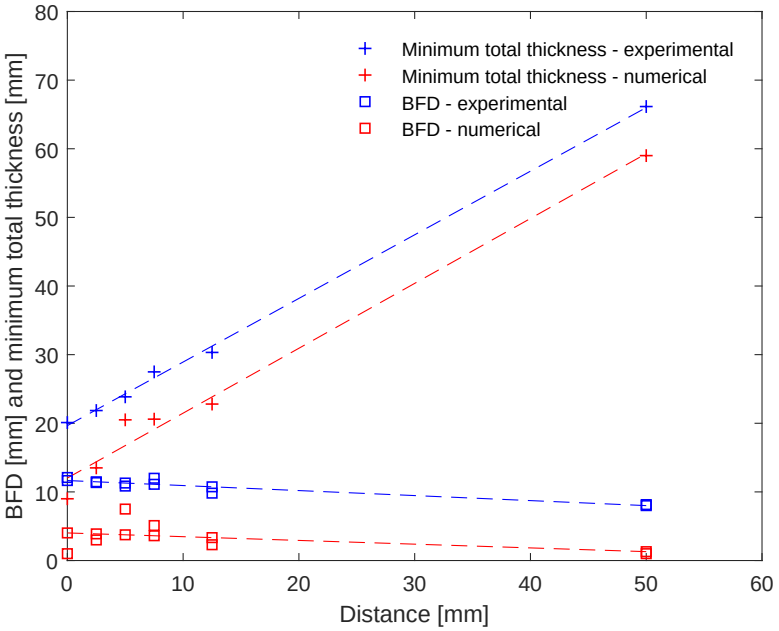

Figure 7.25: Experimental and numerical BFD and minimum total thickness (target + gap + BFD) as a function of the distance.

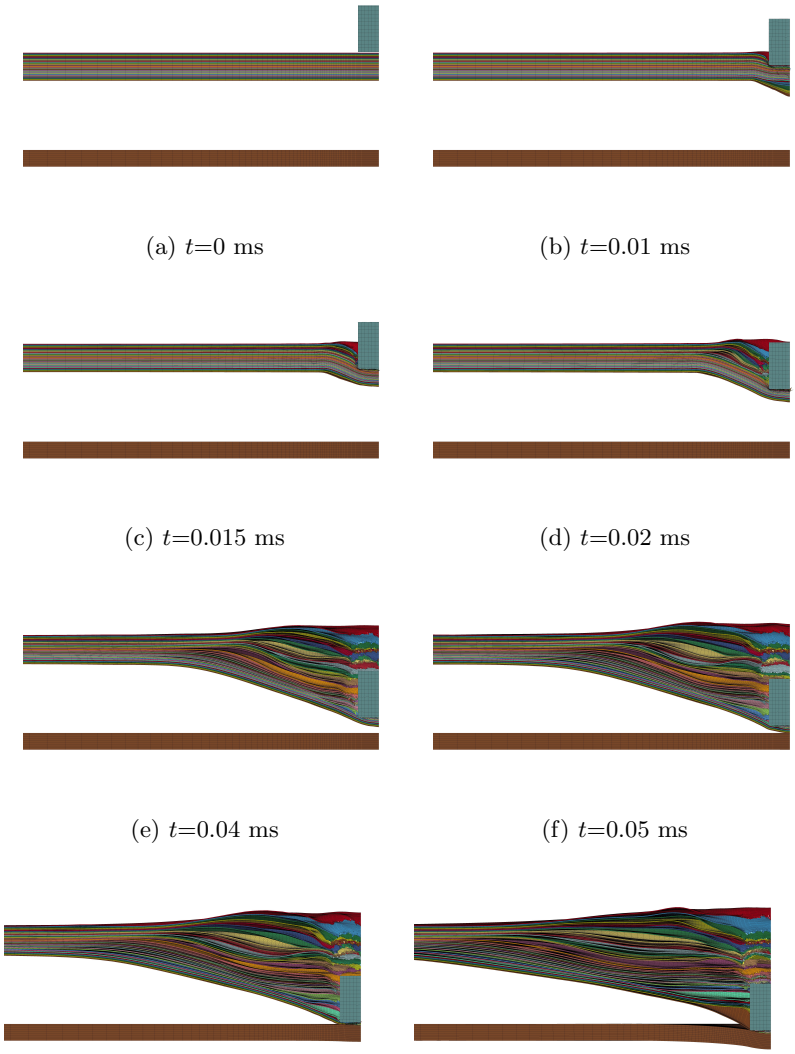

(a) t=0 ms (b) t=0.01 ms

(c) t=0.015 ms (d) t=0.02 ms

(e) t=0.04 ms (f) t=0.05 ms

(g) t=0.06 ms (h) t=0.08 ms

Figure 7.26: Impact from FSP 0.30 on Dyneema HB80 plate at a gap distance of 12.5 mm with an aluminium backing plate.

7.3.2.2 Results and comparison

Figure 7.28 shows the ballistic limit velocity for the two different tested configurations. Comparing the two different configurations, there is no obvious advantage in separating the fibre-composite plate in several single sheets to increase the freedom of movement of the fibres and possibly absorb more energy: the ballistic resistance is comparable for both configurations. It can be observed that the agreement with the experimental results is good.

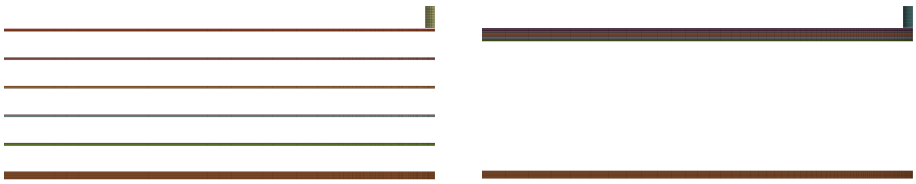

(a) (b)

Figure 7.27: Configuration: (a)= 5 layers of 1 mm Dyneema with 10 mm distance followed by an aluminium backing plate; (b)= 5 mm Dyneema with 50 mm distance followed by an aluminium backing plate.

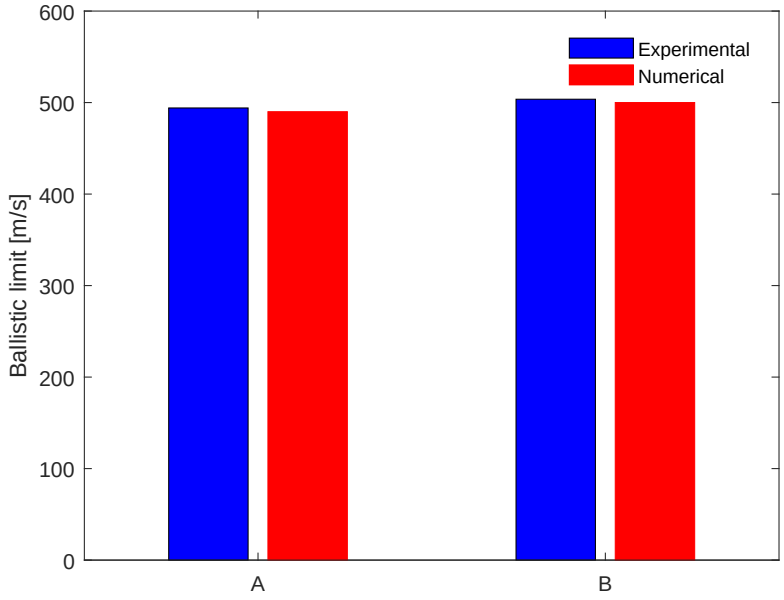

Figure 7.28: Experimental and numerical ballistic limit for the two different configurations: A= 5 layers of 1 mm Dyneema with 10 mm distance followed by an aluminium backing plate; B= 5 mm Dyneema with 50 mm distance followed by an aluminium backing plate.

7.4 Armour helmet concept against 7.62 × 39 mm M43

From this experimental tests and numerical modelling described in the above section, the choice in terms of material (and thickness) for the first three layers of the new helmet concept is: SiC plate with 4.2 mm, followed by Dyneema HB80 with 7 mm and finally an aluminium layer with 2 mm thickness (see Figure 7.29). This choice is based on the results where the SiC shows that is capable of breaking and eroding the impacting projectile, and the Dyneema as a second layer is good to absorb the kinetic energy of the impacting projectile and finally the third layer, the aluminium layer, helps to reduce the back face deformation. In order to validate numerically the configuration, experimental tests were also done.

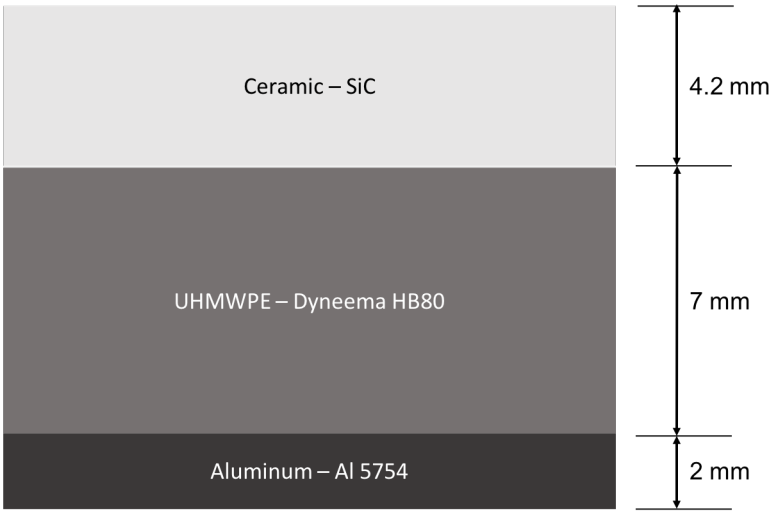

Figure 7.29: Schematic model for the first three layers of the new helmet concept (SiC, Dyneema HB80 and the Al 5754 - H22).

7.4.1 Numerical models

The material models and the mechanical properties of the different materials used in this armour configuration and in the projectile were already described in the previous sections. A tied contact was adopted to simulate the interaction between the ceramic tile and the first layer of the Dyneema composite plate, and the interactions between the last layer of the Dyneema composite layer and the aluminium plate. The element size in the impacted region was chosen (after a mesh convergence study) to be small enough and increased gradually proportional with the distance to the impacted region for the composite and for the aluminium layer at the back of the target. For the ceramic material, the element size is kept constant in the whole plate in order to ensure consistent crack propagation and evolution. The target was modelled with hexahedral solid elements. The ceramic layer is a $50 \times 50 \times 4.2$ [mm^3] SiC plate, the composite is Dyneema HB80 and the aluminium plate as $100 \times 100\times$ (7 and 2) [mm^3] thickness.

The projectile was the 7.62×39 mm M43. The corresponding mechanical properties and dimensions are those presented in Section 7.1.2. The interface between the projectile and the armour material was defined with the eroding contact. In the present study a quarter of the geometry was modelled. The complete model is shown in Figure 7.30.

7.4.2 Results and comparison

Figure 7.31 shows a comparison for the residual length of the projectile core for the experimental impacts against the armour configuration described above. As can be seen the numerical simulation does not show good agreement when compared with the experimental tests (always more than 3 or 4 mm in terms of residual lenght). Figure 7.32 shows the ratio of residual mass over the residual length as a function of residual length for the numerical simulations and the corresponding experimental results. Compared to the results shown in Figure 7.31, the simulations largely duplicated the experimental results. Combining the results of Figure 7.31 and Figure 7.32 it can be concluded that

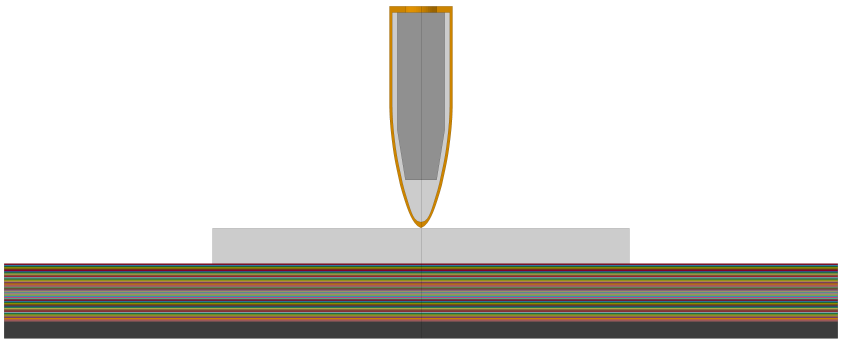

Figure 7.30: Geometric model of 7.62×39 mm M43 projectile and target (SiC, Dyneema HB80 and the Al 5754 - H22).

the deformation and erosion of the projectile have been suitably modelled, but they are too significant at a specific impact velocity, leading to an overestimation of the deformation of the projectile. This is probably due to the fact that the material models for the projectile were representing well the real behaviour, whereas the ceramic model overestimated the resistance of the ceramic material.

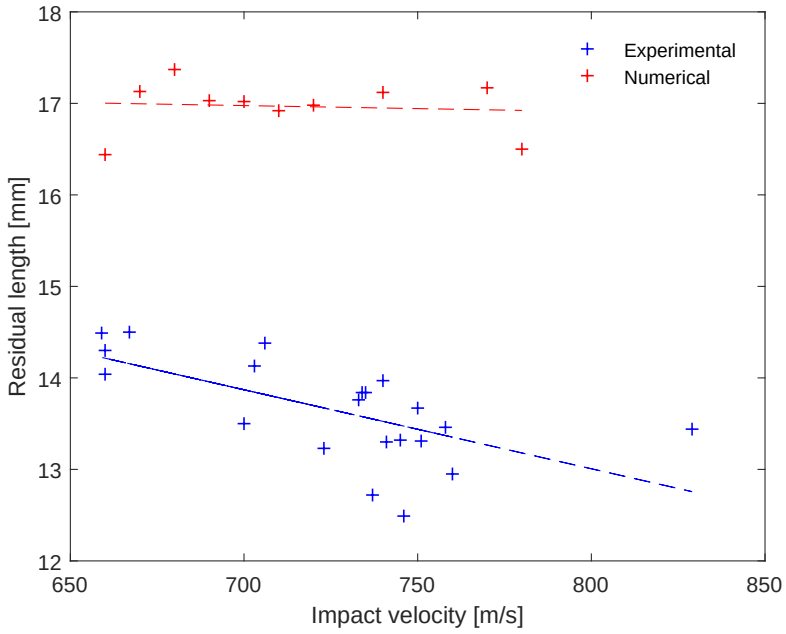

Figure 7.31: Residual length as a function of the impact velocity for the considerated armour configuration, experimental and numerical results.

Figure 7.33 shows frames of the 7.62 × 39 mm projectile with an initial velocity of 750 m/s impacting armour configuration and Figure 7.34 shows frames of the damage propagation of the silicon carbide tile for the same impact conditions.

The ceramic material receives the initial impact of the projectile and its function is to progressively deform and/or fragment the tip of the projectile as it penetrates the

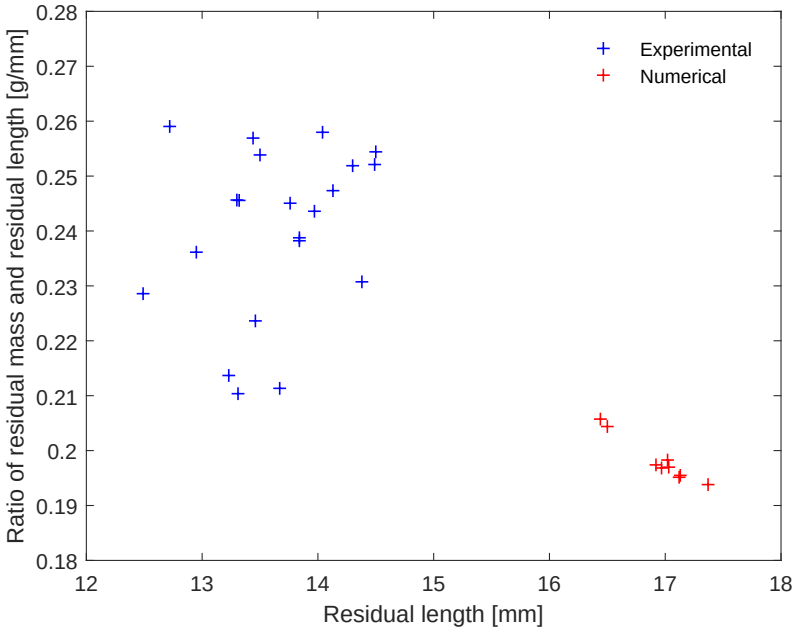

Figure 7.32: Experimental and numerical ratio of residual mass and residual length as a function of the residual length of the core of the projectile.

backing composite material. A major part of the impact energy is dissipated in this initial stage. In this stage there is the destruction of the tip of the projectile without penetrating into the ceramic (see Figure 7.33 (b)), in addition to the formation of cracks in the form of a cone (see Figure 7.34 (c) and (d)). The impact of the projectile generates a compressive shock wave that travels across the ceramic thickness from the front to the rear face at the speed of sound. This wave will reflect back as a tensile wave, which tends to fracture the ceramic. During the formation of the cone the projectile is being eroded but the ceramic does not move. The part of the projectile that is being eroded is called the plastic part. The angle of the cone depends on the type of ceramic plate [Woodward, 1990, Fellows and Barton, 1999]. In the second stage, the main function of the base layer is to absorb the residual impact energy caused by the fragmented parts of the projectile, thus resulting in plastic deformation of the material. In this stage the projectile penetrates the armour and the fractured cone propagates causing lateral spread of ceramic fragments and simultaneously the base armour of the armour starts to deform elastically. The velocity here can be divided into two regions, firstly the rear part of the projectile continues to move, whereas the interface projectile-ceramic moves at a different velocity. The difference between these velocities provide the rate of projectile erosion. Figure 7.35 shows the numerical and experimental angle of the fractured conoid of SiC after and impact. The numerical results are within the range of the experimental results.

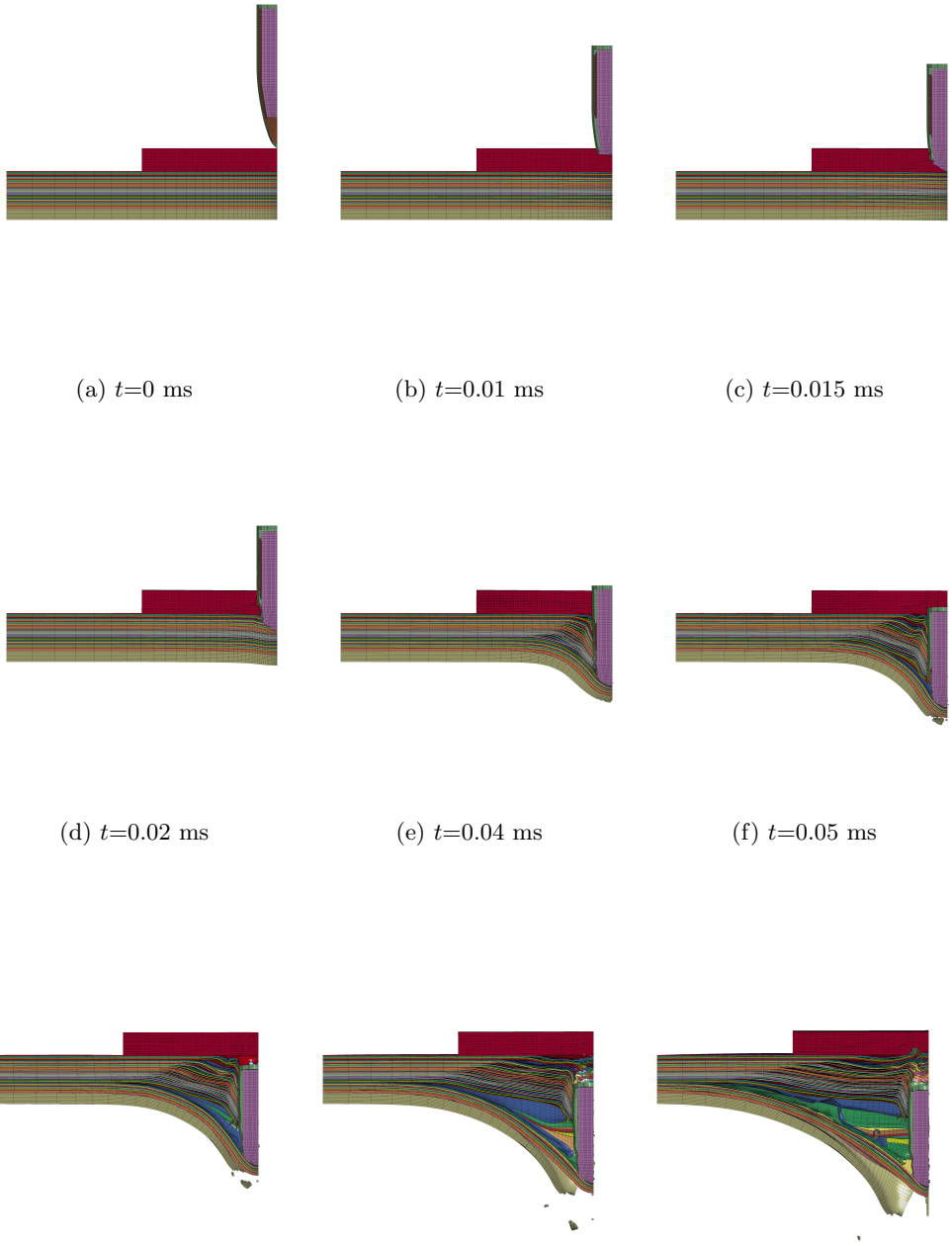

(a) t=0 ms (b) t=0.01 ms (c) t=0.015 ms

(d) t=0.02 ms (e) t=0.04 ms (f) t=0.05 ms

(g) t=0.06 ms (h) t=0.08 ms (i) t=0.1 ms

Figure 7.33: Snapshots of the 7.62×39 mm projectile at 750 m/s impacting against the armour configuration.

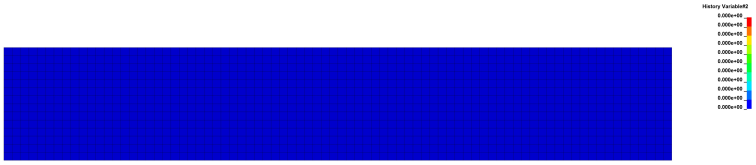

(a) t=0 ms

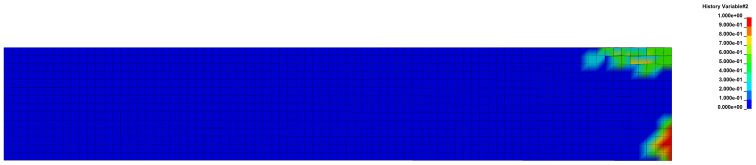

(b) t=0.005 ms

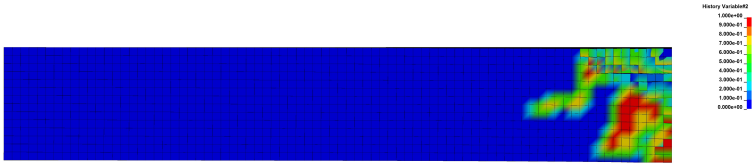

(c) t=0.01 ms

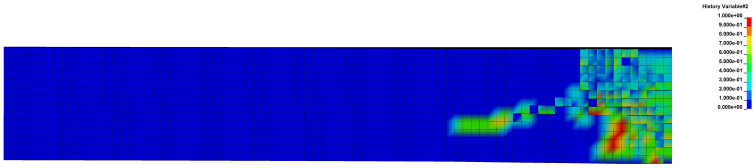

(d) t=0.013 ms

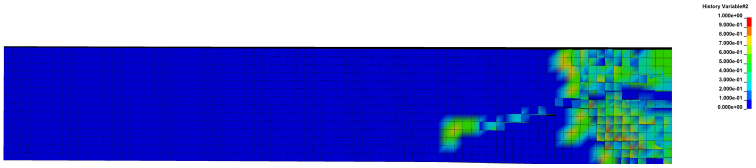

(e) t=0.016 ms

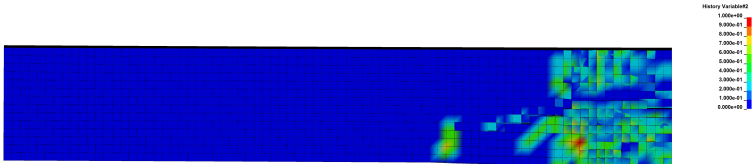

(f) t=0.02 ms

Figure 7.34: Damage propagation in the SiC plate for an impact at 750 m/s.

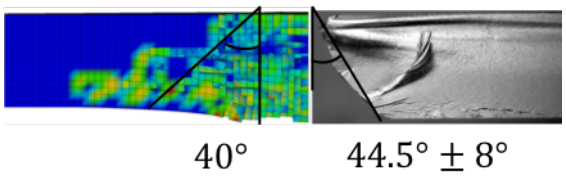

Figure 7.35: Numerical and experimental angle of the fractured conoid of SiC after an impact.

Chapter 8

Numerical modelling of armour concept

This section provides the description and validation of a finite element model for measuring the back face deformation of a prototype armour configuration against the 7.62 × 39 mm M43 round using a clay head form with the special support system developed for testing different helmet armour configurations. Also in this chapter a finite element model approach was used to analise the influence of the shock-absorbing layer on the risk on Behind Helmet Blunt Trauma (BHBT) and to determine a suitable standoff based on a maximum force injury criterion.

The target configuration used in this Chapter is the optimal configuration found for the development of the new helmet design able to stop the rifle ammunition 7.62 × 39 mm M43. This configuration contains a silicon carbide layer, followed by a composite layer of Dyneema HB80 and finally a 5754-H22 aluminium layer. The ceramic material has 4.2 mm thickness, the Dyneema HB80 has 7 mm and the backing aluminium layer has 2 mm thickness (sketch of Figure 7.30).

8.1 FEM validation of a clay head form

When developing high performance ballistic helmets, certain parameters, such as the ballistic resistance, mass and comfort, have to be evaluated. Helmet testing setups are however, expensive and complex, especially during the initial design stages when different layouts, configurations and materials have to be assessed. In order to simplify the problem, a special support system was developed to study the behaviour of different armour configurations without the need to manufacture a complete helmet shell. The support system specifically developed for the testing of new helmet designs, is based on a standard Schuberth helmet, the official helmet of the Belgian Army, similar to the PASGT helmet. The front part of the helmet was cut off and a custom designed clamping system adapted for holding 100×100 [mm^2] samples of different thicknesses was rigidly attached to the helmet. With the current configuration only impacts to the front of the helmet can be evaluated, although a similar approach could be followed for side and back testing. This system, shown in Figure 8.1, is composed of four different parts. The helmet fixtures connect the helmet and the clamps. The front and back clamps are made of 4340 steel, with six bolts to hold the sample in between the clamps.

Although the clamps can be used to vary the angle between the sample and the head form, the current clamp design positions the flat sample parallel to the surface of the head surrogate.

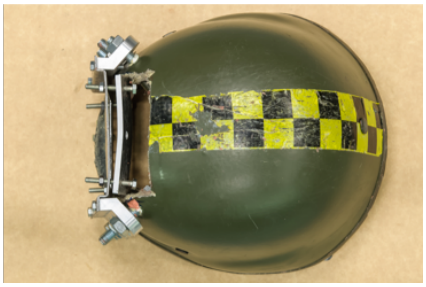

(a) Top view.

(b) Top view with zoom.

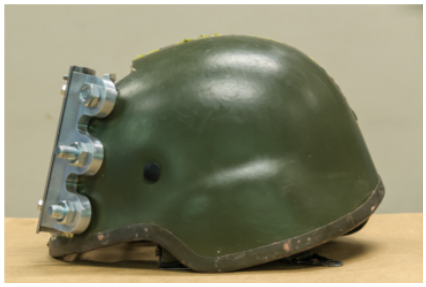

(c) Side view.

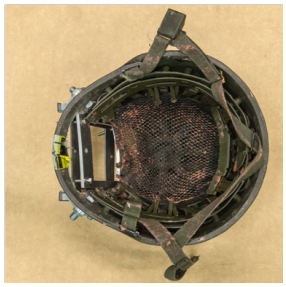

(d) Bottom view.

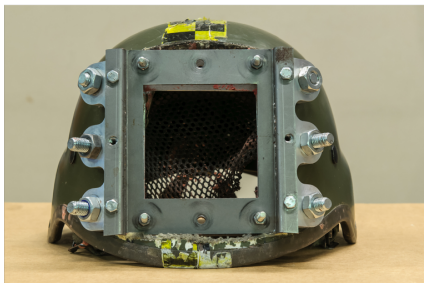

(e) Front view.

Figure 8.1: Experimental support system.

The BFD caused by a ballistic impact was measured with a clay head form in accordance with the NIJ 0106.01 standard [Mukasey et al., 2008] for ballistic penetration tests. This system is composed by two different parts (a metallic part and a modelling clay) and allows to measure of the BFD caused by the projectile.

8.1.1 Numerical modelling

The goal of the numerical simulations was to validate a numerical model of the support system in conjunction with a numerical model of the surrogate head form. Only half of the complete model was used to simulate the impact process as all simulations had one symmetry plane. The following sections describe the numerical models of the support systems developed to test the ballistic helmet concept target and the clay head form. The numerical results of the BFD using the optimal configuration target to stop the 7.62 $\times$ 39 mm projectile are also presented.

8.1.1.1 Support system

In order to numerically represent the experimental test the support system was also modelled. The same parts as in the real support system-helmet combination are implemented in LS-Dyna^{TM}: front clamp, back clamp, helmet fixture, suspension system from a Schuberth helmet (3 parts) and the helmet shell. The subcomponents of the

support system were reproduced in the FEM software: one front clamp and one back clamp able to hold the sample and two fixtures for attaching the structure to the helmet. The different parts and the final assembly are shown in Figure 8.2.

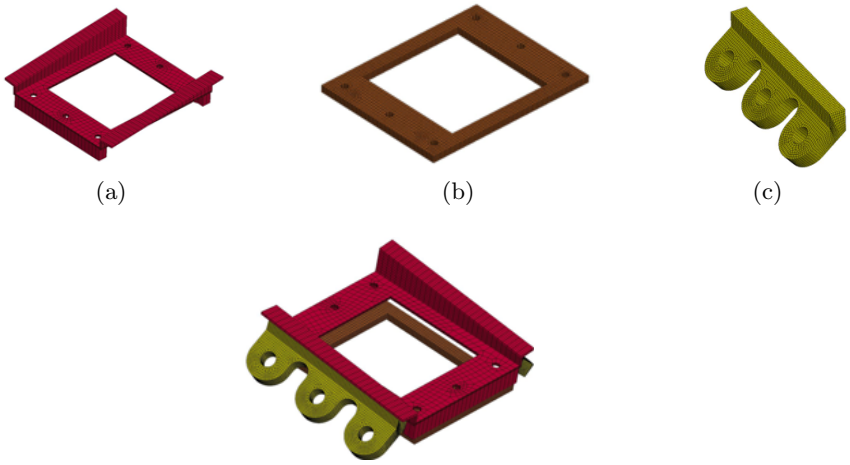

Figure 8.2: Clamp subcomponents: (a) FE mesh of the front clamp; (b) FE mesh of the back clamp; (c) FE mesh of the helmet fixture; (d) FE model of the assembled subcomponents.

The plastic kinematic constitutive model was used for the steel parts of the front clamp and back clamp. The fixtures were modelled with an isotropic elastic plastic constitutive model to represent the aluminium used in the experimental support system. The properties of the aluminium material are described in Section 7.2.3. The mechanical properties for the steel clamp parts are listed in Table 8.1. A tied contact was used to represent the screws and all parts were modelled with hexahedral solid elements.

Table 8.1: Mechanical properties for steel support system subcomponents [Yen, 2002].

Material	Density [kg/m^3]	Young's modulus [GPa]	Poisson's ratio	Yield stress [MPa]	Plastic tangent modulus [GPa]
Steel 4340	7877	207	0.33	1.03	6.9

A composite failure model was used to represent the helmet material. The mechanical properties of the material model correspond to Kevlar 29 composite with a density of 1230 kg/m^3, as this was the armour material used in the real helmet shell. The material properties are listed in Table 8.2. This material is composed of fibres aligned in two different directions. The material model used in LS-Dyna^{TM} allows assigning different directions of composite material on the local coordinate systems of the elements. For the helmet material, axes xx and yy were set as the plane of the shell, and axis zz was perpendicular to the outer shell. In this finite element numerical model a macro scale simulation was also adopted to represent the Kevlar 29 composite as a homogeneous

material once the helmet shell was used only as a support part. Figure 8.3 illustrates the modified finite element model for the Schuberth helmet.

Table 8.2: Material properties of Kevlar 29 composite [Ahn et al., 2010].

Young's modulus [GPa]		Poisson's ratio		Shear modulus [GPa]	
E_{xx}=E_{yy}	E_{zz}	υ_{xy}	$\upsilon_{xz} = \upsilon_{yz}$	G_{xy}	$G_{zx} = G_{yz}$
18.5	6	0.25	0.33	0.77	2.72
Shear strength [GPa]		Compressive strength [GPa]		Tensile strength [GPa]	
S_{xy}	S_{zx}=S_{yz}	$xx = yy = zz$		$xx = yy$	zz
0.098	0.25	1.2		1.7	0.85

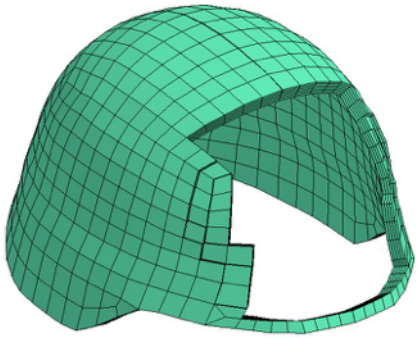

Figure 8.3: Modified finite element model of the Schuberth helmet.

A tied contact between surfaces was used between the clamp parts and the modified helmet shell. The suspension system that provides comfort and protection to the soldier, is composed of three parts: the head strap; the chinstrap and the webbing, as shown in Figure 8.4. The chinstrap and webbing are made of synthetic material (polyester material - Nylon) and the head strap is made of leather. The elastic material model was used to describe the behaviour of these three parts, and the corresponding mechanical properties are listed in Table 8.3. The same material model was used to simulate the head strap (leather). All suspension parts were modelled using shell elements. Figure 8.5 shows the numerical final assembly of the support system.

Table 8.3: Material properties of the different parts of the helmet suspension system.

Material	Density [kg/m^3]	Young's modulus [GPa]	Poisson's ratio
Nylon	1160	2.4	0.35
Leather	810	0.3	0.3

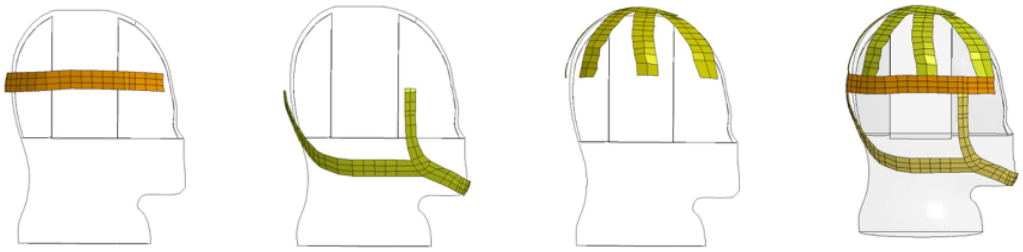

(a) (b) (c) (d)

Figure 8.4: Suspension system: (a) head strap; (b) chinstrap; (c) webbing; (d) assembled suspension system.

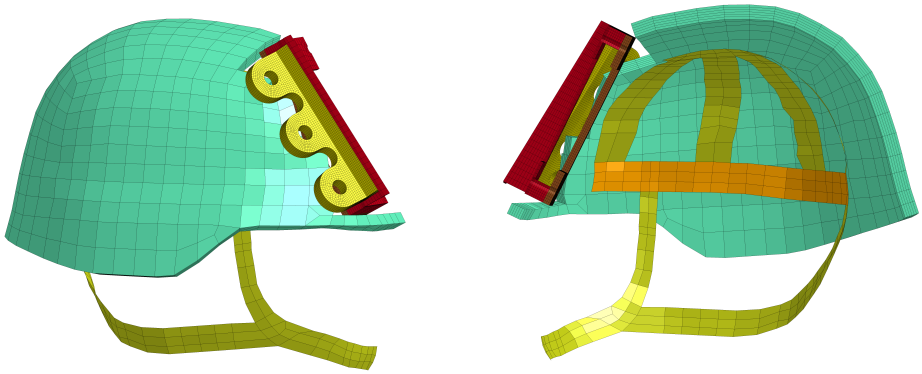

(a) Left side view.

(b) Right side view.

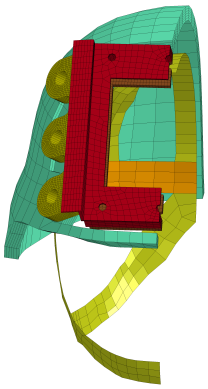

(c) Front view.

Figure 8.5: Numerical model of whole helmet system.

8.1.1.2 Clay head form

The clay head form is a modification of the U.S. Army clay head form defined in the NIJ 0106.01 standard [Mukasey et al., 2008] for ballistic penetration tests. It is possible to conduct tests in five positions (front, back, left, right and coronal). This dummy head consists of two different parts: the aluminium dummy head base, and the modelling clay used to fill the cruciform empty space in the head form in order to measure the back face signature (BFS) of an armour during an impact if a full penetration does not occur in the test. The head form comes in only one size and is made of 6061-T6 aluminium, with a mass of 7.75 kg. The clay embedded in the head is in this case Weible modelling clay (as specified by VPAM [VPAM, 2014]). The properties of the aluminium dummy head model are listed in Table 8.4.

Table 8.4: Material properties of the aluminium head form [Palta et al., 2018].

Material	Density [kg/m^3]	Shear modulus [GPa]	Yield stress [MPa]	Plastic hardening modulus [MPa]	Bulk modulus [GPa]
Al6061-T6	2712	26	276	0.3	75

The LS-Dyna^{TM} material model used for the aluminium was the isotropic plastic model [Palta et al., 2018]. The plastic kinematic material model was adopted for simulating the Weible modelling clay [Kechagiadakis et al., 2017]. The mechanical properties for the Weible modelling clay are listed in Table 8.5.

Table 8.5: Material properties of the modelling clay [Roberts et al., 2007, Kechagiadakis et al., 2017].

Material	Density [kg/m^3]	Young's modulus [GPa]	Poisson's ratio	Yield stress [MPa]	Strain rate parameter C	Strain rate parameter P
Weible plastilina	1750	2.4	0.49	0.196	10	2

Figure 8.6 (a) shows the experimental ballistic headform and Figure 8.6 (b) shows the FE model using hexahedral elements.

The experimental and the finite element model of the head form with the modelling clay is shown in Figure 8.7. An automatic contact between the dummy head model and the modelling clay was used.

8.1.1.3 Results and discussion

Nine experimental tests (shots) were done with the 7.62 × 39 M43 projectile at impact velocities ranging from 650 to 750 m/s for measuring the back face deformation

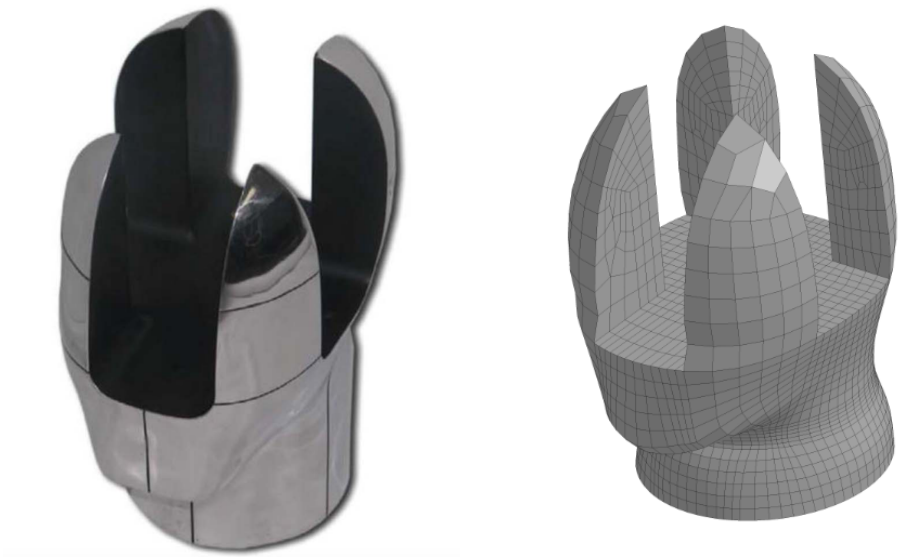

(a) (b)

Figure 8.6: Clay head form: (a) Experimental dummy (Courtesy of Rob Kinsler, U.S. Army Research, Development and Engineering Command/ARL); (b) FE mesh of the dummy head form.

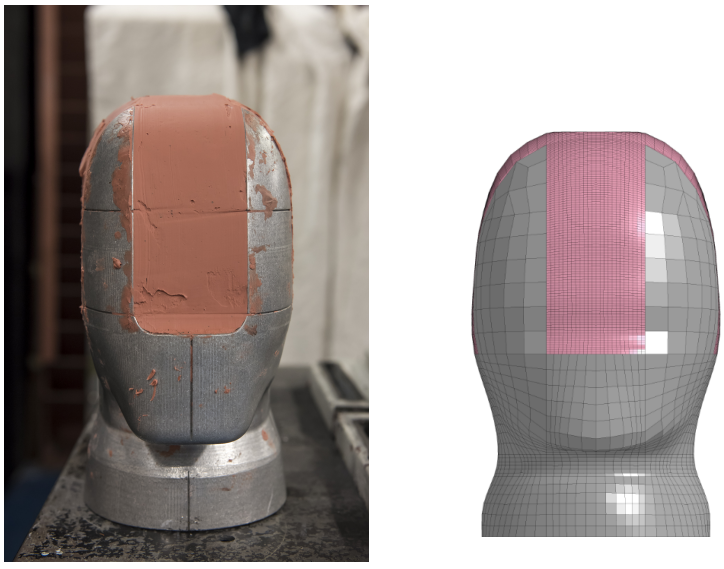

(a) (b)

Figure 8.7: Clay and the headform: (a) experimental setup; (b) FE model.

of a prototype armour configuration. The optimal target configuration composed of SiC, Dyneema HB80 and an aluminium 5754-H22 layer was used (see section 7.4). The target has the same dimensions as those used in previous tests. In this section the validation of the finite element model of the clay head form with special support system developed for testing different helmet armour configuration was done. Figure 8.8 shows the final

assembly of the support system with the sample mounted on the clay head form before impact as used during the experimental and numerical tests.

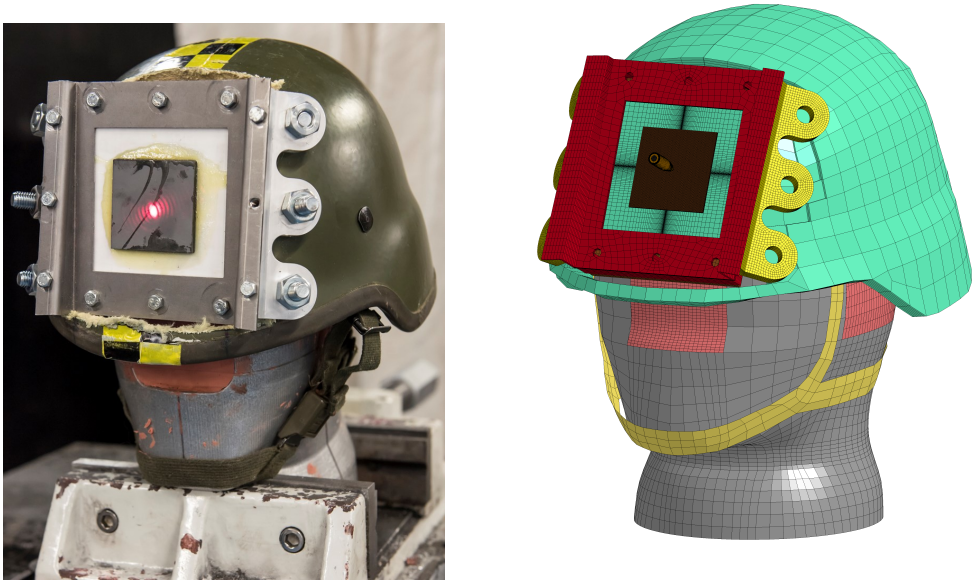

(a) (b)

Figure 8.8: Support system with a clay head form: (a) experimental setup and (b) full numerical model.

The results in Figure 8.9 show the back face signature (BFS) for frontal impact as a function of impact velocity for the numerical simulations and the corresponding experimental results. The error bars for the experimental results correspond a standard deviation $\sigma = 1$, both for BFS and impact velocity. A good fit (all numerical results within standard deviation $\sigma = 1$) between the numerical and experimental results can be observed. It can be noticed that the BFS does not seem to change significantly with increasing impact velocity, which might be due to the fact that the aluminium part of the head form is limiting the maximum back face deformation that is measured in the clay. The simulations reveal (e.g. see the sequence of the impact event shown in Figure 8.10) that the velocity of the sample reaches 0 m/s after approximately 0.1 ms, while the indentation in the modelling clay keeps increasing, only to reach its maximum after 1.6 ms. In order to reduce considerably the computational time, after the projectile reaches zero velocity the support system, the target and the projectile were removed from the simulation since they no longer affected the rest of the simulation. For $t > 0.12$ ms the simulation continues only with the U.S Army clay head form (as can be seen in Figures 8.10 (f), (h) and (i)) .

The modelling results were found to be in good agreement with the experimental tests (all numerical results within standard deviation $\sigma = 1$). However, it was not possible to confirm how realistic the experimental values are because the current helmets that exist in the market do not stop the 7.62 $\times$ 39 M43 projectile.

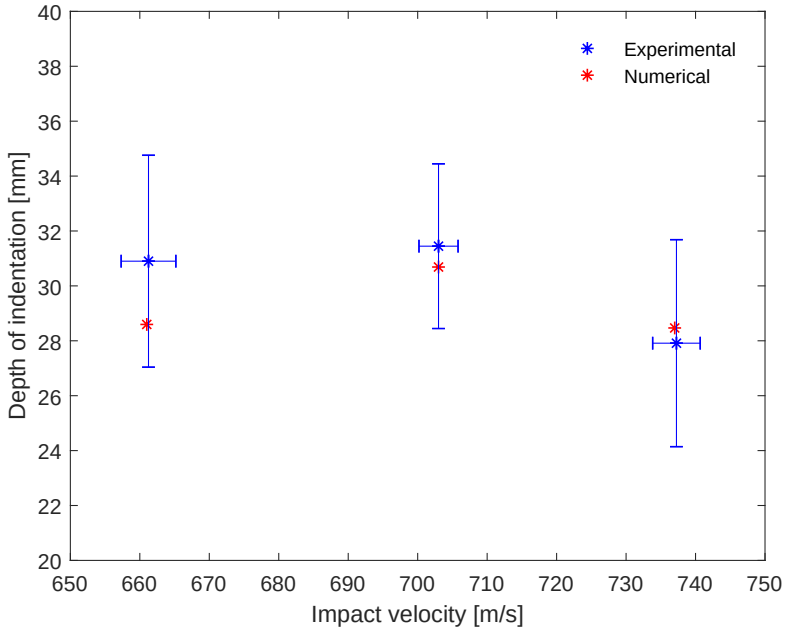

Figure 8.9: Back face signature (BFS) dependence on the impact velocity: experimental and numerical results.

8.2 Shock-absorbing layer

Whereas the previous section gave possible solutions for the first three layers, in this section the focus is on the feasibility of the fourth, shock-absorbing layer. A finite element model approach was used to analyse the influence of the shock-absorbing layer on the risk on behind-helmet blunt trauma and to determine a suitable standoff based on a maximum force injury criterion. In order to reduce the risk on injury due to the local loading of the head without dramatically increasing the required standoff of the helmet, a possible approach is to maximally reduce the dynamic deflection of the helmet shell by 'pushing back' using a shock-absorbing layer. As this shock-absorbing layer is in direct contact with the head, forces on the shock-absorbing layer by the deflecting shell, will be transferred to the head. It is hence necessary to avoid excessive forces transferred from the shock-absorbing layer to the head.

In order to quantify the minimum thickness of the shock-absorbing layer, a numerical study was done on how the dynamic deflection of the helmet shell for the optimal ballistic configuration would be reduced. This study gives an indication of the required standoff for the helmet shell to avoid direct contact loading between the ballistic shell and the head in comparison to a conventional helmet design where the load transfer largely depends on the impact location and the actual suspension or pad design (see e.g. [Freitas et al., 2014]).

8.2.1 Numerical modelling

Two sets of numerical simulations were performed at nominal velocity (740 m/s) of the projectile. A first set of simulations consisted of introducing rigid boundaries to

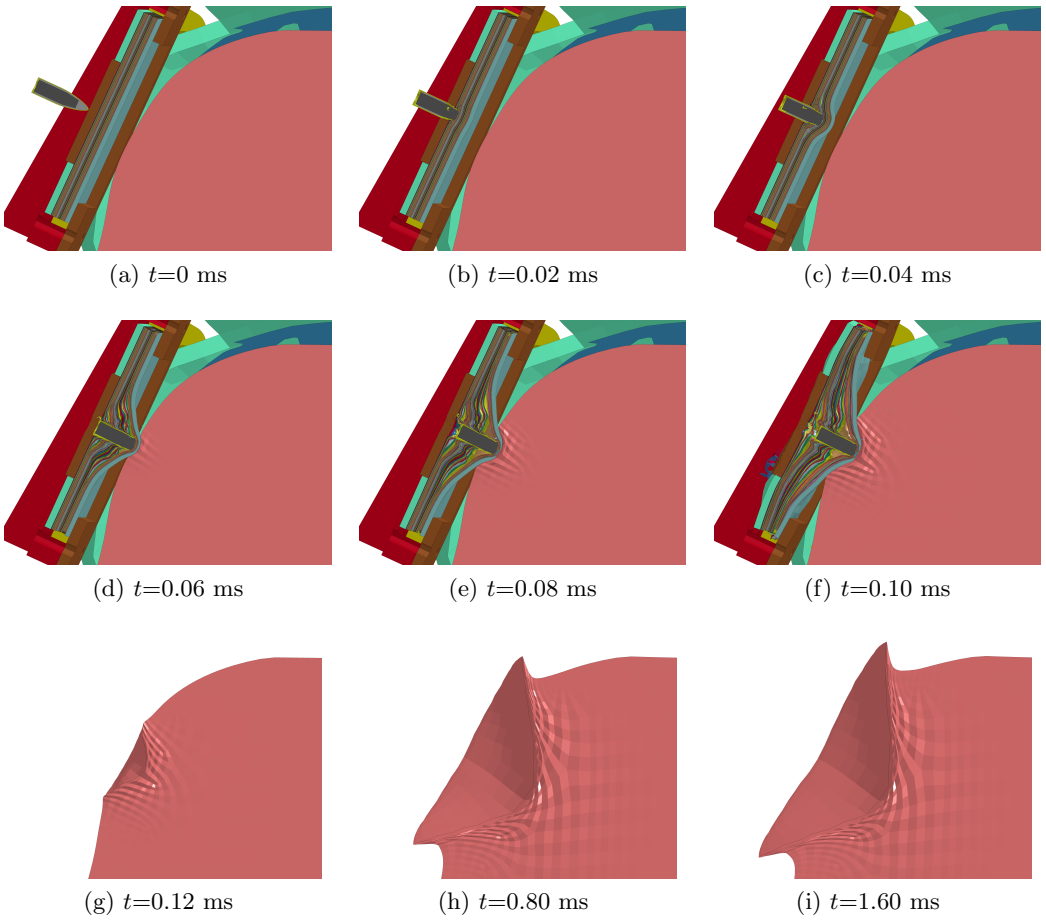

(a) t=0 ms (b) t=0.02 ms (c) t=0.04 ms

(d) t=0.06 ms (e) t=0.08 ms (f) t=0.10 ms

(g) t=0.12 ms (h) t=0.80 ms (i) t=1.60 ms

Figure 8.10: Sequence illustrating an impact event (at 661 m/s) leading to the deformation of the Weible modelling clay.

the composite layer of the flat panel. This fixes the boundaries of the composite layer in the absolute reference system and physically corresponds to the integration of the flat panel in an infinitely rigid and heavy helmet shell. A second set of simulations considered the composite layer of the flat panel to be attached to a rigid, albeit unfixed, frame. The mass of the rigid frame was chosen so that the combined mass of the frame and the flat panel is approximately equal to the mass of the envisioned helmet concept (2.72 kg). This corresponds to the integration of the flat panel in a helmet shell with similar inertia as the actual helmet shell. The difference between the tested flat panels and the full helmet geometry can mainly be attributed to the difference in inertia effect and boundary conditions. Both aforementioned sets considered a helmet shell with and without the presence of a shock-absorbing layer represented by a constant force of 5 kN (average peak force for skull fracture for frontal impacts based on Table 3.1) in slowing down the back face deflection of the ballistic helmet shell. The complete target model is shown in Figure 8.11.

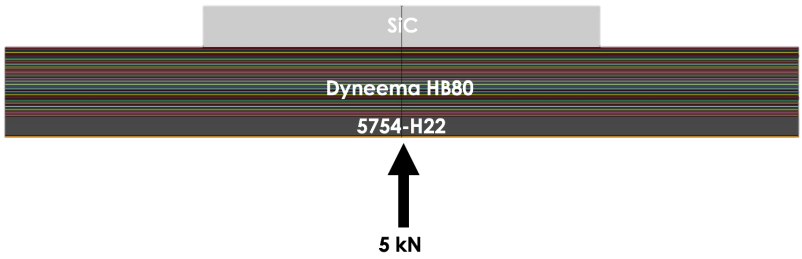

Figure 8.11: Geometrical model of the complete target and the representation of the shock absorbing layer.

8.2.1.1 Results and discussion

Figure 8.12 shows the final assembly of the complete target and projectile with rigid boundaries and attached to a rigid frame. In total, four different cases were modelled:

- Case 1a: rigid boundaries without shock-absorbing layer (Figure 8.13);
- Case 1b: rigid frame (corresponding to helmet inertia effect) without shock-absorbing layer (Figure 8.14);
- Case 2a: rigid boundaries with addition of the shock-absorbing layer (Figure 8.15);
- Case 2b: rigid frame (corresponding to helmet inertia effect) with shock-absorbing layer (Figure 8.16).

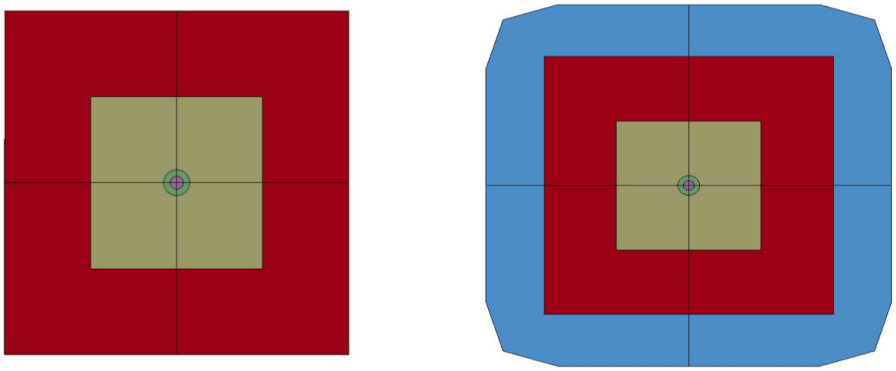

(a) (b)

Figure 8.12: Final assembly of the complete target and projectile: (a) for cases 1a and 2a with rigid boundaries and (b) for cases 1b and 2b attached to a rigid frame.

The results in Figure 8.17 show the back face deflection as a function of time for the four different cases. It is clear that the addition of a shock-absorbing layer can positively influence the back face deflection of a ballistic helmet design, even if the limited mass of the helmet is taken into account. The back face deflection can be reduced by approximately 35% while keeping the risk on behind-helmet blunt trauma on a realistic

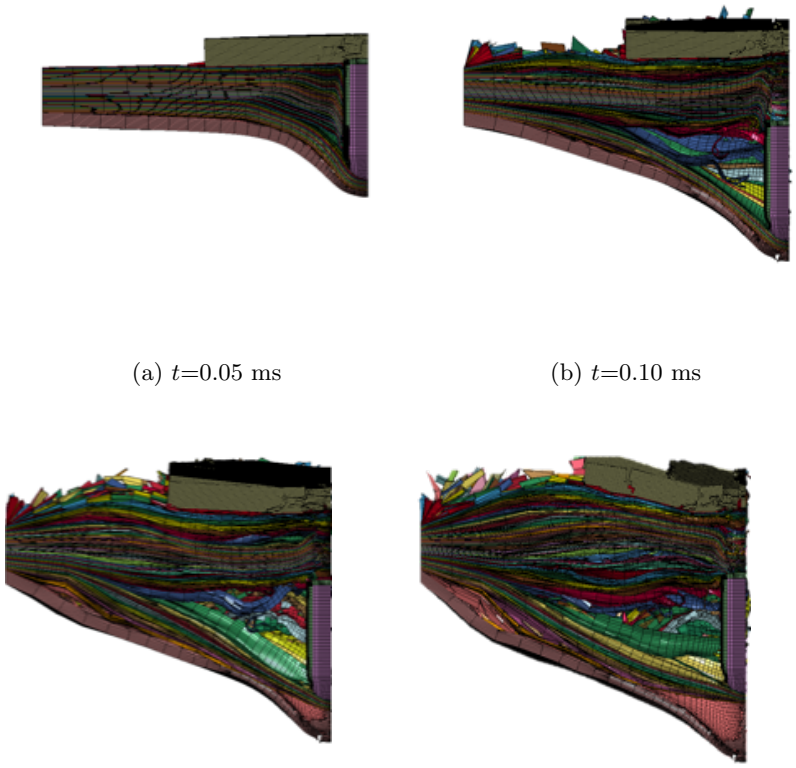

(a) t=0.05 ms (b) t=0.10 ms

(c) t=0.125 ms (d) t=0.15 ms

Figure 8.13: Sequence illustrating Case 1a: rigid boundaries without shock-absorbing layer.

level. Even if the risk level considered for this research (corresponding to a 5 kN contact force) was chosen relatively arbitrarily (i.e. the acceptable risk level might be different for a specific application depending on the risk acceptance criteria of the end-user), it is clear that for a light-weight helmet design, important mass gains can be reached due to an optimised standoff of the helmet shell by doing a combined design of the ballistic shell and the shock-absorbing layer.

Figure 8.18 shows the projectile core velocity as a function of time. Comparing the different curves, Case 2b shows the most constant deceleration due to the constant action of the shock-absorbing layer. Due to this, the loading of the head will be more gradual than on the remanning cases, helping to reduce the risk of behind-helmet blunt trauma. This will minimise the global acceleration of the head (and the brain), which should be beneficial for the risk on brain injury (e.g. commonly used injury severity parameters like HIC and HIP values will be lower, although their applicability to ballistic impact is questionable [Coghe, 2009]).

From the simulation results, a shock-absorbing layer can be designed that is able to significantly reduce the risk on behind-helmet blunt trauma, and with acceptable force transfer to the head. In this way, an optimum standoff distance can be determined for

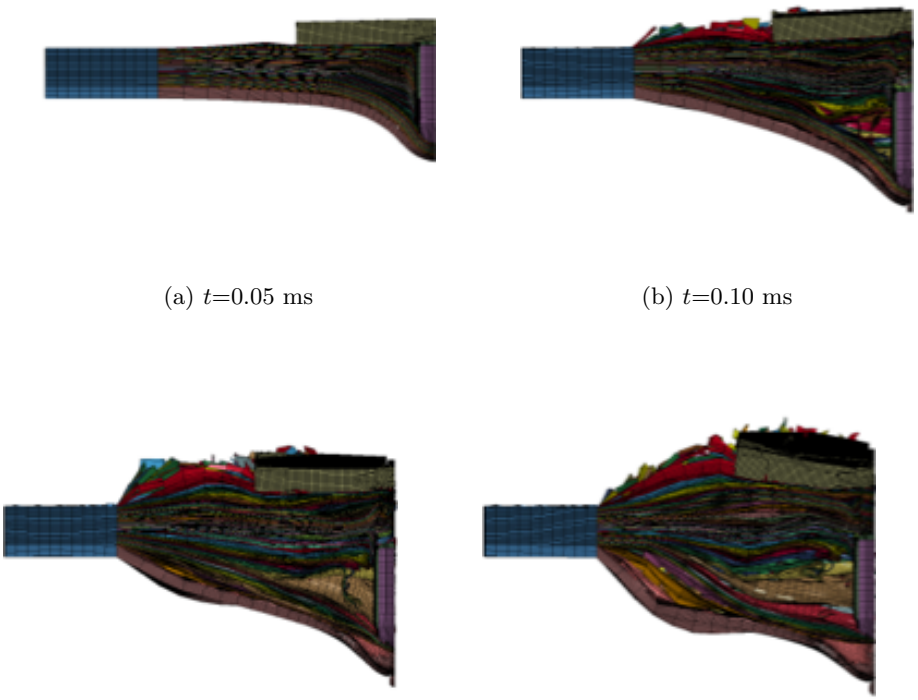

(a) t=0.05 ms (b) t=0.10 ms

(c) t=0.125 ms (d) t=0.15 ms

Figure 8.14: Sequence illustrating Case 1b: helmet inertia effect without shock-absorbing layer.

a ballistic helmet concept able to stop the M43 projectile. The standoff found for the considered ballistic shell was 35% lower than the standoff distance estimated based on the ballistic shell without taking into account the shock-absorbing layer. The actually found standoff is deemed acceptable for the foreseen application.

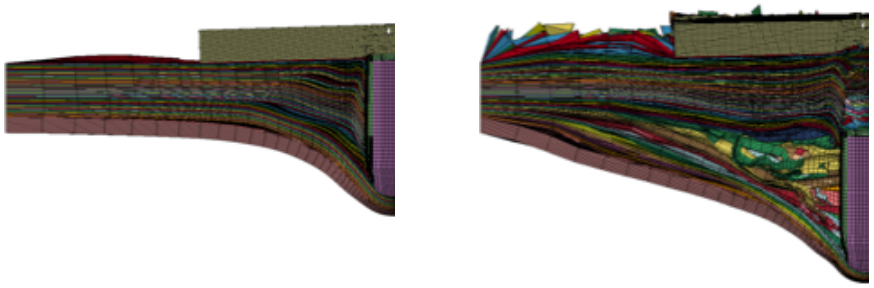

(a) t=0.05 ms (b) t=0.10 ms

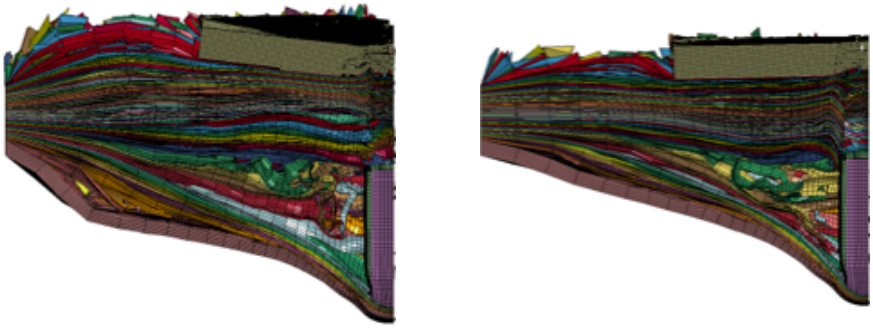

(c) t=0.125 ms (d) t=0.15 ms

Figure 8.15: Sequence illustrating Case 2a: rigid boundaries with addition of the shock-absorbing layer.

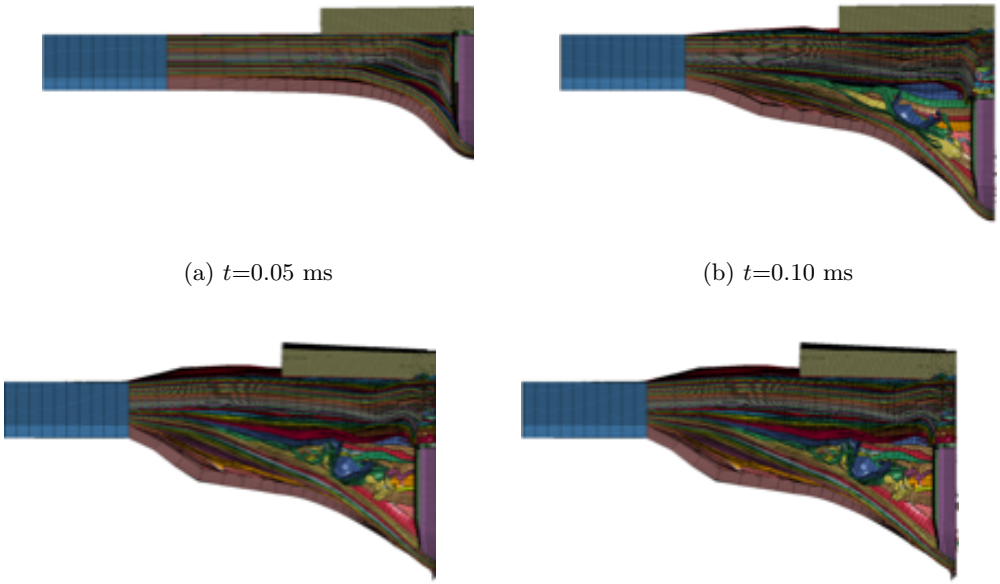

(a) t=0.05 ms (b) t=0.10 ms

(c) t=0.125 ms (d) t=0.13 ms

Figure 8.16: Sequence illustrating Case 2b: helmet inertia effect with addition of the shock-absorbing layer.

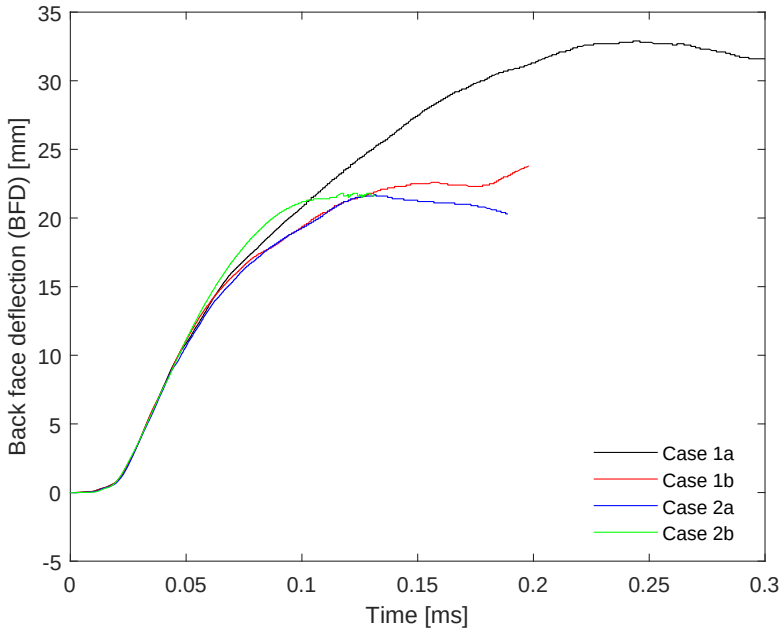

Figure 8.17: Back face deflection as a function of time for the four different cases.

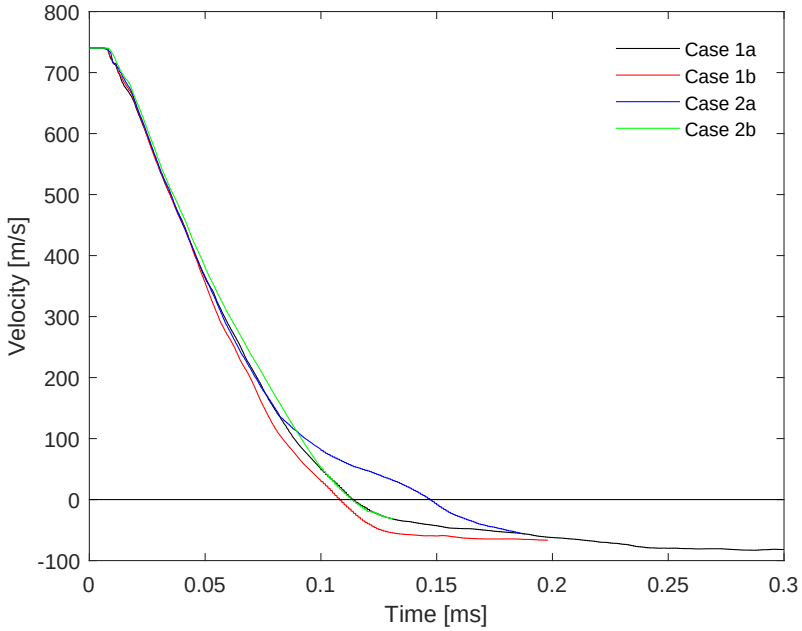

Figure 8.18: Projectile core resultant velocity as a function of time for the four different cases.

Part III

Final remarks

Chapter 9

Conclusions and future work

The main conclusions obtained from this investigation are referred and discussed in this chapter. In the final section of the chapter, possible future lines of research and work are also suggested.

9.1 Conclusions

Unfortunately, terrorism is nowadays an almost daily reality. There are several types of terrorism, such as gun attacks, fire attacks, knives attacks and bombing. The concept of development of an improved ballistic helmet able to stop rifle ammunition assumes consequently high levels of importance since, unfortunately, there are terrorist attacks/acts every day. Thus, strong efforts should be put on research and development concerning issues related to the personal protective equipment, specifically ballistic helmets. This is however complex due to the deformation of the helmet that can cause serious and permanent injuries. Ballistic personal protection equipment is expected to behave in an effective way to protect persons from threats such as fragments or bullets. Nonetheless, in order to aim for the best personal protection equipment, care must be taken, for example, on the weight, comfort, thermal conditions and specially the threats this equipment can protect from. The aim of this work was to develop an optimised armour configuration for an advanced ballistic helmet design using finite element modelling based on results from experimental tests. This not only involves the classical ballistic problem of stopping the bullet, but also determining the risk of head and brain injury for non-penetrating impacts.The main idea behind the research here presented is to create a new concept of helmet able to defeat high velocity rifle bullets using available ballistic materials. The design presented here is based on four layers, where: (i) the first layer is capable of breaking and eroding the impacting projectile, especially the steel core to make it easier to stop it, (ii) the second absorbs the kinetic energy of the projectile, (iii) the third layer limits the back face deflection, and finally (iv) a fourth layer absorbs the shock wave of the initial impact and provides the necessary standoff (required by the back face deflection) for the first three layers, so that direct contact between these layers and the head does not occur.

The finite element (FE) method was the tool used and the commercial software LS-Dyna^{TM} allowed to model the dynamic behaviour of composite armour subjected to ballistic impact. The different materials composing the ballistic helmet were numerically

modelled and validated using experimental tests.

The numerical modelling and validation using experimental results of the 7.62 × 39 M43 projectile against a rigid wall was also done. Two different numerical approaches (with and without thermal effects) were tested, and a study into the effect of EOS on the results was also conducted.

A good correlation between numerical and experimental results of the ammunition and armour materials was achieved (*e.g.* in terms of ballistic limit). Also a good correlation between numerical and experimental results in terms of impact velocity as a function of the depth of indentation of a new ballistic helmet design was observed.

The last numerical analysis made for the helmet shell configuration was relative to the shock absorbing layer. A first set of simulations consisted of introducing rigid boundaries to the composite layer of the flat panel. This basically fixes the boundaries of the composite layer in the absolute reference system and physically corresponds to the integration of the flat panel in an infinitely rigid and heavy helmet shell. A second set of simulations considered the composite layer of the flat panel to be attached to a rigid frame, without fixing this frame. From the simulation results, it is clear that a shock-absorbing layer can be designed in such a way as to significantly reduce the risk on behind-helmet blunt trauma, and with acceptable force transfer to the head. An optimum standoff distance can thus be determined for a ballistic helmet concept able to stop the M43 Kalashnikov projectile.

Since in the proposed work the main objective of stopping the 7.62 × 39 M43 projectile was reached (in terms of ballistic tests), it is possible to conclude that in terms of body armour standards, this proposed ballistic helmet will pass all the proposed standards levels. However, only stopping the projectile does not guarantee avoidance of head injury like skull and/or traumatic brain injury. These two types of head injuries were also considered in this research and in terms of skull fracture, since the design of the shock absorbing layer allows for a maximum of 5 kN force (the maximum supported by the head), it is guaranteed that there is no risk on skull fracture. In terms of brain injury it was not possible to evaluate the actual risk since only flat samples were used in this work and for this work no numerical head model (*e.g.* like a Hybrid III model) with accelerometers was available to measure the Head Injury Criteria (HIC).

9.2 Future work

Possibilities for future work and lines of research are suggested. Firstly, there are several possible improvements that can be made numerically. Further research can focus on the actual design and material selection for the shock-absorbing layer. Currently only a proof-of-concept has been demonstrated. The next steps should include the development of a technology demonstrator and ballistic testing of the technology demonstrator under laboratory conditions. This technology demonstrator would combine the results from the different experimental and numerical approaches, in order to illustrate the available design possibilities to highly increase the survivability of law enforcement and military personnel during high-risk interventions (hostage rescue, high-profile arrests, forced entry, close quarters battle, etc.).

Only the ballistic limit criterion was used in the numerical validation. Further investigations can be made into other criteria, to check if these can be linked to the

experimental and numerical models.

In terms of head injury criteria, other types of criteria (local or global parameter) should also be investigated.

In a more long-term perspective on the future lines of research, the following ideas are suggested:

- Research on a shock absorbing material, with a high energy absorption capacity;
- Since the concept is already demonstrated, it would be interesting to optimise the numerical model to the shape of a ballistic helmet shell;
- Consider the incorporation of a Hybrid III and/or biofidelic numerical head model, in order to test and measure head injuries (like traumatic brain injuries and stress and strain-based injury criteria).

List of Tables

List of Figures

Bibliography

[AAAM, 2018] AAAM (2018). Association for the Advancement of Automotive Medicine.

[Aalco, 2018] Aalco (2018). 5754 - H22 Sheet and Plate.

[Aare and Kleiven, 2007] Aare, M. and Kleiven, S. (2007). Evaluation of head response to ballistic helmet impacts using the finite element method. *International Journal of Impact Engineering*, 34(3):596–608.

[Aare et al., 2003] Aare, M., Kleiven, S., and Halldin, P. (2003). Injury criteria for oblique helmet impacts. *IRCOBI (International Research Council on the Biokinetics of Impacts)*.

[Adanur, 1995] Adanur, S. (1995). *Wellington sears handbook of industrial textiles*. Technomic Publishing Co.

[Advani et al., 1975] Advani, S. H., Powell, W. R., Huston, J., and Ojala, S. J. (1975). Human head impact response experimental data and analytical simulations. *IRCOBI (International Research Council on the Biokinetics of Impacts)*, pages 153–163.

[Ahn et al., 2010] Ahn, J.-H., Nguyen, K.-H., Park, Y.-B., Kweon, J.-H., and Choi, J.-H. (2010). A Numerical Study of the High-Velocity Impact Response of a Composite Laminate Using LS-DYNA. *International Journal of Aeronautical and Space Sciences*, 11(3):221–226.

[Allsop et al., 1988] Allsop, D. L., Warner, C. Y., Wille, M. G., Schneider, D. C., and Nahum, A. M. (1988). Facial impact response: a comparison of the Hybrid III dummy and human cadaver. In *32nd Stapp Car Crash Conference*.

[Anderson et al., 1995] Anderson, C. E., Johnson, G. R., and Holmquist, T. J. (1995). Ballistic experiments and computations of confined 99.5% Al2O3 ceramic tiles. In *15th International Symposium on Ballistic*, pages 65–72, Jerusalem, Israel.

[Arbogast et al., 2003] Arbogast, K. B., Margulies, S. S., Patlak, M., Fenner, H., and Thomas, D. J. (2003). *Review of Pediatric Head and Neck Injury: Implications for Helmet Standards*. The Children's Hospital of Philadelphia, Philadelphia.

[Arora et al., 2009] Arora, C. M., Bhatia, L. C. J. K., and Rana, B. K. (2009). Pattern of Fatal Injuries in Counter Terrorist Operations: An Innovative Analysis through Embalming Services. *Medical Journal Armed Forces IndiaMJAFI*, 65(2).

[Associated Press in Bamako, 2015] Associated Press in Bamako (2015). Two arrested in connection with Bamako hotel attack. *The Guardian*.

[Attwood et al., 2016] Attwood, J., Russell, B., Wadley, H., and Deshpande, V. (2016). Mechanisms of the penetration of ultra-high molecular weight polyethylene composite beams. *International Journal of Impact Engineering*, 93:153–165.

[Attwood et al., 2014] Attwood, J. P., Khaderi, S. N., Karthikeyan, K., Fleck, N. A., OMasta, M. R., Wadley, H. N. G., and Deshpande, V. S. (2014). The out-of-plane compressive response of Dyneema composites. *Journal of the Mechanics and Physics of Solids*, 70:200–226.

[Azevedo et al., 2016] Azevedo, A., Miranda-Vicario, A., Coghe, F., Teixeira-Dias, F., and Matos, J. (2016). Validation of a numerical model for helmet testing with a clay head form. In *Personal Armour System Symposium*, Amsterdam, the Netherlands.

[Bandak, 1995] Bandak, F. A. (1995). On the mechanics of impact neurotrauma: a review and critical synthesis. *Journal of Neurotrauma*, 12(4):635–649.

[Bandak, 1997] Bandak, F. A. (1997). Impact Traumatic Brain Injuries: A Mechanical Perspective. *Neurotraumatology: Biomechanic Aspects, Cytologic and Molecular Mechanisms, M. Oehmichen and H G. Konig*, pages 58–83.

[Bandak and Eppinger, 1994] Bandak, F. A. and Eppinger, R. H. (1994). A Three-Dimensional Finite Element Analysis of the Human Brain Under Combined Rotational and Translational Accelerations. SAE Technical Paper 942215, SAE Technical Paper, Warrendale, PA.

[Barbero, 2013] Barbero, E. J. (2013). *Finite Element Analysis of Composite Materials using Abaqus*. Composite Materials. CRC Press, 1 edition.

[Bass et al., 2003] Bass, C. R., Boggess, B., Bush, B., Davis, M., Harris, R., Rountree, M. R., Campman, S., Ecklund, J., Monacci, W., Ling, G., Holborow, G., Sanderson, E., and Waclawik, S. (2003). Helmet behind armor blunt trauma. In *RTO Applied Technology Panel/Human Factores and Medicine Panel Joint Specialists*, Koblenz, Germany.

[Bass and Yoganandan, 2015] Bass, C. R. and Yoganandan, N. (2015). Skull and facial bone injury biomechanics. In Yoganandan, N., Nahum, A. M., Melvin, J. W., and Yoganandan, T. M. C. o. W. I. o. b. o. N., editors, *Accidental Injury*, pages 203–220. Springer New York.

[Beissel, 2014] Beissel, S. R. (2014). An orthotropic model for composite materials in EPIC. Technical report.

[Belytschko et al., 2014] Belytschko, T., Wing Kam, L., Moran, B., and Elkhodary, K. I. (2014). *Nonlinear Finite Elements for Continua and Structures*. John Wiley & Sons, Ltd, 2nd edition.

[Bhatnagar, 2016] Bhatnagar, A. (2016). *Lightweight Ballistic Composites: Military and Law-Enforcement Applications*. Woodhead Publishing. Google-Books-ID: qZPBCQAAQBAJ.

[Bilmes and Stiglitz, 2008] Bilmes, L. J. and Stiglitz, J. E. (2008). *Hidden wounds and accounting tricks: disguising the true costs.* Penguin, Lessons from Iraq: Avoiding the Next War.

[Bolotion, 1995] Bolotion, D. N. (1995). *Soviet Small-Arms and Ammunition.* Finnish Arms Museum Foundation, first edition.

[Boman, 2010] Boman, R. (2010). *Developpement d' un formalisme Arbitraire Lagrangien Eulerien tridimensionnel en dynamique implicite. Application aux operations de mise forme.* PhD thesis, Universite de Liege, Belgique.

[Bourdin et al., 2007] Bourdin, X., Trosseille, X., Petit, P., and Beillas, P. (2007). Comparison of Tetrahedral and Hexahedral Meshes for Organ Finite Element Modelling: An Application to Kidney Impact. In *20th International Technical Conference on the Enhanced Safety of Vehicles (ESV)National Highway Traffic Safety Administration.*

[Brants, 2016] Brants, G. (2016). Twee explosies op luchthaven in Zaventem: 14 doden en nog een pak zwaargewonden.

[Brown, 2003] Brown, A. (2003). New Options In Personal Ballistic Protection.

[Burger et al., 2012] Burger, D., Rocha de Faria, A., de Almeida, S. F. M., de Melo, F. C. L., and Donadon, M. V. (2012). Ballistic impact simulation of an armour-piercing projectile on hybrid ceramic/fiber reinforced composite armours. *International Journal of Impact Engineering*, 43:63–77.

[Carey et al., 2000] Carey, M. E., Herz, M., Corner, B., McEntire, J., Malabarba, D., Paquette, S., and Sampson, J. B. (2000). Ballistic helmets and aspects of their design. *Neurosurgery*, 47(3):678–688; discussion 688–689.

[Carlucci and Sidney, 2007] Carlucci, D. E. and Sidney, S. J. (2007). *Ballistics: Theory and Design of Guns and Ammunition.* CRC PRess, 1 edition.

[Chabera et al., 2015] Chabera, P., Boczkowska, A., Morka, A., Kdzierski, P., Niezgoda, T., Ozibo, A., and Adam, W. (2015). Comparison of numerical and experimental study of armour system based on alumina and silicon carbide ceramics. *Bulletin of the Polish Academy of Sciences, Technical Sciences*, 63(2).

[Cheeseman and Bogetti, 2003] Cheeseman, B. A. and Bogetti, T. A. (2003). Ballistic impact into fabric and compliant composite laminates. *Composite Structures*, 61(1):161–173.

[Chocron et al., 2014] Chocron, S., Nicholls, A. E., Brill, A., Malka, A., Namir, T., Havazelet, D., van der Werff, H., Heisserer, U., and Walker, J. D. (2014). Modeling unidirectional composites by bundling fibers into strips with experimental determination of shear and compression properties at high pressures. *Composites Science and Technology*, 101:32–40.

[Ciarlet et al., 2004] Ciarlet, P. G., Ayache, N., and Lions, J.-L. (2004). *Computational Models for the Human Body.* Gulf Professional Publishing. Google-Books-ID: xCjTSm49AuoC.

[Claessens, 1994] Claessens, M. H. A. (1994). *Anatomical description of the human head.* DCT rapporten; Vol. 1994.003, Eindhoven: Technische Universiteit Eindhoven.

[Coghe, 2009] Coghe, F. (2009). From the knights helmet to the modern ballistic helmet: have we reached the summit? In *Security and use of innovative technologies against terrorism, Light-Weight Armour Group*, pages 15–31, Aveiro, Portugal.

[Coghe et al., 2010] Coghe, F., Vandeveld, T., Rabet, L., and Mermans, P. (2010). Feasibility study for an improved ballistic helmet design based on optimised ballistic limit and back face deflection. In *Personal Armour Systems Symposium (PASS)*, Quebec, Canada.

[Cordeau, 2016] Cordeau, B. (2016). Assessment of helmet behaviour against high velocity non- penetrating impact with incidence. In *Personal Armour Systems Symposium (PASS)*, Amsterdam, the Netherlands.

[Corporation, 2017] Corporation, G. (2017). Gentex Corporation.

[Council, 2011] Council, N. R. (2011). *Opportunities in Protection Materials Science and Technology for Future Army Applications.*

[Council, 2012] Council, N. R. (2012). *A National Strategy for Advancing Climate Modeling.* National Academies Press, Washington, D.C.

[Croft and Longhurst, 2007] Croft, J. and Longhurst, D. (2007). HOSDB Body Armour Standards for UK Police (2007) Part 2: Ballistic Resistance. Publication No. 39/07/B.

[Cronin et al., 2003] Cronin, D. S., Bui, K., Kaufmann, C., Mclntosh, G., and Berstad, T. (2003). Implementation and validation of the Johnson-Holmquist ceramic material model in LS-Dyna. In *4th European LS-DYNA User Conference (DYNAmore)*, Ulm, Germany.

[Crowley et al., 1992] Crowley, J. S., Licina, J. R., and Bruckart, J. E. (1992). Flight helmets: How they work and why you should wear one. Technical report, US Army Aeromedical Research Laboratory Fort Rucker, United States of America.

[Cunniff, 1999] Cunniff, P. (1999). Dimensionless parameters for optimization of textile-based body armor systems. In *Proceedings of the 18th International Symposium on Ballistics*, pages 1303–1310.

[Daniel and Remy, 2005] Daniel, B. and Remy, W. (2005). Finite element modelling of human head injuries caused by ballistic projectiles. *Revue Europenne des lments Finis*, 14(4-5):559–576.

[Davis, 2001] Davis, J. R., editor (2001). *Alloying: understanding the basics.* ASM International, Materials Park, Ohio, digital printing edition. OCLC: 838971361.

[de Moura et al., 2011] de Moura, M. F. S. F., de Morais, A. B., and de Magalhaes, A. G. (2011). *Materiais Compositos: Materiais, Fabrico e Comportamento Mecanico.* Publindustria, 2 edition.

[Dehmer and Yen, 2010] Dehmer, P. and Yen, C. (2010). High-Speed Photogrammetric Analysis on the Ballistic Behavior of Kevlar Fabrics Impacted by Various Projectiles. Technical Report ARL-TR-5333, Army Research Laboratory, USA.

[Den Reijer, 1991] Den Reijer, P. C. (1991). *Impact on ceramic faced armour*. PhD thesis, TU Delft, The Netherlands.

[Donea et al., 2004] Donea, J., Huerta, A., Ponthot, J.-P., and Rodriguez-Ferran, A. (2004). *Arbitrary Lagrangian Eulerian methods*, volume Encyclopedia of Computational Mechanics. John Wiley & Sons, Ltd, Chichester, UK.

[DSM Dyneema, 2016] DSM Dyneema (2016). DSM Dyneema.

[DuBose et al., 2011] DuBose, J. J., Barmparas, G., Inaba, K., Stein, D. M., Scalea, T., Cancio, L. C., Cole, J., Eastridge, B., and Blackbourne, L. (2011). Isolated severe traumatic brain injuries sustained during combat operations: demographics, mortality outcomes, and lessons to be learned from contrasts to civilian counterparts. *The Journal of Trauma*, 70(1):11–16; discussion 16–18.

[Ernotte and Colens, 2011] Ernotte, A. and Colens, N. (2011). *Amelioration de la protection d'un casque balistique par la caracterisation de certains materiaux*. PhD thesis, Ecole Royale Militaire, Bruxelles.

[Eshel, 2010] Eshel, T. (2010). Dyneema HB80 Composite Material Selected for the U.S. Forces Improved Combat Helmet | Defense Update:.

[Fejdy et al., 2015] Fejdy, M., andwijt, M., Habaj, W., and Struszczyk, M. (2015). Ballistic Helmet Development Using UHMWPE Fibrous Materials. *FIBRES & TEXTILES in Eastern Europe*, 23(1 (109)):89–97.

[Fellows and Barton, 1999] Fellows, N. and Barton, P. (1999). Development of impact model for ceramic-faced semi-infinite armour. *International Journal of Impact Engineering*, 22(8):793–811.

[fivr/Belga, 2015] fivr/Belga (2015). Terroristen hadden politie-uniformen en zware wapens om commissariaten aan te vallen.

[Freitas et al., 2014] Freitas, C. J., Mathis, J. T., Scott, N., Bigger, R. P., and MacKiewicz, J. (2014). Dynamic response due to behind helmet blunt trauma measured with a human head surrogate. *International Journal of Medical Sciences*, 11(5):409–425.

[Gadd, 1966] Gadd, C. W. (1966). Use of a Weighted-Impulse Criterion for Estimating Injury Hazard. pages 164–174, Warrendale, PA. SAE International.

[Gama and Gillespie Jr., 2011] Gama, B. A. and Gillespie Jr., J. W. (2011). Finite element modeling of impact, damage evolution and penetration of thick-section composites. *International Journal of Impact Engineering*, 38(4):181–197.

[Gerald, 2008] Gerald, Q. Z. (2008). *AM17 Protective functional evaluation of helmet against ballistic impact*. Bachelor of Engineering, National University of Singapore, Singapore.

[Giannou and Baldan, 2009] Giannou, C. and Baldan, M. (2009). *War surgery: working with limited resources in armed conflict and other situations of violence*, volume Volume 1. International committee of the red cross.

[Grand view research, 2016] Grand view research (2016). Ultra High Molecular Weight Polyethylene (UHMWPE) Market Analysis By Application (Medical Grade & Prosthetics, Filtration, Batteries, Fibers, Additives, Membranes, Others) And Segment Forecasts To 2022. Technical Report 978-1-68038-506-9.

[Grobert et al., 2016] Grobert, S., Gedon, H., and Peschel, O. (2016). Experimental investigations on dynamic back face deflection caused by ballistic impact on combat helmets and the effect to the human skull. *29th International Symposium on Ballistics*.

[Grujicic et al., 2008] Grujicic, M., Arakere, G., He, T., Bell, W. C., Cheeseman, B. A., Yen, C. F., and Scott, B. (2008). A ballistic material model for cross-plied unidirectional ultra-high molecular-weight polyethylene fiber-reinforced armor-grade composites. *Materials Science and Engineering: A*, 498(12):231–241.

[Gurdjian et al., 1961] Gurdjian, E. S., Lissner, H. R., Evans, F. G., Patrick, L. M., and Hardy, W. G. (1961). Intracranial pressure and acceleration accompanying head impacts in human cadavers. *Surgery, Gynecology & Obstetrics*, 113:185–190.

[Gurdjian et al., 1953] Gurdjian, E. S., Lissner, H. R., Latimer, F. R., Haddad, B. F., and Webster, J. E. (1953). Quantitative determination of acceleration and intracranial pressure in experimental head injury; preliminary report. *Neurology*, 3(6):417–423.

[Hahn and Soyer, 2005] Hahn, E. D. and Soyer, R. (2005). Probit and logit models: Differences in a mul- tivariate realm. *The Journal of the Royal Statistical Society*.

[Hallquist, 2012] Hallquist, J. (2012). *LS-Dyna Keyword Users Manual*, volume II of *Version 971 R6.1.0*. Livermore Software Technology Corporation (LSTC).

[Hatzenbichler and Buchmayr, 2009] Hatzenbichler, T. and Buchmayr, B. (2009). FEM study on the penetration of projectiles into steel sheets. *International Journal of Material Forming*, 2(1):789.

[Hazzard et al., 2018] Hazzard, M., Heisserer, U., van der Werff, H., Curtis, P., and Hallett, S. (2018). Finite Element Modelling of Impact on Composites made with Dyneema. In *Personal Armour Systems Symposium*, pages 208–220, Washington, D.C.

[Heisserer, 2011a] Heisserer, U. (2011a). Numerical modelling of impact - Experiences with Autodyn. Technical, DSM-Dyneema.

[Heisserer, 2011b] Heisserer, U. (2011b). Tensile properties of Dyneema HB plies (HB2, HB26, HB50, HB80). Technical, DSM-Dyneema.

[Hisley et al., 2011] Hisley, D. M., Gurganus, J. C., and Drysdale, A. W. (2011). Experimental methodology using digital image correlation to assess ballistic helmet blunt trauma. *Journal of Applied Mechanics*, 78(5):051022–051022–7.

[Hodgson et al., 1973] Hodgson, V. R., Thomas, L. M., United States, National Highway Traffic Safety Administration, Wayne State University, and Department of Neurosurgery (1973). *Breaking strength of the human skull vs. impact surface curvature*. Dept. of Neurosurgery, Wayne State University, Detroit. OCLC: 1015125.

[Hu et al., 2002] Hu, C.-J., Lee, P.-Y., and Chen, J.-S. (2002). Ballistic performance and microstructure of modified rolled homogeneous armor steel. *Journal of the Chinese Institute of Engineers*, 25(1):99–107.

[Iannucci et al., 2009] Iannucci, L., Pope, D. J., and Dalzell, M. (2009). A Constitutive Model for DYNEEMA UD composites. In *17th International Conference on Composite Materials*, pages 27–31.

[IMA, 2019] IMA (2019). French Imperial M-1858 Curassier Helmet.

[IMA, 2019] IMA (2019). Original Canadian WWII Named 1941 MkI Brodie Helmet by General Steel Wares of Toronto.

[Iremonger, 1999] Iremonger, M. J. (1999). Polyethylene composites for protection against high velocity small arms bullets. In *18th International Symposium on Ballistics*, pages 946–953, San Antonio, TX. Technomic Publishing Co.

[Ivins et al., 2007] Ivins, B. J., Schwab, K. A., Crowley, J. S., McEntire, B. J., Trumble, C. C., Brown, F. H., and Warden, D. L. (2007). How Satisfied Are Soldiers with Their Ballistic Helmets? A Comparison of Soldiers' Opinions about the Advanced Combat Helmet and the Personal Armor System for Ground Troops Helmet. *Military Medicine*, 172(6):586–591.

[Johnson and Cook, 1983] Johnson, G. R. and Cook, W. (1983). A constitutive model and data for metals subjected to larger strains, high strain rates and high temperatures. The Hague, the Netherlands.

[Johnson and Holmquist, 1994] Johnson, G. R. and Holmquist, T. J. (1994). An improved computational constitutive model for brittle materials. In *AIP Conference Proceedings*, volume 309, pages 981–984. AIP Publishing.

[Johnson et al., 2003] Johnson, G. R., Holmquist, T. J., and Beissel, S. R. (2003). Response of aluminum nitride (including a phase change) to large strains, high strain rates, and high pressures. *Journal of Applied Physics*, 94(3):1639–1646.

[Kane and Smith, 1968] Kane, R. L. and Smith, R. S. (1968). A forming technique for soldiers titanium helmets. Technical Report 69-32-GF, General Equipment & Packaging Laboratory U. S. Army Natick Laboratories.

[Karim and Fatt, 2005] Karim, M. R. and Fatt, M. S. (2005). Impact of the Boeing 767 Aircraft into the World Trade Center. *Journal of Engineering Mechanics*, 131(10):1066–1072.

[Kaufmann et al., 2003] Kaufmann, C., Cronin, D., Worswick, M., Pageau, G., and Beth, A. (2003). Influence of Material Properties on the Ballistic Performance of Ceramics for Personal Body Armour. *Shock and Vibration*, 10(1):51–58.

[Kechagiadakis et al., 2017] Kechagiadakis, G., Coghe, F., and Gilson, L. (2017). The development of a Bullet Simulating Projectile for body armor testing. In *30th Internation Symposium on Ballistics*, Long Beach, CA.

[Keene et al., 2016] Keene, D. D., Penn-Barwell, J. G., Wood, P. R., Hunt, N., Delaney, R., Clasper, J., Russell, R. J., and Mahoney, P. F. (2016). Died of wounds: a mortality review. *Journal of the Royal Army Medical Corps*, 162(5):355–360.

[Kelly, 2013] Kelly, P. (2013). *Mechanics Lecture Notes: An introduction to Solid Mechanics*. University of auckland edition.

[Kimpara and Iwamoto, 2012] Kimpara, H. and Iwamoto, M. (2012). Mild traumatic brain injury predictors based on angular accelerations during impacts. *Annals of Biomedical Engineering*, 40(1):114–126.

[King et al., 2003] King, A., Yang, K., Zhang, L., and Hardy, W. (2003). Is Head Injury Caused by Linear or Angular Acceleration? In *IRCOBI Conference*, Lisbon, Portugal.

[Kleiven, 2006] Kleiven, S. (2006). Evaluation of head injury criteria using a finite element model validated against experiments on localized brain motion, intracerebral acceleration, and intracranial pressure. *International Journal of Crashworthiness*, 11(1):65–79.

[Kleiven, 2007] Kleiven, S. (2007). Parametric studies of the ballistic helmet design. In *IMPLAST 2007, 9th Symposium on Plasticity and Impact Mechanics*.

[Kneubuehl, 1996] Kneubuehl, B. (1996). Improved Test Procedure for Body Armour - Statistical Base and Evaluation Program. In *Personal Armour Systems Symposium 1996*, pages 287–294, Colchester, UK.

[Krishnan et al., 2008] Krishnan, K., Rajan, S. D., and Belegundu, A. D. (2008). A General Optimization Methodology for Ballistic Panel Design. In *EngOpt 2008 Conference*, Rio de Janeiro, Brasil.

[Kulkarni et al., 2013] Kulkarni, S. G., Gao, X. L., Horner, S. E., Zheng, J. Q., and David, N. V. (2013). Ballistic helmets - their design, materials, and performance against traumatic brain injury. *Composite Structures*, 101:313–331.

[Lee and Gong, 2010] Lee, H. P. and Gong, S. W. (2010). Finite element analysis for the evaluation of protective functions of helmets against ballistic impact. *Computer Methods in Biomechanics and Biomedical Engineering*, 13(5):537–550.

[Lee and Haut, 1989] Lee, M. C. and Haut, R. C. (1989). Insensitivity of tensile failure properties of human bridging veins to strain rate: implications in biomechanics of subdural hematoma. *Journal of Biomechanics*, 22(6-7):537–542.

[Leigh Phoenix and Porwal, 2003] Leigh Phoenix, S. and Porwal, P. K. (2003). A new membrane model for the ballistic impact response and V50 performance of multi-ply fibrous systems. *International Journal of Solids and Structures*, 40(24):6723–6765.

[Li et al., 2016] Li, X. G., Gao, X. L., and Kleiven, S. (2016). Behind helmet blunt trauma induced by ballistic impact: a computational model. *International Journal of Impact Engineering*, 91:56–67.

[Li et al., 2015] Li, Y. Q., Li, X. G., and Gao, X.-L. (2015). Modeling of advanced combat helmet under ballistic impact. *Journal of Applied Mechanics*, 82(11):111004–111004.

[Lidn et al., 1005] Lidn, E., Seeman, T., Schantz, B., Janzon, B., and Berlin, R. (1005). Marine lethal torso injuries: preliminary findings. Technical report, Carroll AW, Soderstrom CA.

[Lissner et al., 1960] Lissner, H. R., Lebow, M., and Evans, F. G. (1960). Experimental studies on the relation between acceleration and intracranial pressure changes in man. *Surgery, Gynecology & Obstetrics*, 111:329–338.

[Long, 1988] Long, D. (1988). *AK47: The Complete Kalashnikov Family Of Assault Rifles*. Paladin Press, Boulder, Co. Quantity Available: 1.

[LSTC, 2011] LSTC (2011). Livermore Software Technology Corporation (LSTC).

[Marissen, 2011] Marissen, R. (2011). Design with Ultra Strong Polyethylene Fibers. *Materials Sciences and Applications*, 02(05):319.

[Marjoux et al., 2008] Marjoux, D., Baumgartner, D., Deck, C., and Willinger, R. (2008). Head injury prediction capability of the HIC, HIP, SIMon and ULP criteria. *Accident Analysis & Prevention*, 40(3):1135–1148.

[McIntosh, 1998] McIntosh, G. (1998). The Johnson-Holmquist Ceramic Model as used in LS-DYNA 2D. Technical Report DREV-TM-9822, Defence Research Establishment, Valcartier, Quebec.

[Meyer and Mayer, 2011] Meyer, L. W. and Mayer, M. (2011). New strain rate dependent material model for fiber reinforced composites. In Proulx, T., editor, *Time Dependent Constitutive Behavior and Fracture/Failure Processes, Volume 3*, Conference Proceedings of the Society for Experimental Mechanics Series, pages 149–158. Springer New York.

[Meyers, 1994] Meyers, M. A. (1994). *Dynamic Behavior of Materials*. John Wiley & Sons, Inc., Hoboken, NJ, USA.

[MIL-DTL-46593B, 2006] MIL-DTL-46593B (2006). Projectile, Calibres .22, .30, .50, and 20 mm fragment simulating.

[Military, 2017a] Military, R. (2017a). Revision Military.

[Military, 2017b] Military, R. (2017b). Viper A3 Full Cut Helmet.

[Military Trader, 2009] Military Trader (2009). The first modern steel combat helmet: the French 'Adrian'.

[Miranda-Vicario et al., 2014] Miranda-Vicario, A., Azevedo, A., Coghe, F., Matos, J. C., and Pirlot, M. (2014). Experimental and numerical testing of different armour configurations for ballistic helmets. In *Personal Armour Systems Symposium (PASS)*, Cambridge, UK.

[MKU, 2018] MKU (2018). PASGT.

[Monetchikov, 2005] Monetchikov, S. (2005). *[The History of Russian Assault Rifle] (em Russian).* St. Petersburg.

[Moss et al., 2009] Moss, W. C., King, M. J., and Blackman, E. G. (2009). Skull flexure from blast waves: a mechanism for brain injury with implications for helmet design. *Physical Review Letters*, 103(10):108702.

[Mukasey et al., 2008] Mukasey, M. B., Sedgwick, J. L., and Hagy, D. W. (2008). Ballistic Resistance of Body Armor NIJ standard-0101.06. *Law Enforcement Standards Laboratory of the National Bureau of Standards*, page 89.

[Mdlinger et al., 2013] Mdlinger, M., Piccardo, P., Kasztovszky, Z., Kovcs, I., Szkefalvi-Nagy, Z., Kli, G., and Szilgyi, V. (2013). Archaeometallurgical characterization of the earliest European metal helmets. *Materials Characterization*, 79:22–36.

[Nahum et al., 1968] Nahum, A. M., Gatts, J. D., Gadd, C. W., and Danforth, J. (1968). Impact tolerance of the skull and face. In *12th Stapp Car Crash Conference.*

[NATO, 2007] NATO (2007). Test Methodology for Protection of Vehicle Occupants against Anti-Vehicular Landmine Effects, chapter 3: Injury Criteria and Tolerance Levels. Technical Report RTO-TO-HFM-090.

[NATO Standardization Agency, 2016] NATO Standardization Agency (2016). STANAG 2920 Ed. 3 AEP 2920 Ed. A, V2 - PROCEDURES FOR THE EVALUATION AND CLASSIFICATION OF PERSONAL ARMOUR.

[NATO Standardization Office, 2015] NATO Standardization Office (2015). AEP 2920 Procedures for the Evaluation and Classification of Personal Armour, Bullet and Fragmentation Threats, Edition A, Version 1.

[Neto et al., 2008] Neto, E. A. d. S., Peric, D., and Owen, D. R. J. (2008). *Computational Methods for Plasticity: Theory and Applications.* Wiley, Chichester, 1 edition edition.

[Newman, 1986] Newman, J. A. (1986). A generalized acceleration model for brain injury threshold (GAMBIT). In *International IRCOBI Conference on the Biomechanics of Impact.*

[Newman et al., 2000] Newman, J. A., Shewchenko, N., and Welbourne, E. (2000). A proposed new biomechanical head injury assessment function - the maximum power index. *Stapp Car Crash Journal*, 44:215–247.

[News, 2015] News, B. (2015). Paris attacks weapons "made by Zastava Arms in Serbia". *BBC News.*

[News, 2016] News, B. (2016). 2016 Brussels police raids. Page Version ID: 736902005.

[Office, 1936] Office, T. W. (1936). *Text Book of Ammunition*. Naval & Military Press Ltd.

[Olleak and El-Hofy, 2015] Olleak, A. A. and El-Hofy, H. (2015). SPH Modelling of Cutting Forces while Turning of Ti6Al4V Alloy. In *10th European LS-DYNA Conference 2015*, Wrzburg (Germany).

[Othman, 2009] Othman, R. B. (2009). *Finite element analysis of composite ballistic helmet subjected to high velocity impact*. Masters of Science, University Sains, Malaysia.

[Oukara, 2015] Oukara, A. (2015). *Assessment of Non-Lethal Projectile Head Impacts*. PhD thesis, Universite de Liege, Liege, Belgique.

[Palta et al., 2018] Palta, E., Fang, H., and Weggel, D. C. (2018). Finite element analysis of the Advanced Combat Helmet under various ballistic impacts. *International Journal of Impact Engineering*, 112:125–143.

[Parisien, 2015] Parisien, L. (2015). Je suis Charlie.

[Patrick et al., 1963] Patrick, L. M., Lissner, H. R., and Gurdjian, E. S. (1963). Survival by design: head protection. In *7th Stapp Car Crash and Field Demonstration Conference*.

[Pauker, 2007] Pauker, B. (2007). Congo: On the Trail of an AK-47. *Frontline world*.

[Pierazzo and Collins, 2004] Pierazzo, E. and Collins, G. (2004). A Brief Introduction to Hydrocode Modeling of Impact Cratering. In Koeberl, C., Dypvik, H., Burchell, M. J., and Claeys, P., editors, *Cratering in Marine Environments and on Ice*, pages 323–340. Springer Berlin Heidelberg, Berlin, Heidelberg.

[Pingxiang, 2017] Pingxiang (2017). Pingxiang Chemshun Ceramics Co.,Ltd.

[Pintar et al., 2013] Pintar, F. A., Philippens, M. M. G. M., Zhang, J. Y., and Yoganandan, N. (2013). Methodology to determine skull bone and brain responses from ballistic helmet-to-head contact loading using experiments and finite element analysis. *Medical Engineering & Physics*, 35(11):1682–1687.

[Prasad and Mertz, 1985] Prasad, P. and Mertz, J. M. (1985). The position of the United States Delegation to the ISO working group 6 on the use of HIC in the automotive environment. Technical Report 94(5), SAE Trasactions.

[Rafaels et al., 2015] Rafaels, K. A., Cutcliffe, H. C., Salzar, R. S., Davis, M., Boggess, B., Bush, B., Harris, R., Rountree, M. S., Sanderson, E., Campman, S., Koch, S., and Bass, C. R. (2015). Injuries of the head from backface deformation of ballistic protective helmets under ballistic impact. *Journal of Forensic Sciences*, 60(1):219–225.

[Rahbek et al., 2017] Rahbek, D. B., Simons, J. W., Johnsen, B. B., Kobayashi, T., and Shockey, D. A. (2017). Effect of composite covering on ballistic fracture damage development in ceramic plates. *International Journal of Impact Engineering*, 99:58–68.

[Ramezani and Rothe, 2017] Ramezani, A. and Rothe, H. (2017). A New Approach to Modelling Fiber-Reinforced Plastics for Hydrocode Analysis - Experimental Model Validation of Composite Materials Under Ballistic Impact. In *International Conference on Advances in System Simulation*, pages 41–50, Athens, Greece.

[Rank, 2019] Rank, S. M. (2019). Mesopotamian Warfare: The Sumerians, Akkadians and Babylonians.

[Raymond, 2008] Raymond, D. E. (2008). *Biomechanics of blunt ballistic temporo-pariental head impact*. PhD thesis, Wayne State University, Detroit, Michigan.

[Roberts et al., 2007] Roberts, J. C., Ward, E. E., Merkle, A. C., and O'Connor, J. V. (2007). Assessing Behind Armor Blunt Trauma in Accordance With the National Institute of Justice Standard for Personal Body Armor Protection Using Finite Element Modeling:. *The Journal of Trauma: Injury, Infection, and Critical Care*, 62(5):1127–1133.

[Rodriguez Millan et al., 2014] Rodriguez Millan, M., Vaz-Romero, A., Rusinek, A., Rodriguez-Martinez, J., and Arias, A. (2014). Experimental Study on the Perforation Process of 5754-H111 and 6082-T6 Aluminium Plates Subjected to Normal Impact by Conical, Hemispherical and Blunt Projectiles. *Experimental Mechanics*, 54.

[Rohani, 1977] Rohani, B. (1977). Mechanical Constitutive Models for Engineering Materials. Technical report, U.S. Army Engineer Waterways Experiment Station, Washington, DC.

[Runesson, 2006] Runesson, K. (2006). Constitutive modeling of engineering materials - teory and computation. Lecture Notes, Dept. of Applied Mechanics, Chalmers University of Technology, Goteborg.

[Salimi Jazi et al., 2014] Salimi Jazi, M., Rezaei, A., Karami, G., Azarmi, F., and Ziejewski, M. (2014). A computational study of influence of helmet padding materials on the human brain under ballistic impacts. *Computer Methods in Biomechanics and Biomedical Engineering*, 17(12):1368–1382.

[Sarron et al., 2004] Sarron, J. C., Dannawi, M., Faure, A., Caillou, J. P., Da Cunha, J., and Robert, R. (2004). Dynamic effects of a 9 mm missile on cadaveric skull protected by aramid, polyethylene or aluminum plate: an experimental study. *The Journal of Trauma*, 57(2):236–242; discussion 243.

[Schmitt et al., 2014] Schmitt, K.-U., Niederer, P. F., Cronin, D. S., Muser, M. H., and Walz, F. (2014). *Trauma Biomechanics: An Introduction to Injury Biomechanics*. Springer-Verlag, Berlin Heidelberg, 4 edition.

[Schneider and Nahum, 1972] Schneider, D. C. and Nahum, A. M. (1972). *Impact studies of facial bones and skull*. Proc. 16th Stapp Car Crash Conference, sae 720965 edition. OCLC: 173389429.

[Seeber et al., 2018] Seeber, H., Ramezani, A., and Rothe, H. (2018). Advances in the Development of Combat Helmet Systems - Constructional Contributions for Lightweight Ballistic Composites. 11(1 & 2):166 – 172.

[Segala and Cavallaro, 2014] Segala, D. B. and Cavallaro, P. V. (2014). Numerical investigation of energy absorption mechanisms in unidirectional composites subjected to dynamic loading events. *Computational Materials Science*, 81:303–312.

[Serway and Jewett, 2003] Serway, R. A. and Jewett, J. W. (2003). *Physics for Scientists and Engineers*. Brooks Cole, 6th edition.

[Sone et al., 2017] Sone, J. Y., Kondziolka, D., Huang, J. H., and Samadani, U. (2017). Helmet efficacy against concussion and traumatic brain injury: a review. *Journal of Neurosurgery*, 126(3):768–781.

[Sparks, 2012] Sparks, E. (2012). *Advances in Military Textiles and Personal Equipment*. Elsevier. Google-Books-ID: Xs5ZAgAAQBAJ.

[SSAB, 2016] SSAB (2016). Data sheet 195 Armox 500t.

[Stanton, 1994] Stanton, S. L. (1994). *U.S. Army uniforms of World War II*. Stackpole Books, United States of America, 1st edition.

[Stattenschek and Tauffkirchen, 1970] Stattenschek, A. and Tauffkirchen, W. (1970). Critical evaluation of assessment methods for head impact applied in appraisal of brain injury hazard, in particular in head impact on windshields. In *1970 International Automobile Safety Conference Compendium*, pages 1084–1112.

[Studies, 2011] Studies, B. (2011). 7.62x39 (M43).

[Tan et al., 2012] Tan, L. B., Tse, K. M., Lee, H. P., Tan, V. B. C., and Lim, S. P. (2012). Performance of an advanced combat helmet with different interior cushioning systems in ballistic impact: Experiments and finite element simulations. *International Journal of Impact Engineering*, 50:99–112.

[Teixeira-Dias et al., 2010] Teixeira-Dias, F., Pinho-da Cruz, J., Fontes Valente, R. A., and Alves de Sousa, R. J. (2010). *Metodo dos Elementos Finitos - Tecnicas de Simulacao Numerica em Engenharia*. ETEP, Edicoes Tecnicas e Profissionais.

[Terrio et al., 2009] Terrio, H., Brenner, L. A., Ivins, B. J., Cho, J. M., Helmick, K., Schwab, K., Scally, K., Bretthauer, R., and Warden, D. (2009). Traumatic brain injury screening: preliminary findings in a US Army Brigade Combat Team. *The Journal of Head Trauma Rehabilitation*, 24(1):14–23.

[Tham et al., 2008] Tham, C. Y., Tan, V. B. C., and Lee, H. P. (2008). Ballistic impact of a KEVLAR helmet: experiment and simulations. *International Journal of Impact Engineering*, 35(5):304–318.

[Tse et al., 2014] Tse, K. M., Lim, S. P., Tan, V. B. C., and Lee, H. P. (2014). A Review of Head Injury and Finite Element Head Models. *American Journal of Engineering, Technology and Society.*, 1(5):28–52.

[Ulbrichts Witwe GmbH, 2009] Ulbrichts Witwe GmbH (2009). ZENTURIO- The newest development of Ulbrichts Edition: NR 01/11.11.2009.

[van den Bosch, 2006] van den Bosch, H. (2006). *Crash helmet testing and design specifications*. PhD thesis, Technische Universiteit Eindhoven.

[van Hoof, 1999] van Hoof, J. (1999). *Modelling of Impact Induced Delamination in Composite Materials*. PhD thesis, Ottawa-Carleton Institute for Mechanical and Aerospace Engineering, Ottawa, Ontario.

[van Hoof et al., 2001] van Hoof, J., Cronin, D. S., Worswick, M. J., Williams, K. V., and Nandlall, D. (2001). Numerical head and composite helmet models to predict blunt trauma. In *19th International Symposium on Ballistics*, Interlaken, Switzerland.

[van Hoof et al., 1999] van Hoof, J., Deutekom, M. J., Worswick, M. J., and Bolduc, M. (1999). Experimental and numerical analysis of the ballistic response of composite helmet materials. In *18th International Symposium on Ballistics*, San Antonio, TX (USA).

[van Hoof and Worswick, 2000] van Hoof, J. and Worswick, M. J. (2000). Combining head models with composite helmet models to simulate ballistic impacts. Technical Report DREV-CR-2000-160.

[Vargas-Gonzalez et al., 2011] Vargas-Gonzalez, L., Walsh, S. M., and Wolbert, J. (2011). Impact and ballistic response of hybridized thermoplastic laminates. Technical report, DTIC Document.

[Voigt and Thomas, 1973] Voigt, R. and Thomas, L. M. (1973). Breaking Strength of the Human Skull vs. Impact Surface Curvature. Technical Report Final rept. 20 Dec 71-31 Mar 73., Wayne State University School of medicine, Department of Neurosurgery., Wayne State University.

[Voo et al., 1994] Voo, L., Pintar, F. A., Yoganandan, N., Sanees, A., Ewing, C. L., Thomas, D. J., and Snyder, R. G. (1994). Biomechanical Analysis of Tractor Induced Head Injury. *SAE Transactions*, 103:178–183.

[VPAM, 2014] VPAM (2014). VPAM APR 2006 Allgemeine Prfgrundlagen fr ballistische Material-, Konstruktions- und Produktprfungen. *Vereiningung der Prufstellen fur Angriffshemmende Materialien und Konstruktionen*.

[VPAM, 2017] VPAM (2017). VPAM HVN 2009 Durchschusshemmender Helm mit Visier und Nackenschutz 2009. *Vereiningung der Prufstellen fur Angriffshemmende Materialien und Konstruktionen*.

[W. Gadd, 1971] W. Gadd, C. (1971). Tolerable Severity Index in whole-head nonmechanical impact. In *15th Stapp Car Crash Conference*, pages 809–816.

[Wade et al., 2007] Wade, A. L., Dye, J. L., Mohrle, C. R., and Galarneau, M. R. (2007). Head, face, and neck injuries during Operation Iraqi Freedom II: results from the US Navy-Marine Corps Combat Trauma Registry. *The Journal of Trauma*, 63(4):836–840.

[Wallsten and Kosec, 2005] Wallsten, S. and Kosec, K. (2005). The economic costs of the war in Iraq. SSRN Scholarly Paper ID 848408, Social Science Research Network, Rochester, NY.

[Walsh, 2003] Walsh, N. P. (2003). Mikhail Kalashnikov: Mikhail Kalashnikov. *The Guardian*.

[Walsh et al., 2005] Walsh, S. M., Scott, B. R., Spagnuolo, D. M., and Army Research laboratory (ARL) (2005). *The development of a hybrid thermoplastic ballistic material with application to helmets.* Defense Technical Information Center, Ft. Belvoir. OCLC: 74284220.

[Wambua et al., 2007] Wambua, P., Vangrimde, B., Lomov, S., and Verpoest, I. (2007). The response of natural fibre composites to ballistic impact by fragment simulating projectiles. *Composite Structures*, 77(2):232–240.

[Warren et al., 2004] Warren, T. L., Hanchak, S. J., and Poormon, K. L. (2004). Penetration of limestone targets by ogive-nosed VAR 4340 steel projectiles at oblique angles: experiments and simulations. *International Journal of Impact Engineering*, 30(10):1307–1331.

[Wendy, 2019] Wendy, T. (2019). EPIC Combat Helmet Liner System.

[Wikipedia, 2016a] Wikipedia (2016a). January 2015 anti-terrorism operations in Belgium. Page Version ID: 738309413.

[Wikipedia, 2016b] Wikipedia (2016b). Jewish Museum of Belgium shooting. Page Version ID: 735866393.

[Wikipedia, 2016c] Wikipedia (2016c). November 2015 Paris attacks. Page Version ID: 738870768.

[Winterbone, 1997] Winterbone, D. E. (1997). 7 - Equations of State. In *Advanced Thermodynamics for Engineers*, pages 121–134. Butterworth-Heinemann, Oxford.

[Woodward, 1990] Woodward, R. L. (1990). A simple one-dimensional approach to modelling ceramic composite armour defeat. *International Journal of Impact Engineering*, 9(4):455–474.

[Woodward et al., 1994] Woodward, R. L., Egglestone, G. T., Baxter, B. J., and Challis, K. (1994). Resistance to penetration and compression of fibre-reinforced composite materials. *Composites Engineering*, 4(3):329–341.

[Yang and Dai, 2010] Yang, J. and Dai, J. (2010). Simulation-based assessment of rear effect to ballistic helmet impact. *Computer-Aided Design and Applications*, 7(1):59–73.

[Yen, 2002] Yen, C.-F. (2002). Ballistic impact modeling of composite materials. In *7th International LS-DYNA Users Conference*, Detroit, Michigan, USA.

[Yoganandan et al., 1995] Yoganandan, N., Pintar, F. A., Sances, A., Walsh, P. R., Ewing, C. L., Thomas, D. J., and Snyder, R. G. (1995). Biomechanics of skull fracture. *Journal of Neurotrauma*, 12(4):659–668.

[Zebra Armour, 2018] Zebra Armour (2018). Zebra Armour - Armour for life.

[Zienkiewicz et al., 2013] Zienkiewicz, O. C., Taylor, R. L., and Zhu, J. Z. (2013). *The Finite Element Method: Its Basis and Fundamentals, Seventh Edition*. Butterworth-Heinemann, Amsterdam, 7 edition edition.

[Zook, 1977] Zook, J. (1977). An Analytical Model of Kinetic Energy Projectile/Fragment Penetration. Technical Report BRL MR2797, Ballistic Research Laboratory, U.S.A.